The Effect of Repeated Post Weld Heat Treatment on the Mechanical Properties of ASTM A 302 Grade B

Rudi Filmalter

A dissertation submitted to the Faculty of Engineering and the Built Environment, University of the Witwatersrand, in fulfilment of the requirements for the degree of Master of Science in Engineering.

Johannesburg 2015

DECLARATION

I, Rudi Filmalter, declare that this dissertation is my own unaided work, except where otherwise acknowledged. It is being submitted for the degree of Master of Science in Engineering at the University of the Witwatersrand, Johannesburg. It has not been submitted previously at this, or any other university for any degree or examination.

Digitally signed by Rudi Filmalter
Date: 2015.11.13 08:10:46 +02'00'

13-11-2015

Signature

Date

ACKNOWLEDGEMENTS

I would like to thank the following people and organisations, without which this work would not have been possible:

- Metallurgical Engineering Department, Sasol Secunda, for making their laboratory and work shop available for test work on this project.
- Nico Venter, laboratory assistant at the Metallurgical Engineering Department, Sasol Secunda, for his patience in spending countless hours in performing the test work.
- In memory of Christiaan Hattingh [1987Hat], by whom this work was inspired.
- Cornelis Verhoef, for his work [2002Ver] on the bottom cone of the ash lock.
- To Gasification plant, Sasol Secunda, for providing the material for testing.
- To Sasol Secunda Study Aid Office, for financial assistance.
- My supervisor, Josias van der Merwe, for his guidance and mentorship.

ABSTRACT

Erosion-corrosion on ash lock internal surfaces means that these equipment are continuously refurbished through weld build-up, followed by post weld heat treatment (PWHT). The deterioration of mechanical properties of the ash locks after numerous PWHT cycles has been a concern. A graphical prediction model based on experimental work on this material grade has been derived previously to predict the mechanical properties after a number of PWHT cycles. The validity of the model was, however, questioned. Ash lock, 210AL-3401, was scrapped for the purpose of testing the effect of several PWHT cycles on the mechanical properties and microstructure to determine whether the current model is valid or needs to be optimised.

Test samples of the ASTM A 302 Grade B manganese-molybdenum material were cut from the shell and top dome parent metal and shell-to-dome weld of the test ash lock and subjected to a number of additional simulated PWHT cycles with holding times ranging from 2 to 100 hours. This was followed by mechanical testing, i.e. tension -, hardness - and Charpy V-notch impact testing, in accordance with SA-370, and metallographic examination after each PWHT cycle.

Test results showed that actual measured tensile properties for the shell and dome samples were generally higher than what was predicted by the current model and, similar to hardness, followed an overall downward trend with increasing PWHT cycles for the shell, dome and weld. Impact toughness for the shell and dome was mostly above the minimum required values, but after 100 hours of additional PWHT impact toughness was below the minimum required values when tested at 0°C and above minimum required values when tested at higher temperatures. Impact toughness for the shell-to-dome weld showed an overall increase with increasing PWHT. Metallographic examination showed an overall increase in quantity and size of molybdenum carbides and spheroidisation of the cementite phase for the shell and dome samples with increasing PWHT. Significant coarsening of the carbides together with an increase in the level of spheroidisation resulted in a rapid decrease in tensile properties and impact toughness with increasing PWHT. Similar effects were observed on the microstructure of the weld samples, but no significant effect on impact toughness was observed.

TABLE OF CONTENTS

i. LIST OF FIGURES

ii. LIST OF TABLES

iii. ABBREVIATIONS AND SYMBOLS

ASME	American Society for Mechanical Engineers
ASTM	American Society for Testing and Materials
BSED	Backscattered electron detector
DBTT	Ductile to brittle transition temperature
EDX	Energy dispersive X-ray spectroscopy
EOL	End of life
ETD	Everhart-Thornley detector
FFS	Fitness-for-service
GO	General Overhaul
HAZ	Heat affected zone
Hp	Hollomon-Jaffe parameter
Hp_{eff}	Effective Hollomon-Jaffe parameter
ICRCG HAZ	Intercritically reheated coarse-grained heat affected zone
M/A	Martensite/austenite constituent
M_6C	Complex metal carbides
Mo_2C	Network of fine molybdenum carbide precipitates
Mo_3C	Coarse molybdenum carbides
MPa	Megapascal
MS	Mass Spectrometry
nm	nanometre
PWHT	Post weld heat treatment
SEM	Scanning electron microscope
SCHAZ	Sub-critical heat affected zone
t_{eff}	Effective holding time
UTS	Ultimate Tensile Strength
YS	Yield Strength
µm	micrometre

CHAPTER 1: INTRODUCTION

1.1. Background

The ash locks at the Sasol Secunda Gasification plants (East and West) are pressure vessels manufactured from ASTM A 302 Grade B manganese-molybdenum alloy steel plate material. The gasifiers, also pressure vessels on these plants, are situated on top of the ash locks converting coal to gas. Hot ash as a byproduct from this reaction is dropped from the gasifier into the ash lock periodically. The hot ash and water mixture is highly erosive as well as corrosive and as a result severe wall loss occurs during operation on the internal surface of the shell, top dome and bottom cone (see figure 1.1) of the ash locks.

During General Overhauls (GO) of the equipment, generally 4-yearly although history has shown this to be more frequent, weld build-up of the affected areas back to original dimensions is performed followed by a post weld heat treatment (PWHT). PWHT at 595°C minimum after weld build-up is a requirement from ASME VIII Division 1 Paragraph UCS-56 [1980As3] for this material to relieve residual stresses induced during welding. It is known that mechanical properties of steel deteriorate with repeated PWHT. The ash locks, more than 80 in total, have been operating since 1980/1982 and have been subjected to a number of weld repairs and PWHT cycles throughout their service life.

In the early life of the ash locks (1980's) the question was raised as to how many more of these PWHT cycles can the material be subjected to before the mechanical tensile properties would be below the minimum required properties as specified in ASME II-A/ASTM.

Test work was subsequently conducted by Hattingh [1987Hat] on this type of material, i.e. ASTM A 302 Grade B. This showed that mechanical tensile properties generally decreased with an increasing number of PWHT cycles. Tensile properties initially showed a slight increase, followed by a gradual decrease and then a substantial decrease at a certain stage of PWHT exposure, after which properties decreased to a lesser extent until no further significant decrease in properties occurred. Tensile properties of the test samples were still above minimum required ASME/ASTM values for this material after additional simulated

PWHT. No definitive conclusion was, however, reached with regards to the maximum number of PWHT cycles allowed for the ash locks (refer to Chapter 2 “Literature Study” for more in-depth detail on this test work).

In 2001 it was proposed that destructive mechanical testing be performed on the bottom cone of an ash lock (equipment number 210AL-3401) after it was calculated, using Hollomon-Jaffe parameter (Hp) formulas [2009Sas], that the qualified* PWHT cycle of the material had been used up and that mechanical tensile properties of the ash lock were approaching the minimum required ASME/ASTM values for A 302 Grade B material. The ash lock was consequently scrapped in 2001. This ash lock had been in service for approximately 19 years (since 1982) and subjected to a number of PWHT cycles (8 cycles for the shell and 5 cycles for both the dome and cone) throughout its service life. Test results [2002Ver] showed that the actual measured mechanical properties of the bottom cone compared with the estimated results in certain areas of the parent metal and welds, but were conservative in other areas (refer to Chapter 2 “Literature Study” for more in-depth detail on this test work).

**Qualifying a material for multiple PWHT cycles entails removal of test specimens from the batch, subjecting them to a simulated long PWHT cycle (equivalent to at least three PWHT cycles, including the installation PWHT cycle plus two repairs) and performing mechanical tests on these test specimens. The test results are then displayed on the material certificate, therefore, in effect guaranteeing that the component can withstand an effective number of PWHT cycles equivalent to the qualified PWHT cycle before mechanical properties of the component will have reached the values stated on the material certificate. The Hp [2009Sas] is used to determine whether a material still has part of its qualified cycle left after multiple PWHT cycles had been performed during weld repairs. Hollomon-Jaffe methodology will be used throughout this project to obtain the mechanical strength (UTS and YS) of the various material batches at different stages of exposure to repeated PWHT.*

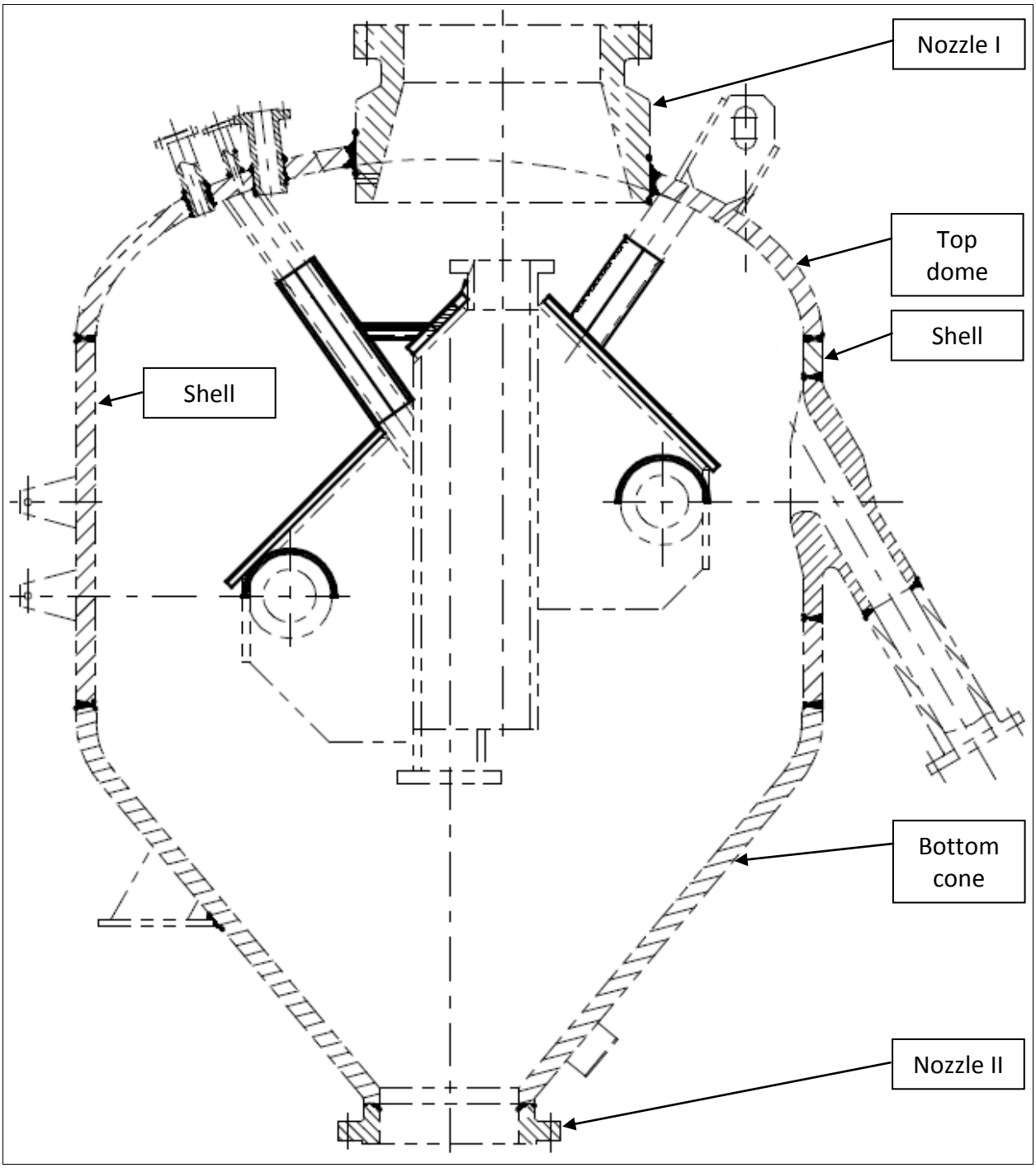

Figure 1.1: Extract from general arrangement drawing showing a vertical cross-section through an ash lock. The top dome, shell and bottom cone components are indicated [1980Sas].

In 2007 test results from Hattingh's work [1987Hat] were used by SecMet, the metallurgical department of MegChem Engineering in Secunda, to derive a graphical prediction model consisting of linear equations (refer to Chapter 4 "Results", figures 4.31 and 4.32) by which mechanical tensile properties for the ash locks after being subjected to PWHT could be predicted [2009Me1, 2009Me2]. The model was based on straight line fitting through the data points obtained from Hattingh's test results. It was, however, suspected that the

predictions were too conservative and that the actual properties after PWHT could be much higher (as much as 10%) than the predicted values. This would lead to ash locks being scrapped prematurely. It was requested that the model be investigated to determine its validity and relevance and whether the model could be optimised for future predictions of ash lock properties.

It was proposed that destructive mechanical testing be performed on the shell and top dome of the ash lock 210AL-3401, i.e. the ash lock of which the bottom cone had been previously tested. Samples of the shell and top dome were made available for extensive testing. Test results are discussed in this report (see Chapter 4 “Results”).

1.2. Research problem statement

Due to repeated PWHT cycles the ash locks are running out of available PWHT cycles [2009Me1, 2009Me2] for which they were initially qualified during initial fabrication. A graphical prediction model based on previous work [1987Hat] for predicting mechanical tensile properties for the ash lock components has shown that predicted mechanical properties for certain ash lock components have decreased below the minimum required ASME/ASTM values for the material. As a result the ash locks have to be replaced. This graphical prediction model needs to be thoroughly investigated and revised if possible to be able to predict whether these ash locks can still be subjected to more PWHT cycles and up to what point before the mechanical properties have reached a point where the material integrity is no longer adequate for service. The hypothesis is, thus, that resulting from the adoption of an overly conservative life limit approach, ash locks at Sasol are being prematurely scrapped.

1.3. Rationale for the study

There are more than 80 ash locks in total at the Gasification plants. Replacement cost per ash lock runs into millions of Rands. The total cost of replacement is significant. Extended life of the ash locks could potentially result in a substantial cost saving to the plant. However, unanticipated failures could result in substantial cost. The study is intended to provide an independent unbiased review that informs decision making.

The study will also contribute to an increase in fundamental knowledge regarding the metallurgical transformations and mechanisms involved during repeated PWHT of ASTM A 302 Grade B material through the use of modern analytical and observation techniques.

The following were identified as objectives for the research project in order to determine whether or not the current life prediction method is appropriate to life extension prediction.

1.4. Research aim and objectives

The overall aim of the study is to determine whether the current prediction model is valid for predicting mechanical properties for the ash locks after PWHT.

The following were identified as objectives for this research project:

a. Determine the mechanical properties (tensile -, hardness -, impact properties) and microstructure of the ASTM A 302 Grade B shell and top dome components and the shell-to-dome weld of the test ash lock 210AL-3401 in the as-received condition.
b. Determine the effect of several repeated PWHT cycles on the mechanical properties and microstructure of the ASTM A 302 Grade B materials and whether the mechanical properties will reach a minimum limiting value beyond which no further degradation occurs.
c. Investigate whether there is a correlation between hardness and ultimate tensile strength (UTS) of the material and whether surface hardness measurements before and after PWHT can accurately predict the through-thickness UTS of the ash lock material.

1.5. Research questions

As a result of achieving the above-mentioned objectives the following research questions were posed:

a. Can microstructural examination (i.e. replication) be performed to accurately determine the mechanical properties of the ash locks after PWHT? This was suggested by Hattingh [1987Hat] as a practical means during GO's to determine the mechanical properties of the components of the ash lock to confirm whether it can undergo any further PWHT.
b. Can the results obtained from mechanical testing on this ash lock, 210AL-3401, be considered representative of the other ash locks still in service?
c. Can a new graphical prediction model be derived from these test results or should the current model be optimised to more accurately predict the mechanical tensile properties after repeated PWHT on the other ash locks still in service?

1.6. Methodology used

Test samples of the ASTM A 302 Grade B manganese-molybdenum plate material were cut from the shell and top dome parent metal and shell-to-dome weld of the test ash lock and subjected to a number of additional simulated PWHT cycles with holding times ranging from 2 hours to 100 hours. These heat treatments were then followed by mechanical testing, i.e. tension testing, hardness testing and Charpy V-notch impact testing, in accordance with SA-370, and metallographic examination of the respective microstructures after each PWHT cycle. Tension test results were then plotted as a graphical prediction model to be used for predicting mechanical tensile properties after repeated PWHT on the other ash locks still in service.

1.7. Limitations of the study

It was initially intended for additional tension tests to be carried out at the design temperature of the ash locks to test the mechanical strength at elevated temperature after extended PWHT. However, due to the limiting size of the shell and dome of the test ash lock there were no additional samples available for elevated temperature tension testing and as a result these tests could not be carried out.

The integrity of the forged components (nozzles, dip pipe and internals) was not tested in this study as the study was aimed at testing only the ASTM A 302 Grade B material of the shell, top dome and bottom cone. The top and bottom nozzle and dip pipe, as well as non-pressure bearing internals, are made from ASTM A 182 Grade F1 forged material. Testing of the forgings did not form part of this project.

1.8. Subdivision of the dissertation

The rest of the dissertation will consist of the following subdivisions: Literature Study, Research Methodology, Results, Discussion and Conclusions with References and an Appendix.

CHAPTER 2: LITERATURE STUDY

2.1. Introduction

The effect of PWHT on the mechanical properties of carbon and low alloy steels has been a popular research topic, both internationally and locally. At Sasol Secunda, Hattingh [1987Hat] used ASTM A 302 Grade B material to investigate the effect of repeated PWHT on the mechanical properties of the ash locks. Verhoef [2002Ver] performed mechanical testing on the bottom cone of ash lock 210AL-3401. The fundamentals behind these studies, mechanical test results and significance of previous test work are discussed in this chapter.

2.2. Fundamentals

Mechanical tensile properties of carbon and low alloy steels generally decrease with increasing PWHT exposure. This phenomenon has been studied by various researchers. Sparkes [1986Spa] found that the tensile strength of a C-Mn-Nb and a C-Mn-Nb-V pressure vessel steel deteriorated when the temperature of PWHT exceeded 600°C. De Brito et al. [2001deB] found that after subjecting A 537 pressure vessel carbon steel samples to PWHT at 650°C for 5 hours a reduction in tensile properties and hardness was noted.

Canonico and Berggren [1971Can] found a variation in mechanical tensile properties through the thickness of the plate with higher ultimate tensile strength measured at the surface than at mid-section. This results from the effect of rolling and is expected. The ultimate tensile strength of welded samples was, however, found to be uniform through the thickness with similar strength measured at the surface than at midsection. Similarly the weld area represents a cast structure and can be expected to show more similar through-thickness strengths.

The effect of multiple PWHT cycles on impact toughness was studied by a number of researchers. Hu, Du, Wang et al. [2014Hu] found that during cooling after welding of V-N steel ultra-fine grained ferrite forms along prior austenite grain boundaries, where V(C,N) precipitates provide potential nucleation sites for ferrite leading to extraordinary

refinement of martensite/austenite (M/A) constituent. With subsequent heat treatments these precipitates consume carbon content in the austenite, leading to a decrease in the carbon content in the M/A constituent, with consequent decrease in hardness and increase in toughness.

Wei, Shang and Wu [2010Wei] investigated grain refinement in the coarse-grained region of the heat affected zone (HAZ) in low-carbon high-strength microalloyed steels using optical microscopy, scanning electron microscopy, and electron backscattering diffraction. They found that the coarse-grained region of the HAZ consists of predominantly bainite and a small proportion of acicular ferrite. Bainite packets are separated by high angle boundaries. Acicular ferrite laths or plates in the coarse-grained region of the HAZ formed prior to bainite packets partition the austenite grains into many smaller and separate areas, resulting in fine-grained microstructures. Electron backscattering diffraction analysis indicated that the average crystallographic grain size of the coarse-grained region of the HAZ was much smaller than that of the austenite grains.

However, the effect of several repeated PWHT cycles on the mechanical properties and microstructure were not found to have been adequately studied. Literature [1986Spa, 2001deB, 1971Can] has shown that mechanical tensile properties generally decrease gradually with increasing PWHT cycles and then drop rapidly at some point of PWHT exposure, after which with more PWHT the decrease in properties became less severe. No literature could, however, be found to explain what happens beyond this point when several additional PWHT cycles are performed on such material. The advantage of knowing exactly what the effect of numerous PWHT cycles long after this point has been reached would be on the mechanical properties and microstructure, is that this information may help the plant to understand how to operate the equipment safely beyond the point where the equipment would normally have been scrapped due to too low mechanical properties. In effect, this could drastically extend the useful life of the equipment and result in a substantial cost saving to the plant.

The effect of several repeated PWHT cycles on the mechanical properties and microstructure of welds were also not thoroughly studied. Welds and the associated HAZ are generally seen as the potential weak points in a vessel and many failures occur at welds

first before parent metal is affected. It would also be beneficial to understand what happens to weld properties after numerous PWHT cycles.

2.2.1 The physical metallurgy of ASTM A 302 Grade B

Pressure vessel steel plate specification ASTM/ASME A/SA-302 Grade B is a manganese-molybdenum alloy steel plate intended particularly for welded boilers and other pressure vessels [2013As1]. According to their strength levels, there are different grades in the A/SA-302 specification, such as Grade A, Grade B, Grade C and Grade D.

Steel is considered an alloy of mainly iron and carbon, with iron being present as the major element and carbon interstitially dissolved in the iron matrix. According to Joarder [1995Joa] manganese-molybdenum alloy steel, such as A/SA-302 Grade B, is a hypoeutectoid steel (containing between 0 and ~0.8% carbon). A/SA-302 Grade B has a maximum specified [2013As1] carbon content of 0.2% max. and contains maximum 0.6% molybdenum (Mo) as an alloying element.

Honeycombe [1982Hon] explains that the iron phase in the steel at room temperature is present as alpha ferrite (α), one of three allotroic forms of iron, the other possible forms being delta ferrite (δ) and austenite (γ). The iron-carbon equilibrium phase diagram only applies to plain carbon steels. However, the addition of alloying elements changes this diagram significantly. Chromium (Cr), molybdenum (Mo), tungsten (W) and vanadium (V) are all ferrite stabilisers, implying that presence of such elements in a steel will result in a contraction of the γ-field on the iron-carbon equilibrium phase diagram. These α-stabilisers will result in an increase in the eutectoid transformation temperature (723°C) and a change in eutectoid composition of the iron-carbon phase diagram. The austenite stabilising elements, namely carbon (C), nitrogen (N), nickel (Ni) and manganese (Mn), will result in an expansion of the γ-field. The γ-stabilisers will result in a decrease in eutectoid transformation temperature.

According to Smallman [1985Sma] the crystal structure of both alpha ferrite (α) and delta ferrite (δ) is body-centered cubic (BCC), while austenite is face-centered cubic (FCC). In

carbon and low alloy steel austenite only exists above the lower critical (A1) temperature. Austenite in pure iron exists between 910 to 1400°C.

Iron and carbon form an intermetallic compound called cementite upon cooling from austenite. This compound is very hard and brittle, and is represented by the formula Fe_3C. The crystal structure of cementite (Fe_3C) is orthorhombic.

The microstructure of normalised and tempered A/SA-302 Grade B consists of a mixture of ferrite and pearlite [1982Hon]. Upon cooling from autenite to below the A1 temperature, coarse pearlite is formed. On further decreasing the isothermal transformation temperature down to about 550°C, a fine lamellar pearlite structure is produced.

Pearlite is a mixture of two phases i.e. ferrite and carbide (Fe_3C), in which each micro-constituent takes shape like lamella. When A/SA-302 Grade B has been normalised, quenched and tempered, two additional phases called bainite and martensite are formed.

The microstructural definition of bainite is non-lamellar and forms due to a eutectoid reaction between ferrite and carbide. Bainite is formed below the nose of the time-temperature-transformation (TTT) diagram and above the martensite start temperature. Upper bainite is formed at the higher transformation temperature and lower bainite is formed above the martensite start temperature.

The martensitic transformation is a solid state phase transformation, which occurs by the co-operative movement of atoms by a shear mechanism without involving any diffusion of atoms. Transformation occurs below the martensite start temperature. The crystal structure of martensite in steels is body-centered tegragonal (BCT) and the degree of tetragonality depends on the percentage of carbon in the steel.

2.2.2 Post weld heat treatment (PWHT)

Gillissie [1981Gil] defines PWHT as a stress relieving heat treatment designed to relieve a proportion of the welding imposed residual stresses by reducing the hardness and increasing ductility, thus reducing the danger of cracking in the vessel weldments. Welding

processes used to join metals together, result in the base materials near the weldment, the deposited weld metal and, in particular, the HAZ to transform through various metallurgical phases. Depending upon the chemistry of the metal, hardening then occurs in the HAZ adjacent to the weld metal deposit where the highest stresses due to melting and solidification occur.

PWHT at 595°C minimum after welding is a requirement from ASME VIII Division 1 Paragraph UCS-56 [1980As3] for carbon and low alloy steels to relieve residual weld stresses. ASME further specifies the rate of heating and cooling before and after PWHT above 427°C and also specifies the holding time, usually one hour per inch (25.4mm) of thickness of the material. Following the holding (soaking) time, controlled cooling down to 427°C or lower is vitally important as many carbon and low alloy steels are subject to surface cracking if cooled too rapidly [1981Gil].

According to Verhoeven [2007Ver] tempering is a heat treatment technique applied to steel to improve toughness and ductility by decreasing the hardness and tensile strength. Tempering is usually performed after quenching or in some cases after normalising without quenching. Tempering is accomplished by heating to a temperature below its lower critical temperature. This is also called the lower transformation temperature or lower arrest (A1) temperature. For iron-carbon alloys containing between ~0.02% and 6.67% carbon the A1 temperature is 723°C. Above this temperature the crystalline phases of the alloy, called ferrite and cementite, are transformed to a single-phase solid solution phase referred to as austenite. Heating above this temperature must be avoided in order not to destroy the quenched microstructure called martensite. Tempering of carbon and low alloy steel is typically stage IV tempering as described by Raghavan [2006Rag] during which coarsening of Fe_3C particles occurs resulting in softening of the steel. These coarsened particles become visible under the optical microscope when tempering was performed above 500°C. With molybdenum-containing alloys, such as A/SA-302 Grade B, a stage V tempering (secondary hardening) occurs when tempering temperature exceeds 550°C resulting in an increase in hardness. PWHT is generally performed in the same temperature range as tempering and, thus, has the same effect on the microstructure and properties.

API RP 582 [2009Api] states that for quenched and tempered or normalised and tempered material, the PWHT holding temperature should be maintained at least 15°C below the original tempering temperature of the base metal, as there is a risk of reducing the mechanical strength below the specified minimum for the steel. The Sasol Specification SP-90-17 [2007Sas] recommends that PWHT should be performed at least 20°C below the original tempering temperature.

Toyooka and Terai [1972Toy] found that the effects of PWHT on carbon steel were: (1) a reduction of residual stress value, (2) removal of strain-aging embrittlement, (3) reduction of HAZ hardness, (4) recovery of impact values, and (5) dimensional stability. According to Toyooka and Terai the low fracture stress values of as-welded tensile specimens have recovered by PWHT even in short soaking time. The recovery of fracture stress values after PWHT was substantially affected by the heating temperature level, but not as much by the soaking time. The recovery of fracture stress values highly correlated with the reduction of hardness of strain-hardened specimens. Wan, Xiong and Suo [2005Non] agree that tempering is an absolutely necessary process in which the modification of the microstructure, the removal of the stress, lowering of hardness and improvement in certain mechanical properties, such as impact strength and fracture toughness in quenched steel, are achieved.

Fletcher and Cohen [1944Fle] found that increase in tempering temperature and time resulted in a decrease in hardness of 1.02% carbon steel quenched from 1575°F (857°C). Steel samples tempered for 100 hours at 420°F (215°C) measured a hardness of 58 Rockwell C, compared to 63 Rockwell C for samples tempered for 0.1 hour at the same temperature. The same phenomenon was observed by Guo [1999Guo] and by Wan, Xiong and Suo [2005Non].

2.2.3 Hollomon-Jaffe parameter (Hp)

Tests were carried out by Hollomon and Jaffe [1945Hol], whereby it was determined that repeated tempering of carbon and low alloy steels resulted in a degradation in mechanical properties, i.e. tensile properties and hardness. The degree of exposure to tempering heat treatment was derived as a parameter called the Hollomon-Jaffe parameter (Hp).

As per Hollomon and Jaffe's work this tempering parameter is non-linear, dependent on variable heat treatment temperature and time, and holding and cooling times, according to the following equation [1947Hol]:

$$Hp = T(C+\log \tau)x10^{-3}$$

where, Hp = Hollomon-Jaffe parameter,
T = Temperature (°K),
C is a constant, and,
τ = Effective holding time (which includes the heating and cooling portions of the cycle), in hours.

Hollomon and Jaffe [1947Hol] determined that the constant C varies linearly for carbon contents between 0.30% and 1.10%. C = 15 is appropriate for steels containing 0.90-1.20%C and C = 19.5 is used for steels containing 0.15-0.45% carbon. In practice, C = 20 is commonly used for carbon-manganese and low alloy steels. A constant of 30 can be employed for more highly alloyed steels, such as 9%Cr steels.

Heating and cooling cycles are included in the parameter:

$$t = t + T/(2.3K1(20-\log K1)) + T/(2.3K2(20-\log K2))$$

where, t is the holding time in hours,
K1 = heating rate in K/hour, and,
K2 = cooling rate in K/hour.

According to Kate and Bhapkar [2009Kat] in mathematics the logarithm of a number is the exponent to which another fixed value called the base must be raised to produce that number. The logarithm to base 10 is called the common logarithm and as written as $\log_{10}$ or log. Logarithms are used as a means to simplify calculations and to reduce wide-ranging quantities to smaller scales.

The Hp is used to compare the response of a steel to a tempering heat treatment or PWHT by defining an equivalence of time and temperature [1947Hol]. A PWHT that was performed on a piece of steel at a specific holding time and temperature can, thus, be quantified by a certain Hp value. The formulas above can also be used to calculate the holding time required if the steel was to be subjected to PWHT at a different holding temperature to achieve the same tempering effect (i.e. the same Hp). This parameter can also be used to determine how much effective time of a qualified PWHT cycle is left and whether another PWHT cycle can be performed without exceeding the effective time of the simulated PWHT cycle for which the material was qualified during manufacturing [2009Sas].

The correctness of the Hollomon-Jaffe parameter derivation above was demonstrated by Brooks [1996Bro], whereby tempering hardness was plotted against Hp for plain carbon steel and higher carbon steels after quenching to form martensite. It was also shown that the parametric plotting was valid for tempering structures other than martensite, namely pearlite and bainite. When plotted data for martensite, pearlite and bainite were compared (see figure 2.1) it was found that at higher Hp values (Hp>14.000 when C=14.4; equivalent to Hp=15.554 when C=20), thus higher tempering temperatures and longer times, the hardness values of pearlite and bainite were closer to that of martensite than at lower Hp. The slopes of the curves and, thus, the rate of tempering achieved at these higher Hp's were

generally lower for pearlite and bainite than for martensite. Note that for tempering and PWHT of carbon and low alloy steels, generally and in this study, the Hp is expected to be at the higher end of the graph (refer to paragraph 2.3 where Hp>17.93 [1987Hat]).

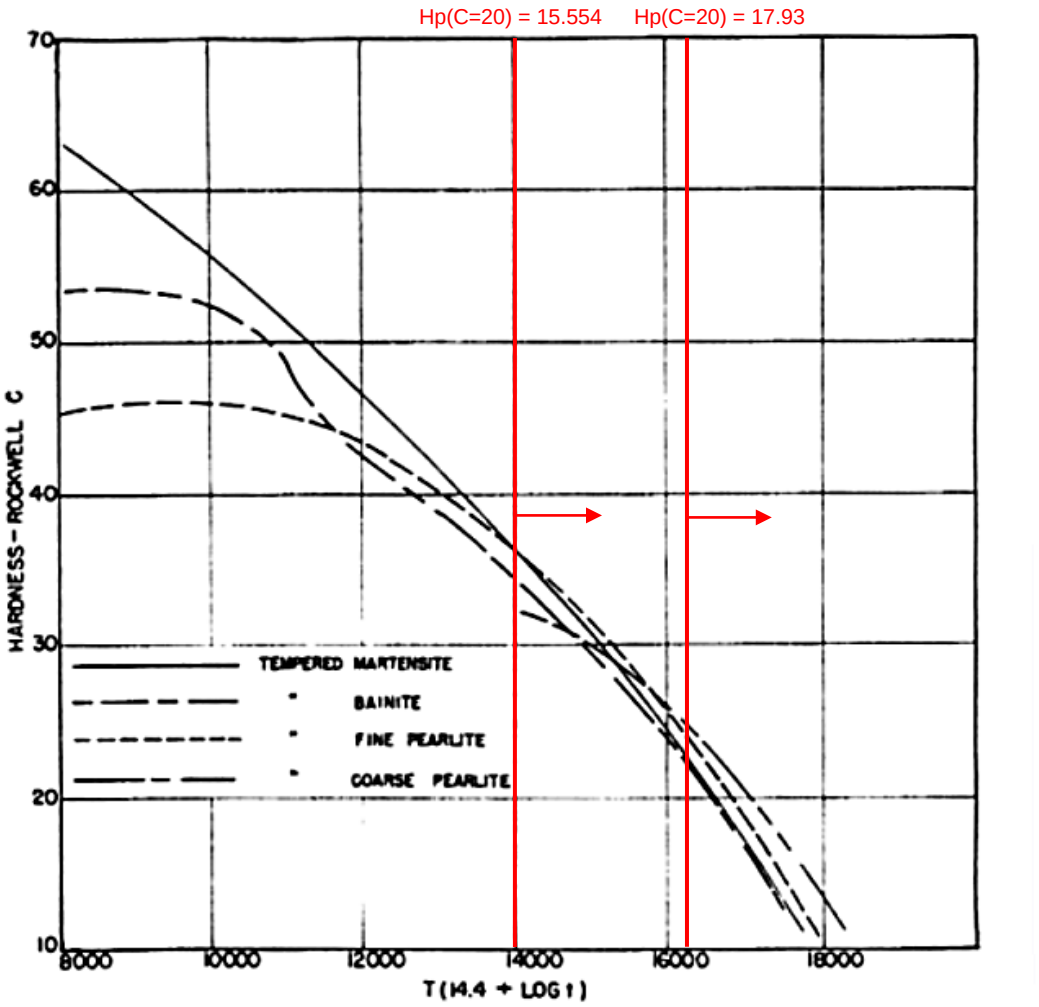

HARDNESS VS. TIME-TEMPERATURE PARAMETER FOR TEMPERING 0.94 PER CENT CARBON STEEL FROM VARIOUS INITIAL STRUCTURES. (*Data from Engel.*[3])
Temperature of formation of isothermal structures: bainite, 600°F.; fine pearlite, 900°F.; coarse pearlite, 1200°F.

Constant = 14.4
Time t in seconds.
Temperature T in deg. K.

Figure 2.1: Tempering data for martensite, bainite and pearlite plotted parametrically [1945Ho2 in 1996Bro].

It was also observed by Brooks [1996Bro] that the decrease in tensile properties and hardness, and structural change in carbon steels was due to coarsening of the cementite (Fe_3C) with increasing Hp. The rate of hardness decrease was noted to be reduced in low alloy steels. This was ascribed to the influence of substitutional solutes, such as manganese, silicon, molybdenum and chromium, on the diffusion of carbon. When the alloy content is

sufficiently high, carbides other than Fe_3C may form which have a high solute content. These alloying elements diffuse much slower in ferrite than carbon. The rate of softening in low alloy steels will, thus, be less than in carbon steel.

2.2.4 Stages of spheroidisation

Spheroidisation is a change in the microstructure of carbon and low alloy steels after prolonged and accumulative exposure in the 440°C to 760°C range, where the carbide phases are unstable and may agglomerate from their normal plate-like form to a spheroidal form, or from small, finely dispersed carbides such as in low alloy steels to large agglomerated carbides [2011Api]. Spheroidisation may cause a loss in strength and creep resistance.

The spheroidisation of pearlitic and/or bainitic microstructures of mild and low alloy steels subjected to elevated temperature service above the creep threshold for a period of time is a common phenomenon. Toft and Marsden [1961Tof] developed a system using samples of 1Cr-½Mo steel, which allows the degree of carbide spheroidisation of all ferritic steels to be categorized into six stages. Each stage is indicated with a letter, which represents a microstructural appearance. A description of each microstructure and its corresponding letter depicting the different stages proposed by Toft and Marsden are given in table 2.1.

The threshold temperature for spheroidisation of carbon-molybdenum and manganese-molybdenum alloy steels, such as the ASTM A 302 Grade B materials of the ash locks, is 440°C [2011Api]. The PWHT temperature of 595°C minimum for this material [1980As3] is above this threshold and, therefore, spheroidisation due to PWHT is expected.

Table 2.1: Stages of carbide spheroidisation in ferritic steel after Toft and Marsden [1961Tof].

Stage	Degree of spheroidisation
A	Typical of the structure of a new material, consisting of ferrite and a very fine pearlite.
B	The first stage of carbide spheroidisation, usually coinciding with the appearance of small particles of carbides at the grain boundaries.
C	An intermediate stage of spheroidisation showing more distinct signs of carbide spheroidisation in the pearlite areas, but some carbide plates still evident. Increased carbide

	precipitation within the ferrite grains and at the grain boundaries.
D	Spheroidisation of the carbide is virtually complete, but they are still grouped in the original pearlitic pattern.
E	Spheroidisation is complete and the carbides are dispersed leaving little trace of the original pearlite areas.
F	There is a marked increase in the size of some of the carbide particles, partly due to coalescence.

According to Toft and Marsden [1961Tof] an overall decrease in creep rupture strength was noted with increasing stages of spheroidisation and precipitation. With each stage the precipitation of Mo_2C carbides in the ferrite increased, an effect known as secondary hardening or precipitation hardening [1962Cla]. When ferritic steel containing Mo (also Cr, V, W and Ti), a carbide former, is heated in the tempering range between 500-600°C for this type of material [2004Key], a network of fine molybdenum carbides (Mo_2C) precipitate within the microstructure. Precipitation occurs mainly on the grain boundaries but also intragranular in the ferrite and in the cementite (Fe_3C) phase of the pearlite. The presence of these fine carbides directly result in an initial increase in tensile properties [1962Cla, 1986Spa]. According to Toft and Marsden transformation from Fe_3C to Mo_2C in the pearlite phases also became more evident. Eventually the decrease in coherency due to the presence and size of the Mo_2C carbides and later Mo_3C carbides and complex M_6C carbides caused a decrease in creep ductility and rupture strength and consequently an increased susceptibility for creep damage. At higher stages of spheroidisation (E-F) the creep rupture strength is lower than at early stages, i.e. stages A-B; therefore, the material is more susceptible to creep rupture. Hattingh's work was in agreement with the work done by Toft and Marsden [1961Tof] on carbon and low alloy steels where the degree of spheroidisation increased with increasing tempering time.

2.2.5 Possibility of creep damage

According to work done by Neubauer and Wedel [1983Neu] on carbon and low alloy steel, cavities relating to creep damage occur over time in the microstructure under stress and at temperatures operating in the creep range (above 399°C for this material [2011Api]). Neubauer and Wedel developed a system for classifying the various stages of creep for

carbon and low alloy steels by means of replicas (see table 2.2). According to their report at the end of the steady-state creep regime the first cavities are formed (damage parameter A). The transition from secondary to tertiary creep is associated with orientated cavities (damage parameter B). The link-up of cavities to micro cracks (damage parameter C) and the formation of macro cracks (damage parameter D) precede fracture.

Table 2.2: Cavitation damage classification after Neubauer and Wedel [1983Neu].

Damage parameter	Microstructural feature	Remedial action
Undamaged	No secondary creep damage observed.	None
A	Cavities are isolated on grain boundaries.	Observe
B	Orientated cavities i.e., the cavities are distributed so that an alignment of damaged boundaries normal to the maximum stress can be seen.	Requires inspection at fixed intervals, usually between $1^1/_2$ and 3 years.
C	Some micro cracks, coalescence of cavities causing the separation of grain boundaries.	Requires repair or replacement within 6 months.
D	Macro cracks	Requires immediate replacement.

The operating temperature of the ash locks is between 360 and 400°C and, therefore, creep damage is not expected due to normal operation. Microstructure changes are also not expected. The total effective time to which the ash locks will be exposed during PWHT at 620°C is not expected to have a significant effect on creep life and no creep voids are, therefore, expected to occur in the material. In Hattingh's tests, the material was exposed to a maximum of 40 cycles of 30 minutes each, i.e. between 20 to 30 hours at 620°C. Creep is known to take many years of operation under stress in the creep range to occur [1952Lar].

2.3. Background - PWHT of ash locks

This study was inspired by previous test work performed by Hattingh [1987Hat] in 1987, where the effect of simulated PWHT (i.e. tempering heat treatment) on the mechanical properties of ASTM A 302 Grade B manganese-molybdenum plate material was determined.

2.3.1 Chemical composition and initial mechanical properties of test batch

Hattingh's experiments were performed on a batch of 20 mm thick ASTM A 302 Grade B plate material with chemical composition and initial (as-fabricated) mechanical tensile properties as indicated in tables 2.3 and 2.4.

Table 2.3: Chemical composition of Hattingh's test batch [1987Hat].

	Chemical composition [weight %]	
Element	**Specification for A 302 Grade B [1980As1]**	**Test plate**
Carbon (C)	0.20 max.	0.17
Manganese (Mn)	1.50 max.	1.13
Sulphur (S)	0.04 max.	0.021
Phosporous (P)	0.035 max.	0.012
Silicon (Si)	0.30 max.	0.22
Chromium (Cr)	-	0.19
Molybdenum (Mo)	0.60 max.	0.51
Nickel (Ni)	-	0.23
Copper (Cu)	-	0.39
Vanadium (V)	-	0.005
Niobium (Nb)	-	0.005
Iron (Fe)	Remainder	Remainder

Table 2.4: Initial tensile properties of Hattingh's test batch [1987Hat].

	Specification for A 302 Grade B [1980As1]	**Test plate**
Yield Strength [MPa]	345 min.	532.6
Ultimate Tensile Strength [MPa]	550 - 690	736.96

2.3.2 Additional simulated PWHT

The Hp prediction methodology played a significant part in Hattingh's work. Hp was also used extensively in this study. In Hattingh's work additional simulated PWHT was performed on samples of the batch over an Hp range equivalent to 40 PWHT cycles of 30

minutes each at a holding temperature of 620°C (up to an Hp of 19.36). Various sets of samples were subjected to a number of single long simulated PWHT cycles, each with varying holding times representing different Hp values. The various holding times for each long cycle were calculated, using Hp methodology, to be equivalent to a number of shorter PWHT cycles of 30 minutes each (for an explanation on the methodology used refer to Chapter 3 Par. 3.4.1 "Simulated PWHT parameters"). The various heat treatments were followed by mechanical testing and metallographic examination on samples subjected to the various PWHT cycles.

2.3.3 Mechanical properties vs. PWHT

The graph in figure 2.2 shows the tensile properties plotted against the Hp. The Hp value on the X-axis of the graph represents the degree of total effective PWHT performed on the material. The Y-axis represents the tension test results for samples subjected to the various PWHT cycles. For example, an Hp value of 17.93 on this graph represents the mechanical tensile properties (ultimate tensile strength (UTS) and yield strength(YS)) of samples that were subjected to 1 simulated PWHT cycle of 30 minutes at 620°C, while an Hp of 18.47 represents the mechanical properties of samples subjected to a single long simulated PWHT cycle equivalent to 4 shorter PWHT cycles of 30 minutes each. Similarly, an Hp of 18.82 represents the mechanical properties of samples subjected to a single long simulated PWHT cycle equivalent to 10 shorter PWHT cycles of 30 minutes each, etc. An Hp of 19.36 represents 40 such simulated PWHT cycles.

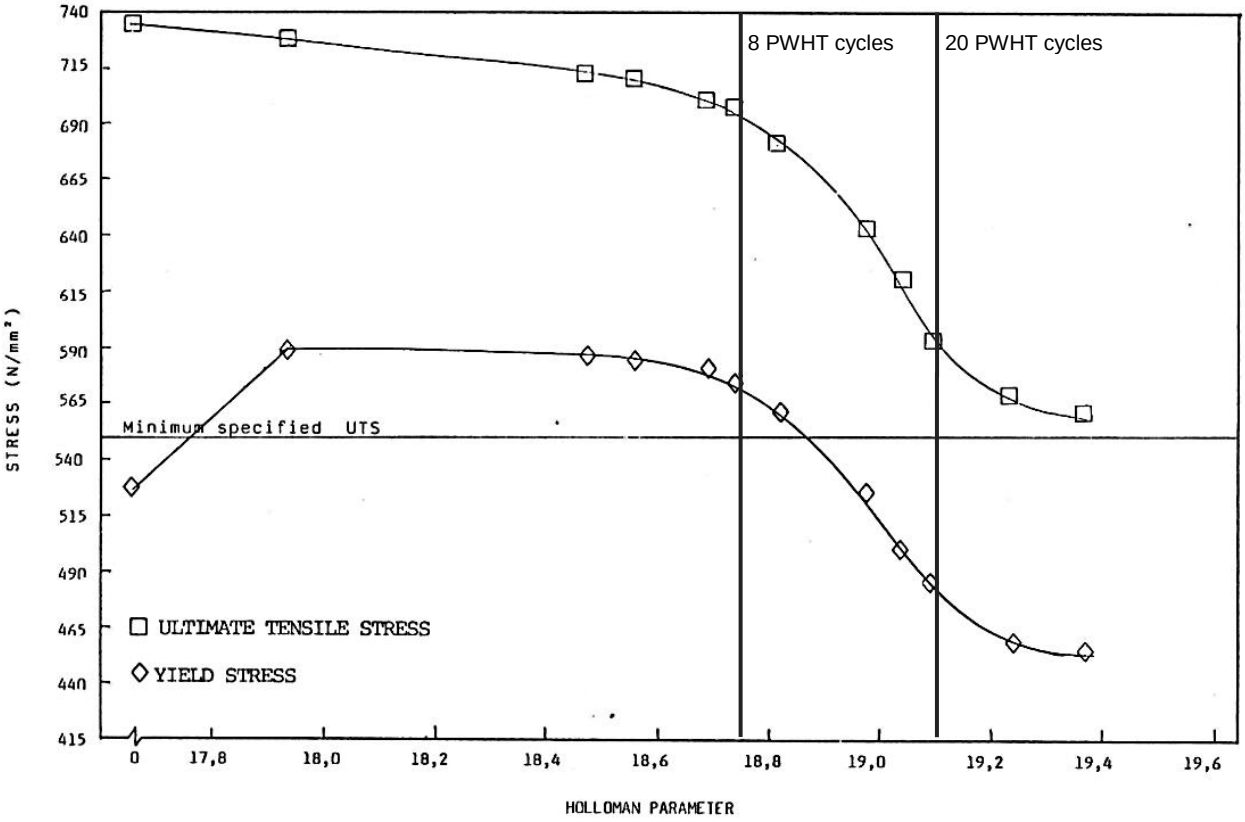

Figure 2.2: Effect of repeated PWHT on the tensile properties of ASTM A 302 Grade B [1987Hat].

The graph in figure 2.2 shows that there is an overall decrease in UTS with increasing Hp value. A significant drop in UTS was noticed after approximately 8 PWHT cycles (Hp of 18.74). After 20 cycles (Hp of 19.10) up to 40 cycles (Hp of 19.36) the decrease in properties was significantly lower and tended to flatten with increasing Hp.

Hattingh's test results further confirmed that after 40 PWHT cycles of 30 minutes each the UTS and YS for this specific batch were still above the minimum specified ASTM values for A 302 Grade B material. This, however, according to Hattingh, depends strongly on the initial properties after fabrication. Hattingh's test batch had a relatively high initial UTS and YS compared to the minimum required ASME/ASTM values (refer to table 2.4).

A marked decrease in hardness values with an increasing Hp was observed. Decrease in hardness followed the same trend as for the UTS, with a sharp decrease after 8 PWHT cycles (Hp of 18.74). After 20 cycles (Hp of 19.10) the decrease in properties was significantly lower. ASME II-A specification SA-370 [1980As2] confirmed that for ferritic steel, hardness follows the same trend as UTS. It was also noted that the precipitation of Mo_2C after the

first PWHT cycle that caused secondary hardening did not cause an increase in microhardness after one PWHT cycle.

2.3.4 Impact properties

Hattingh also performed Charpy V-notch impact tests on samples tested at different Hollomon-Jaffe parameters and temperatures. A considerable decrease in the ductile to brittle transition temperature (DBTT) with an increasing Hp was noticed. The DBTT measured at a minimum specified average value of 35 Joules [2003Sas] decreased from 40°C for the as-received material to 9°C for the samples heat treated at Hp=19.36 (40 cycles), indicating an increase in ductility with increasing Hp. The scatter in energy values at Hp=18.47 (4 cycles) was not explained. A significant upwards shift in uppershelf energy with increasing Hp (increasing PWHT) was noticed, which was attributed to increased toughness of the material.

The increase in toughness and ductility with increasing heat treatment time was attributed to a decrease in tensile properties, spheroidisation of planar carbides (cementite) as well as precipitation of fine molybdenum carbides (Mo_2C). PWHT was therefore considered to have a beneficial influence on the impact properties of the material.

2.3.5 Metallographic examination

Metallographic examination was performed by Hattingh on samples in the as-received condition as well as samples subjected to varying number of PWHT cycles. This was done to determine the effect repeated PWHT had on the microstructure as well as on the mechanical properties.

2.3.5.1 Effect on microstructure

Hattingh found during metallographic examination of the test samples that at an Hp of 18.74 the cementite plates in the microstructure reached an advanced stage of spheroidisation (stage C on the Toft and Marsden classification system [1961Tof]), which was associated with the corresponding decrease in the UTS. After 20 cycles (Hp of 19.10) spheroidisation was virtually complete (stage D) and no significant further decrease in UTS was noted.

Hattingh confirmed that the stages of spheroidisation of the cementite increased with increasing heat treatment time. The initial microstructure of the as-received material was characteristic of a quenched and tempered material, i.e. tempered martensite, bainite and ferrite. The microstructure before simulated PWHT was performed (as-received condition) was typical plate-like (lamellar) cementite, evident of an undamaged structure (stage A [1961Tof]).

Subjecting the material to tempering heat treatment caused a change in morphology of the cementite. The microstructure after 1 simulated PWHT cycle revealed that the cementite, having a high interfacial energy, tended to break (spheroidise) forming smaller packets (stage B [1961Tof]). A network of fine molybdenum carbide precipitates (Mo_2C) also started to form.

Later with increasing heat treatment time, after 8 simulated PWHT cycles, spheres formed from the cementite plates (stage C [1961Tof]), and eventually a small number of globular precipitates formed in the cementite. This would minimise the interfacial energy of the cementite. This phenomenon was also observed by other researchers [1986Spa].

Almost total breakdown of cementite into spheres was noted after 20 PWHT cycles (stage D [1961Tof]) with complete spheroidisation (stage E [1961Tof]) of the pearlite phase (cementite plates) reached after 40 PWHT cycles (Hp of 19.36).

Metallographic examination further confirmed that after 1 PWHT cycle a network of fine molybdenum carbide precipitates (Mo_2C) was observed in the microstructure, typically secondary hardening [1962Cla]. Secondary hardening results in an initial increase in YS after which, with further heat treatment, the effect gradually dissappears as the Mo_2C coarsens.

No evidence of creep cavities (voids) was found in the microstructure before or after any of the PWHT cycles in Hattingh's work. During PWHT the material was exposed to a maximum of 40 cycles of 30 minutes each, i.e. between 20 to 30 hours, at 620°C. The total effective time to which the ash locks were exposed during PWHT at 620°C was not expected to have a significant effect on creep life.

2.3.5.2 Effect on mechanical properties

An initial increase in yield strength (YS) was noticed after only 1 PWHT cycle, which then gradually decreased up to an Hp of 18.74, after which it dropped significantly (see figure 2.1).

In Hattingh's work these molybdenum carbides resulted in an initial increase in YS. With further heat treatment, overaging of the Mo_2C occurred leading to coarsening and as a result a gradual decrease in YS. He found after 8 PWHT cycles a similar sharp drop in YS was observed, which was also seen with the UTS. The exact cause of this sharp drop in properties was not explained, but may be ascribed to coarsening of the Mo_2C, possibly formation of M_6C carbides, possibly transformation from Fe_3C to Mo_2C in the pearlite phases, and spheroidisation of the cementite phase. After 20 cycles (Hp=19.10) spheroidisation was virtually complete and the decrease in YS became lower.

Hattingh's tests confirmed that sheroidisation of planar carbides (cementite) together with precipitation of fine molybdenum carbides (Mo2C) with increasing PHWT, resulted in an

overall increase in toughness and ductility. The samples heat treated at Hp=19.36 (40 cycles), indicated an upwards shift in uppershelf energy, i.e. increased ductility, with increasing Hp.

2.3.6 Single long PWHT cycle vs. multiple shorter PWHT cycles

It was further confirmed by Hattingh [1987Hat] that a single long PWHT cycle had the same effect on the mechanical properties as a number of shorter individual PWHT cycles, with equivalent total effective holding time (similar Hp) (linear cumulative effect). A set of samples was subjected to 8 repeated PWHT cycles corresponding to an Hp of 18.77, while another set of samples was subjected to one single cycle equivalent to an Hp of 18.77. The tensile properties (UTS and YS), Charpy V-notch impact values and hardness measured in both cases were comparable.

2.3.7 Current state

Due to the sharp drop in mechanical properties experienced at an Hp value of 18.74 (8 PWHT cycles), it was suggested by Hattingh as a conservative approach that an Hp of 18.74 be considered as a safe cut-off point for continued operation of an ash lock to ensure integrity of the ash locks and that mechanical properties can still be above the minimum required ASTM/ASME values. Note that certain ash locks have now been heat treated past this Hp value and based on Hattingh's predictions the properties of the shell and dome components of these ash locks should now be very close to or even below the minimum required ASTM/ASME values (as confirmed with the calculated predictions [2009Me1, 2009Me2]).

2.4. Initial work done on bottom cone section of test ash lock 210AL-3401

After it was realised via calculated predictions that the tensile properties of the ash locks are approaching the minimum required ASTM values it was decided to perform tests on an actual ash lock to confirm the predicted values. An ash lock, 210AL-3401, was scrapped in 2001 for the purpose of testing after it was found that the qualified PWHT cycle of the bottom cone had almost been used up due to repeated PWHT [1945Hol, 2009Sas].

2.4.1 Background

Initial mechanical testing on the test ash lock 210AL-3401 was carried out on the ASTM A 302 Grade B material of the bottom cone (refer to figures 1.1 and 2.3) by Verhoef [2002Ver] in 2002. The bottom cone material had been qualified during fabrication for 6.6 hours at 605°C. The bottom cone had been subjected to a number of weld repairs during which PWHT was performed over its lifetime from 1982 to 2001. The total effective time of all these previous PWHT cycles was 8.99 hours at 620°C (this equates to an Hp of 18.712 as calculated using Hollomon-Jaffe [1945Hol] formulas), thus close to the cut-off point of 18.74 as suggested by Hattingh [1987Hat]. Total effective time after the simulated PWHT cycle was 20.01 hours at 620°C (Hp of 18.920).

In Verhoef's work, samples were taken across the longitudinal weld seam (section A1 and A2 in figure 2.2), as well as at a cone parent metal area away from the weld at Section H, from both the internal and external surfaces of the plate and subjected to an additional simulated PWHT cycle of 14 hours at 615°C (equivalent to 11.023 hours effectively at 620°C and Hp=18.79, as determined using Hollomon-Jaffe calculations [1945Hol]). This was done to determine the effect of an additional PWHT cycle on the mechanical properties and microstructure of the parent metal of the bottom cone as well as the vertical weld seam. Actual measured mechanical properties were determined on samples in the as-received condition, as well as samples subjected to the additional simulated PWHT cycle.

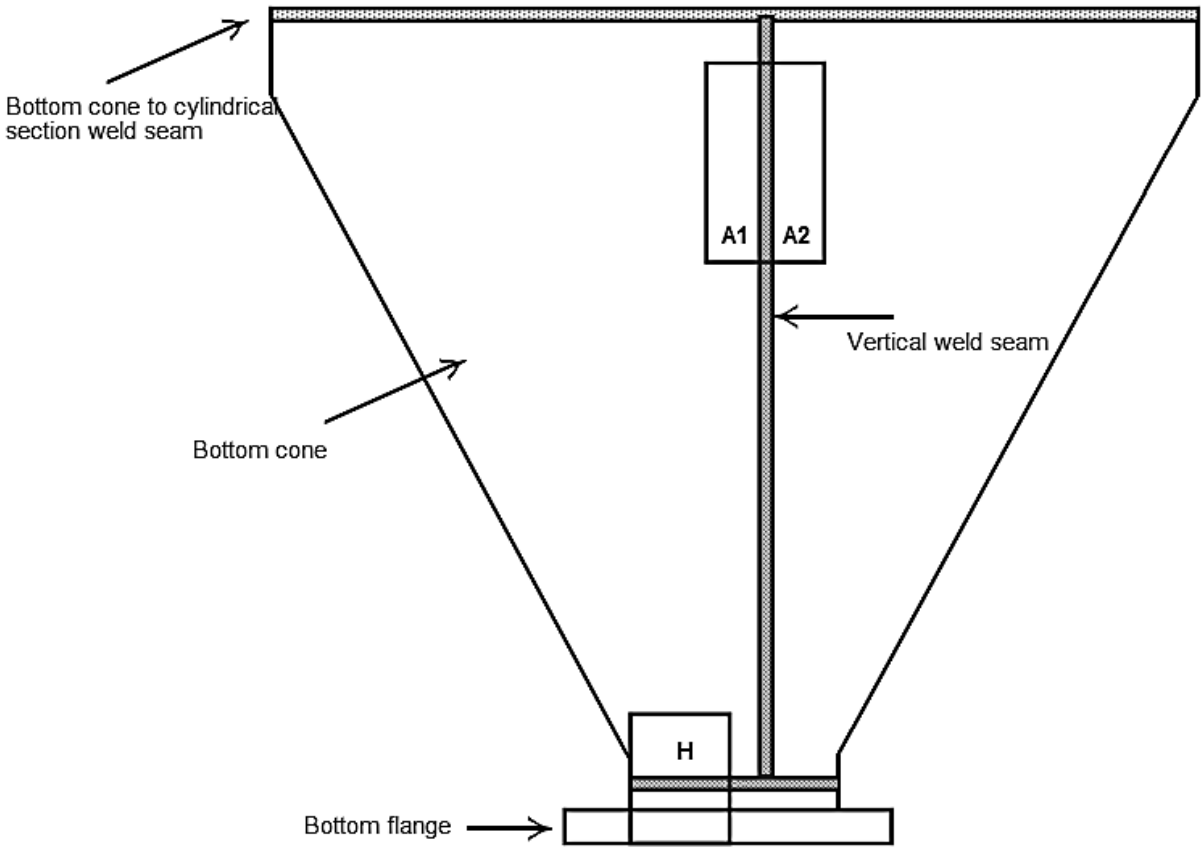

Figure 2.3: Cross-sectional drawing of the bottom cone of ash lock 210AL-3401 showing the areas where samples were removed for testing [2002Ver].

2.4.2 Chemical composition and initial mechanical properties

Tables 2.5 to 2.7 show the chemical composition of the bottom cone material and the initial (as-fabricated) mechanical properties as obtained from the material certificates for this ash lock.

Table 2.5: Chemical composition of the bottom cone as per material certificates [2002Ver].

	Chemical composition [weight %]	
Element	**Specification for A 302 Grade B [1980As1]**	**Plate as-received**
Carbon (C)	0.25 max.	0.20
Manganese (Mn)	1.50 max.	1.40
Sulphur (S)	0.04 max.	0.004
Phosporous (P)	0.035 max.	0.017
Silicon (Si)	0.30 max.	0.25

Chromium (Cr)	-	0.03
Molybdenum (Mo)	0.60 max.	0.57
Vanadium (V)	-	0.002
Niobium (Nb)	-	0.001
Iron (Fe)	Remainder	Remainder

Table 2.6: Initial tensile properties of the bottom cone as per material certificates [2002Ver].

	Specification for A 302 Grade B [1980As1]	**Plate initial**
Yield Strength [MPa]	345 min.	463
Ultimate Tensile Strength [MPa]	550 - 690	629

Table 2.7: Initial Charpy V-notch impact properties of the bottom cone (tested at 0°C) as per material certificates [2002Ver].

	Minimum required [2003Sas]*	**Plate initial**
Energy absorbed [J]	35J ave / 24J min	122, 134, 94 (Ave. 117)

*Minimum requirements not given in ASTM/ASME A/SA-302.

2.4.3 Mechanical testing

2.4.3.1 Tension test results

Verhoef found that the as-received (Hp of 18.712) mechanical tensile properties for the cone parent material adjacent to the vertical weld seam (section A1 and A2 in figure 2.3) compared well with the estimated properties obtained through the use of the Hp [1945Hol] and based on Hattingh's test work [1987Hat]. However, the tensile properties of the cone parent material after being subjected to an additional PWHT cycle of 14 hours at 615°C (Hp of 18.920) were considerably higher than the estimated calculated values.

Actual mechanical tensile properties for the transverse weld samples of the vertical weld seam in both the as-received and heat treated conditions compared well with the estimated properties. The tensile properties of the transverse weld samples and the all weld samples after PWHT were below the required specified ASTM limit. No Hollomon-Jaffe predictions were made for the all weld samples.

Tensile properties for the as-received cone parent material in Section H were higher than the estimated calculated values. The tensile properties for the heat treated samples was below the estimated and below the minimum specified ASTM limit. This was explained by the possibility that the vessel may have been subjected to multiple localised post weld heat treatments in this area (instead of bands around the vessel circumference).

For the parent metal there was initally a decrease in UTS and YS from intial properties to current condition followed by an increase in UTS and YS after the simulated PWHT cycle, while the weld metal showed a decrease in properties after each condition. The cause of this phenomenon was not explained in Verhoef's report.

Verhoef found no significant differences in the UTS and YS between samples taken from the internal and external surfaces of the cone. No tension testing was done on samples removed from the middle of the plate.

2.4.3.2 Hardness testing

Verhoef also performed hardness testing on as-received samples and on samples subjected to an additional PWHT cycle of 14 hours at 615°C. Laboratory Vickers hardness tests were performed on cross-sectional samples cut through the vertical weld seam in Section A1 and A2 on the parent metal, HAZ and weld metal. Hardness tests using a MicroDur MIC10 portable hardness tester were also performed on the samples in exactly the same locations as was done with the laboratory Vickers hardness indenter.

Verhoef found that the average laboratory measured Vickers weld metal hardness of the vertical weld seam of samples in an as-received condition was 178 HV_{10}. The weld metal hardness of the heat treated vertical weld seam was slightly lower at 175 HV_{10}. The average HAZ hardness of the vertical weld seam in the as-received conditions was measured to be 190 HV_{10}, compared to after PWHT, which were slightly lower at 180 HV_{10}. The average parent metal hardness adjacent to the vertical weld seam in the as-received conditions was measured as 180 HV_{10}. The results of the heat treated samples indicated an average parent metal hardness of 180 HV_{10}. This is similar to the hardness of the as-received samples.

Hardness values on samples removed from the middle of the plate compared well with that on the internal and external surface.

In general Verhoef found that the laboratory measured Vickers hardness of the material, when converted to tensile strength [1980As2], compared favourably with the actual tensile properties. However, in most cases, this was not true for the portable hardness tests, which measured on average 32% lower compared to that of the laboratory Vickers hardness values. Verhoef attributed the inconsistency of these portable hardness tests to sample dimensions, with larger specimens providing more accurate results.

2.4.3.3 Impact testing

Additionally in Verhoef's work [2002Ver] Charpy V-notch impact tests were performed on the as-received material and after subjecting samples to an additional PWHT cycle of 14 hours at 615°C.

In the case of the weld seams, the weld metal as well as HAZ were tested. Three Charpy specimens per location were tested; one set of 3 specimens at the external surface, one set at the internal surface and one set in the middle of the plate. At Section A1 specimens were only taken from the internal surface. The tests were conducted at a temperature of 0°C, which is the same temperature specified on the material certificates for this ash lock. The impact toughness of the material in all the areas tested was well above the minimum specified requirements in SP-110-6 [2003Sas] for both the as-received samples as well as after the additional PWHT cycle. The results generally did not show a definite improvement or reduction in toughness. The impact values for samples removed from the middle of the plate compared well with the values on the internal and external surface. DBTT's before and after PWHT were not determined in this investigation.

2.4.3.4 Metallographic examination

Metallographic examination of the as-received material microstructures, which included parent metal, HAZ and weld metal, was performed. The cone parent metal microstructure comprised of ferrite and partially spheroidised pearlite. The original pearlite colonies could

still be observed. Repeated PWHT resulted in the partial decomposition of the pearlite islands. The heat treated cone parent metal microstructure consisted of only slightly more spheroidised pearlite. No significant differences between the parent metal microstructures at the internal surface and the external surface were found. No examination was done on the microstructure in the middle of the plate.

2.5. Significance of previous test work

When the ash lock was scrapped in 2001 only the bottom cone was tested. The shell and dome, also ASTM A 302 Grade B material, were never tested. These components were, however, tested in the current study.

The key significance of Hattingh's work [1987Hat] is that the graphical prediction model based on his test results has been and is still being used to predict the mechanical tensile properties (UTS & YS) of the ASTM A 302 Grade B manganese-molybdenum plate material of the ash locks after repeated PWHT following weld repairs, to determine whether the ash lock is still suitable for continued service. It is, however, questionable due to various reasons whether Hattingh's test results can really be considered representative of the ash locks.

One noteworthy difference between the actual ash lock material and the material used in Hattingh's experiments is the material thickness of his plates. a) He used 20 mm thick plate material purchased specifically for the purpose of testing. The thickness of the test ash lock shell and dome are 70 mm and 75mm, respectively. b) The plates in Hattingh's tests were also cut into smaller samples before being heat treated, while actual PWHT on an ash lock is performed through the entire thickness of the plate. It is, therefore, possible that the middle of the ash lock plate thickness is not exposed to the same extent of heat as the surfaces during PWHT. Slower cooling is expected in the middle of the sample due to its thickness, leading to smaller Mo_2C carbides and thus a lower YS in the middle of the plate than at the surface [1980Ued]. With increased PWHT cycles slow cooling will also lead to increased spheroidisation and consequently lower tensile strength [1986Spa].

c) Furthermore, Verhoef's test results [2002Ver] on the bottom cone of test ash lock 210AL-3401 showed that actual measured values did not completely correspond to calculated predictions of tensile properties after repeated PWHT using results from Hattingh's tests. This shows that Hattingh's test results may have been too conservative.

It would, therefore, be more relevant if actual samples from the same batch of which the ash locks were made were used for testing and that heat treatment is done on through-thickness samples as well as samples removed from both the surface and middle of the plate. It is also possible that the ash lock material has different initial mechanical properties, chemistry, grain shape and size and initial heat treatment as compared to the material used in Hattingh's tests. Initial microstructure depends mainly on the initial heat treatment condition, for example normalised, quenched and tempered, and to some extent on the chemical composition and method of production [1961Tof, p279].

By using actual ash lock material the aim would be to provide a more closely matched representation of the condition of the ash locks still in service. The effect of PWHT on weld metal has also been investigated in this study and will be discussed in this report.

2.6. Conclusion

Literature study has shown that extended PWHT has an overall detrimental effect on the mechanical properties of carbon and low alloy steels. Work done by Hattingh [1987Hat] has shown that the ash locks may have a limited life, which is dependant on the number of PWHT cycles performed during refurbishments. Verhoef's test results [2002Ver] on the bottom cone of test ash lock 210AL-3401, however, showed that actual measured values did not completely correspond to calculated predictions of tensile properties after repeated PWHT using results from Hattingh's tests. According to literature various possible reasons can contribute to the different results obtained in the test work of these two researchers. It was decided that it would be be more relevant if samples from an actual ash lock was used for testing.

CHAPTER 3: RESEARCH METHODOLOGY

3.1 Introduction

Test samples of the ASTM A 302 Grade B manganese-molybdenum plate material were cut from the shell and top dome parent metal and shell-to-dome weld of test ash lock 210AL-3401 and subjected to a number of additional simulated PWHT cycles. These heat treatments were then followed by mechanical testing (including tension -, hardness - and impact testing) in accordance with SA-370. Metallographic examination of the respective microstructures was performed. The integrity of the nozzle materials, dip pipe and internals (forgings) were not tested in this study. The following section provides a detailed description of the experimental work that was carried out.

3.2 Sample Cutting

3.2.1 Locations of test specimens on the ash lock

The locations of all test specimens were marked out on the ash lock, on the top dome and shell components, as well as across the shell-to-dome weld (refer to figures 3.1 and 3.2). The rolling direction of the plate was verified by performing a macro-etch on the various components of the ash lock prior to cutting. All test specimen areas on the ash lock were stamped by the AIA (Authorised Inspection Agency) prior to cutting, following a pre-determined naming convention, to ensure traceability of samples.

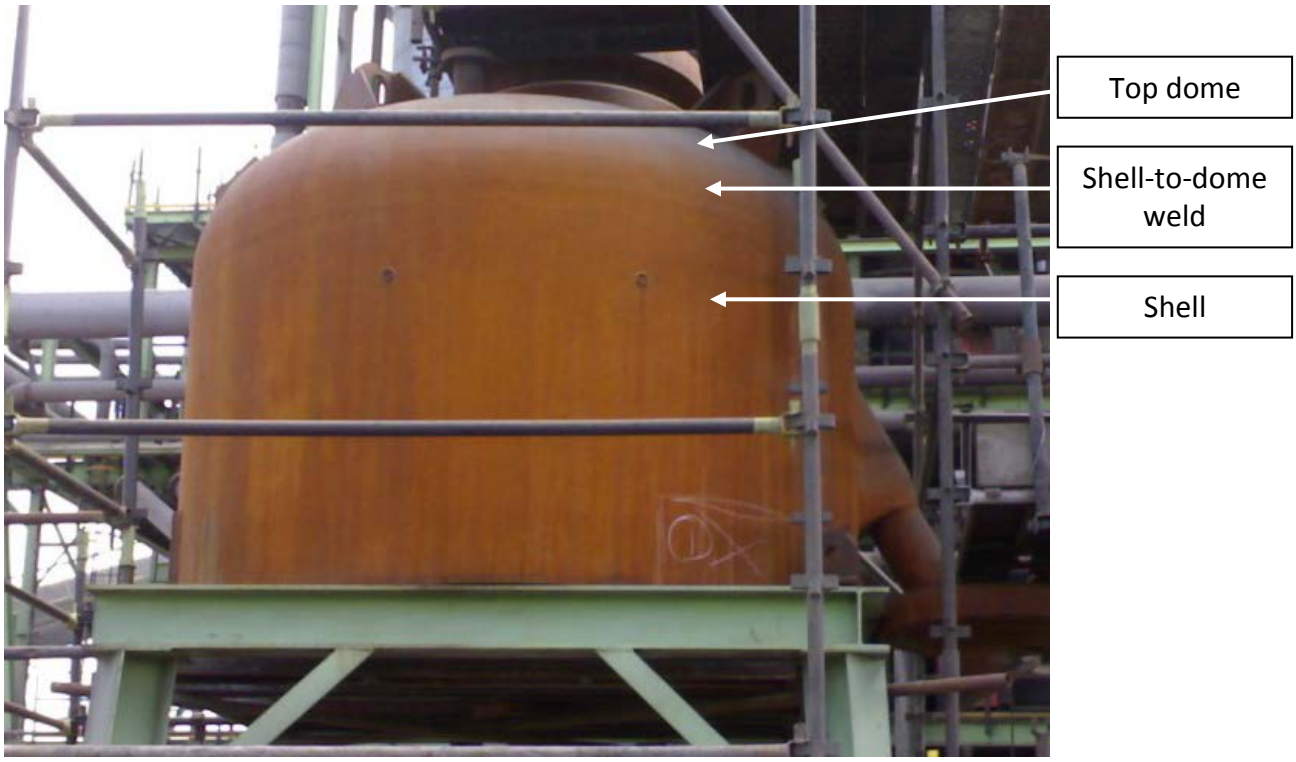

Figure 3.1: Photograph of the test ash lock resting on a support structure without its bottom cone before cutting of samples from the shell and top dome.

Figure 3.2: Representative photograph showing sample areas as marked out on the shell of the ash lock.

Figure 3.3: Representative photograph showing samples cut from the top dome.

3.2.2 Procedure for sample removal

The following procedure was used to remove samples from the ash lock to ensure that no damage was caused to the sample and the surrounding material. Samples were removed along the marked areas using a cutting torch, without damaging the sample area or the surrounding material (refer to figure 3.3). Once samples were cut a band saw was used to remove the area affected by the cutting torch by cutting 15 mm away from the edge of the samples. Large samples were cut into smaller sizes using a band saw, ensuring that the AIA stamp on each sample was not damaged and carried over as required. Final cutting and machining to the desired dimensions was performed.

Removal of samples was performed by the appointed fabricator. Final cutting and machining of samples to the desired dimensions was done by the Sasol Synfuels Metallurgical Engineering department.

3.3 Testing Procedure

Testing was performed in accordance with Test Methods and Definitions SA-370 [2013As2]. The following section outlines the minimum testing requirements. Tests were performed on material in the as-received condition and material subjected to further PWHT (see section 3.3).

3.3.1 ASTM A 302 Grade B - parent metal of shell and dome

3.3.1.1 Tension testing

The test temperature selected for tension testing was room temperature (18-22°C). The ASTM specification does not give a test temperature and recommends that this is decided by the purchaser. Room temperature was selected since this is the temperature that was specified on the material certificates for the test ash lock. Acceptance criteria for testing were as per the ASTM/ASME specification for this material [1980As1]. Although the specification only requires 2 tension tests per heat treatment the number of test specimens that were tested per heat treatment and location (internal -, external surface and middle of plate) varied on average between 10 and 30 test specimens. This high number of tension tests would ensure the accuracy of the test results. Tension test specimens (full size) were removed from both the internal and external surfaces and middle of the plate for each component (shell and dome). The longitudinal axis of the tension-test specimens was transverse to the final rolling direction of the plate. A reduction of area measurement was recorded while conducting the required tension test to obtain other real stresses as distinct from engineering stress.

3.3.1.2 Hardness testing

Brinell hardness tests on cross-sections of the samples was performed according to the Test Methods and Definitions in SA-370 [2013As2]. Hardness testing was performed by the Brinell method and procedures using the stationary laboratory Brinell hardness tester in accordance with ASTM Method E10 and E110 as applicable. The area to be tested was ground flat to a surface finish (Ra) of 2 µm max (80 grit). The instrument was calibrated at

the start and end of each batch of tests. In addition, Vickers hardness tests using the stationary laboratory Vickers hardness tester and Vickers hardness tests using the MicroDur MIC10 portable hardness tester were performed on a sectioned and polished surface. The relationship between Brinell and Vickers is given in SA-370.

3.3.1.3 Impact testing

The test temperature selected for Charpy V-notch impact testing was 0°C. The ASTM specification does not give a test temperature and recommends that this is decided by the purchaser. A test temperature of 0°C was selected as this is the temperature that was specified on the material certificates for the test ash lock. Impact testing was performed in accordance with SA-370 [2013As2] and SP-110-6 [2003Sas] using Charpy V-notch Type A full size specimens (10x10mm). Acceptance criteria for testing were as per SP-110-6. The recorded results included test-bar orientation, specimen size, test temperature, absorbed energy and lateral expansion opposite the notch. The percentage shear fracture appearance was also recorded. Each impact test consisted of one set of three impact specimens from the same material, of the same size and having the same transverse orientation (figure 3.4). Test specimens for rolled plate was cut transverse to the final rolling direction. Impact test coupons were removed adjacent to tension test coupons. The number of sets of impact specimens required was one set at the internal surface, external surface and middle of the plate (figure 3.5).

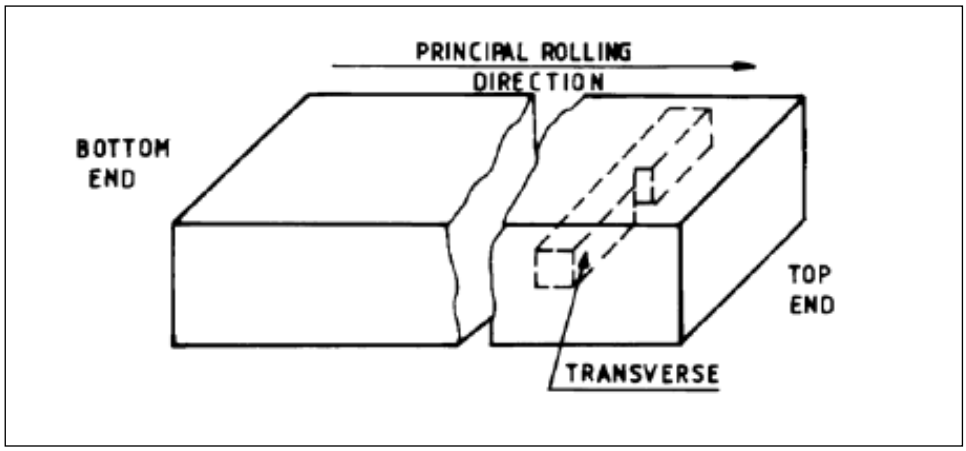

Figure 3.4: Illustration of impact test specimen [2013As2].

3.3.2 Weld seam - between the shell and top dome

3.3.2.1 Tension testing

The test temperature was room temperature for all heat treatments (18-22°C). Two tension tests were performed per heat treatment and location. Tension test specimens were removed from both the inside - and outside surfaces and in the middle of the plate. Tension tests were performed in the longitudinal (all-weld) and transverse directions. Due to limited weld samples available not all planned tests could be performed. Testing was performed in accordance with SA-370 using the largest feasible specimens. The gauge length for measuring elongation was four times the diameter of the test section.

3.3.2.2 Hardness testing

Brinell hardness tests on cross-sections of the samples was performed according to the Test Methods and Definitions in SA-370. Hardness testing was performed by the Brinell method and procedures using the stationary laboratory Brinell hardness tester in accordance with ASTM Method E10 and E110 as applicable. Brinell hardness tests was done on the weld metal, HAZ and parent material adjacent to the HAZ. The area to be tested was ground flat to a surface finish (Ra) of 2 µm max (80 grit). The instrument was calibrated at the start and end of each batch of tests. In addition, Vickers hardness tests using the stationary laboratory Vickers hardness tester and Vickers hardness tests using the MicroDur MIC10/20 portable hardness tester were performed on a sectioned and polished face along a line parallel to, and within 1 mm of, the inner and outer surfaces, and in the centre of the cross section in the HAZ, fusion zone and unaffected parent material. The relationship between Brinell and Vickers is given in SA-370.

3.3.2.3 Impact testing

The test temperature was 0°C. Impact testing was performed in accordance with SA-370 and SP-110-6 using Charpy V-notch (Type A) full size specimens (10 by 10 mm). The longitudinal axis and mid-length of the impact specimen was located similarly to the longitudinal axis of the tension test specimens. One set of three tests was performed at

each location in the as-received condition and after the various heat treatments. Impact test specimens were removed from the external surface, internal surface and middle of the plate. Due to limited weld samples available not all planned tests could be performed. One set of all-weld-metal test specimens and located as specified in figure 3.5 below shall be made on each weld.

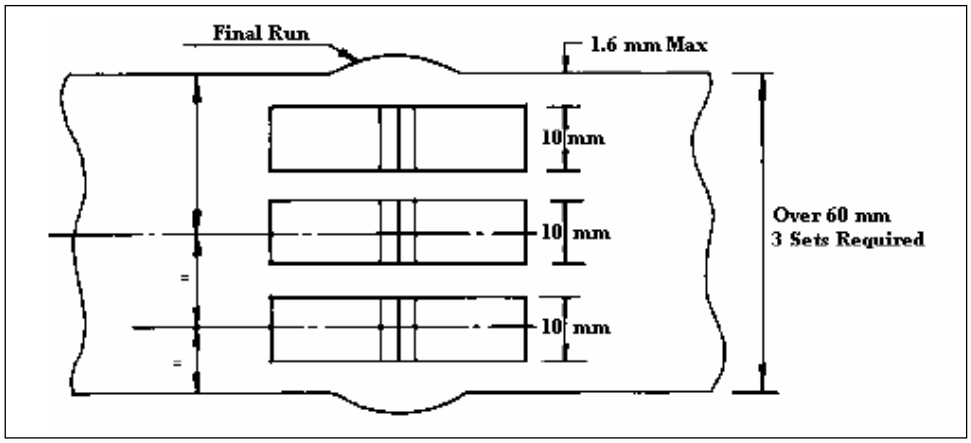

Figure 3.5: Illustration of impact test specimen sets [2013As2].

One set of HAZ test specimens per each heat treatment was tested within the locations as specified in figure 3.6.

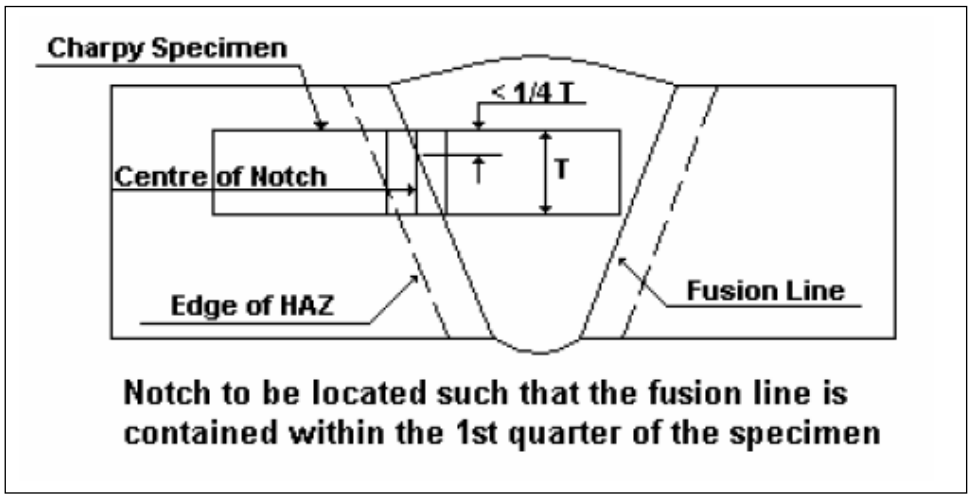

Figure 3.6: Location of impact test specimen within the HAZ [2013As2].

3.4 Heat treatment parameters

3.4.1 Simulated PWHT parameters

Additional heat treatments with holding times ranging from 2 hours up to 100 hours were performed in a muffle furnace on samples in the as-received condition to simulate additional PWHT. Thermocouples connected to a data logger were attached on samples to ensure heat distribution through the furnace was recorded. A single long simulated PWHT cycle represented a number of multiple shorter individual PWHT cycles. Heat treatment parameters for each long cycle were calculated [2013As3]. Unrestricted heating rate was applied from ambient temperature up to 350°C. Heating rate above 350°C in °C per hour for this material thickness was calculated as 80°C/hour. The holding temperature was chosen as 620°C (maximum PWHT temperature to be at least 20°C lower than the original tempering temperature shown on the material certificate [2007Sas]). Cooling rate above 350°C in °C per hour was calculated as 101°C/hour. Unrestricted cooling rate was applied from 350°C down to ambient temperature.

A single long simulated PWHT cycle of 100 hours, for example, represented approximately 36 individual PWHT cycles of 140 minutes each, based on a sample thickness of 70mm. The Hp of the single long PWHT cycle, Hp = 19.651, was equivalent to the total Hp of the multiple shorter PWHT cycles, therefore the combined effect of tempering (PWHT) exposure on the material can be considered to be the same. Figures 3.7 and 3.8 show graphical representations of the 100 hours long PWHT cycle compared to the ~36 individual PWHT cycles of 140 minutes each. Note the total time it would take do perform 36 individual cycles compared to one long cycle. This is due to the time that would be spent on heating and cooling between ambient and 350°C, which is not considered to contribute towards tempering [2007Sas].

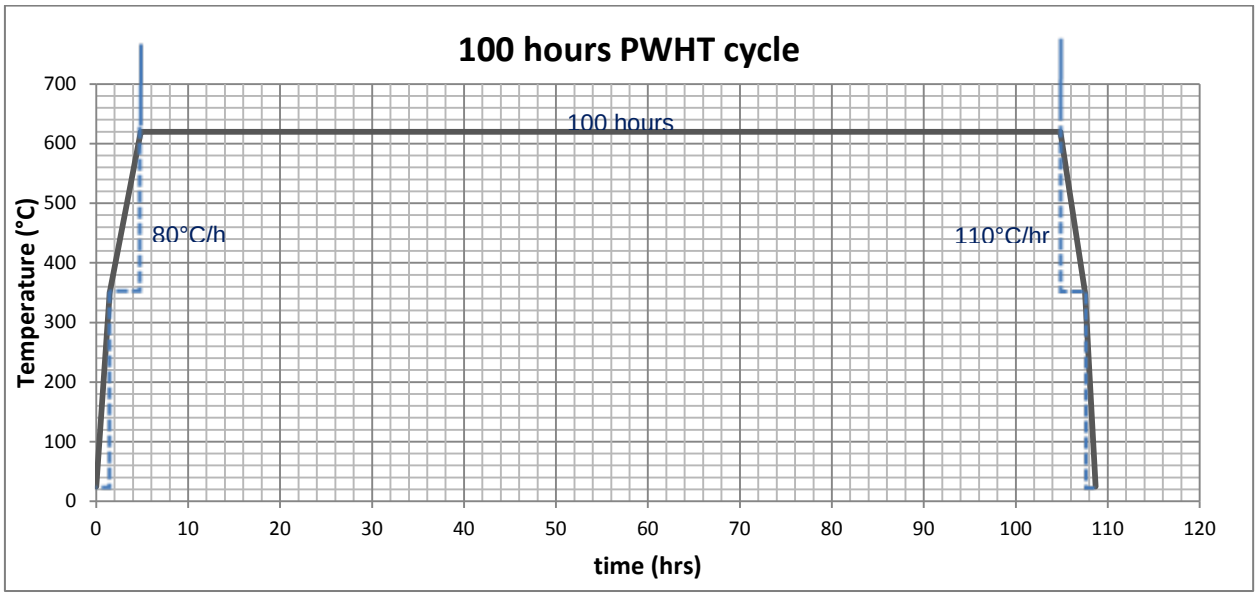

Figure 3.7: Graphical representation of the 100 hours simulated PWHT cycle.

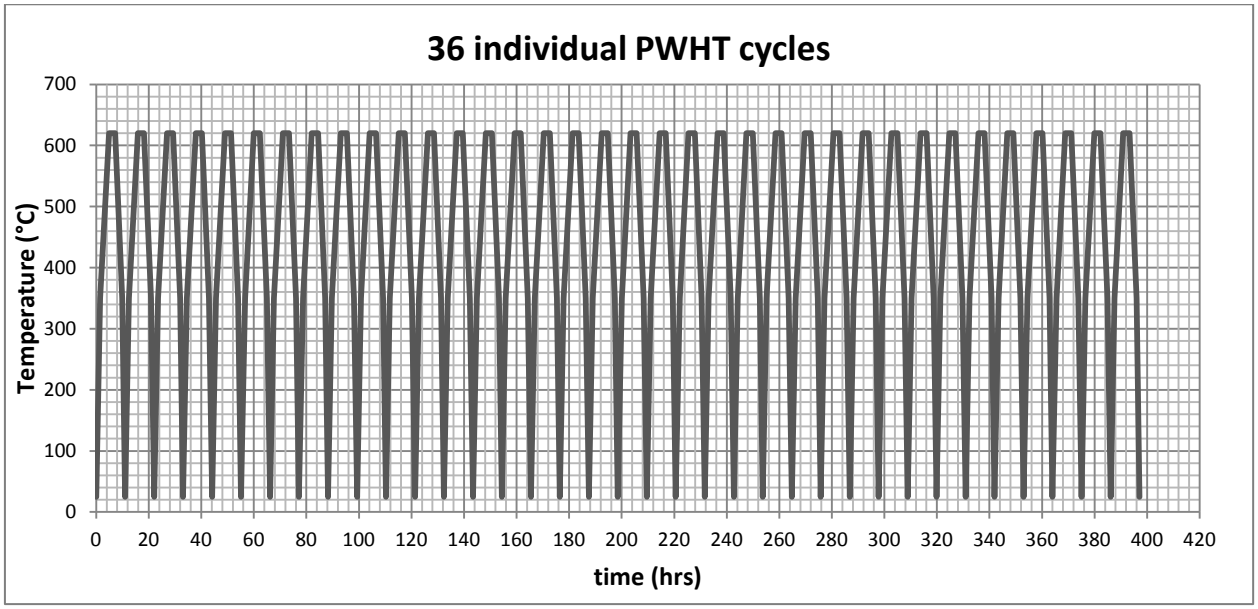

Figure 3.8: Graphical representation of the ~36 shorter individual PWHT cycles.

3.5 Metallographic examination

Metallographic examination on the various samples was performed as follows. Samples from each heat treatment condition and area was cut and mounted as a micro in bakelite for the purpose of microscropic evaluation. Bright field optical microscopy was performed on the parent metal, HAZ and weld metal of samples in the etched condition (etched with 5% Nital) to identify and study the microstructure of the samples at the different heat treatment conditions. The Everhart-Thornley detector (ETD) and backscattered electron detector (BSED) of the SEM together with the energy dispersive X-ray spectroscopy (EDX) analyser was used to examine and analyse phases in the microstructure.

3.6 Chemical analysis

Spectrographic chemical analysis was performed on a sample from the shell and dome using the quantitative mass spectrometer. Samples were first polished and cleaned with acetone to remove oxides and contaminants.

Mass spectrometry (MS) is an analytical chemistry technique used to identify the amount and type of chemicals present in a sample by measuring the mass-to-charge ratio and abundance of gas-phase ions. As part of the MS procedure a sample is ionized by bombarding it with electrons causing some of the sample's molecules to break into charged fragments. These ions are then separated according to their mass-to-charge ratio by accelerating them and subjecting them to an electric or magnetic field. Ions of the same mass-to-charge ratio will undergo the same amount of deflection [2000Spa]. The ions are detected by an electron multiplier, a mechanism capable of detecting charged particles. Results are displayed as spectra of the relative abundance of detected ions as a function of the mass-to-charge ratio. The atoms or molecules in the sample are identified by either correlating known masses to the identified masses or through a characteristic fragmentation pattern.

3.7 Conclusion

Mechanical testing on samples of the shell and dome and shell-to-dome weld, in the as-received condition and after repeated PWHT, was performed as planned in accordance with Test Methods and Definitions SA-370 [2013As2]. Metallographic examination on the various samples was also performed as intended. Nozzle materials (forgings) will be tested in a different study. Test results will be presented in the next chapter (see Chapter 4 “Results”).

CHAPTER 4: RESULTS

4.1 Introduction

The initial chemical composition and mechanical properties of the shell and dome of test ash lock 210AL-3401, as obtained from the code data book, are shown in the first section of this chapter. Results of mechanical tests and metallographic examination on samples from the shell and dome and shell-to-dome circumferential weld of the test ash lock 210AL-3401, in the as-received condition as well as after being subjected to a series of simulated PWHT cycles, are also displayed. The remainder of the chapter consists of the current graphical prediction model used to predict tensile properties of the ash locks after PWHT as well as a new mathematical model based on the current test results.

4.2 Initial chemical composition and mechanical properties

The chemical composition and initial mechanical properties of the shell and dome of ash lock 210AL-3401, as obtained from material certificates in the code data book, are presented in tables 4.1 to 4.4.

Table 4.1: Chemical composition of shell and dome of test ash lock 210AL-3401

	Chemical composition [weight %]		
Element	**Specification for A 302 Grade B [1980As1]***	**Shell**	**Dome**
Carbon (C)	0.25 max.	0.18	0.19
Manganese (Mn)	1.50 max.	1.40	1.44
Sulphur (S)	0.04 max.	0.004	0.004
Phosporous (P)	0.035 max.	0.014	0.013
Silicon (Si)	0.30 max.	0.25	0.24
Chromium (Cr)	-	0.03	0.02
Molybdenum (Mo)	0.60 max.	0.55	0.54
Nickel (Ni)	-	-	-
Copper (Cu)	-	-	-
Vanadium (V)	-	0.001	0.001

Niobium (Nb)	-	0.001	0.002
Iron (Fe)	Remainder	Remainder	Remainder

*Specified chemical composition in the latest design code [2013As1] is similar to that of the original design code [1980As1].

Table 4.1 shows that the chemical composition of the shell and dome conformed to chemical composition requirements for A 302 Grade B low alloy steel.

Table 4.2 shows the mechanical tensile properties of test specimens removed from the original batch during manufacturing, after the test specimens were subjected to a simulated qualified PWHT cycle of 198 minutes at 605°C (excluding the heating and cooling times above 350°C) as obtained from the code data book. This qualified cycle was similar for both the shell and dome. Initial properties of the batch before simulated PWHT (as-fabricated) were not provided in the code data book.

Table 4.2: Initial qualified mechanical tensile properties of shell and dome of test ash lock 210AL-3401

	Specification for A 302 Grade B [1980As1]*	**Shell**	**Dome**
Yield Strength [MPa]	345 min.	383	418
Ultimate Tensile Strength [MPa]	550 - 690	557	585

*Specified mechanical properties in the latest design code [2013As1] are similar to that of the original design code [1980As1].

The Charpy V-notch impact properties for the shell and dome after the simulated PWHT cycle are shown in table 4.3. The impact properties conformed to the minimum requirements for this material [2003Sas].

Table 4.3: Initial Charpy V-notch impact properties of shell and dome of test ash lock 210AL-3401 (tested at 0°C).

	Minimum required [2003Sas]*	**Shell**	**Dome**
Energy absorbed [J]	35 min. / 24 ave.	123, 130, 123 (Ave. 126)	143, 152, 144 (Ave. 146)

*Minimum requirements not given in ASTM/ASME A/SA-302.

Initial hardness values of shell and dome of test ash lock 210AL-3401 were not given in the code data book. Initial weld metal properties were also not contained in the code data book.

4.3 Chemical analysis

In the current study, spectrographic chemical analysis was performed via mass spectrometry (MS) on shell and dome samples obtained from test ash lock 210AL-3401 in the as-received condition (see table 4.4). The chemical analyses of the materials were comparable to the chemical requirements for A 302 Grade B material. The analyses compared well with the initial compositions shown in the code data books.

Table 4.4: Spectrographic chemical analysis of shell and dome of test ash lock 210AL-3401

	Chemical composition [weight %]		
Element	**Specification for A 302 Grade B [2013As1]**	**Shell**	**Dome**
Carbon (C)	0.25 max.	0.18	0.19
Manganese (Mn)	1.50 max.	1.48	1.52
Sulphur (S)	0.04 max.	0.013	0.014
Phosporous (P)	0.035 max.	0.048*	0.042*
Silicon (Si)	0.30 max.	0.24	0.24
Chromium (Cr)	-	0.033	0.029
Molybdenum (Mo)	0.60 max.	0.53	0.53
Nickel (Ni)	-	0.007	0.008
Aluminimum (Al)		0.017	0.016
Copper (Cu)	-	0.013	0.013
Vanadium (V)	-	<0.002	<0.002

Niobium (Nb)	-	<0.003	<0.003
Iron (Fe)	Remainder	Remainder	Remainder

*The slightly higher than specified phosphorous content is not seen as a concern. At most this would have resulted in a slightly higher UTS, YS and hardness, improved machinability and a slight decrease in toughness and ductility [2007Key]. No significant effect was noted on the actual properties shown in tables 4.2 and 4.3. Note that specified chemical composition in the latest design code [2013As1] is similar to that of the original design code [1980As1].

4.4 Mechanical testing

For the current study, samples were cut from the shell and dome and shell-to-dome circumferential weld (see Chapter 1 figure 1.1) from both the internal surface, external surface and middle of the plate thickness (see Chapter 3 for methodology and sample dimensions). These samples were subjected to a series of additional simulated PWHT cycles with holding times ranging from 2 hours to 100 hours. After PWHT the samples were subjected to tension testing, hardness testing and Charpy V-notch impact testing.

This section shows the results of these tests after each PWHT cycle and the corresponding effective Hollomon-Jaffe parameter (Hp_{eff}) and effective PWHT time (t_{eff}). The term "effective time" refers to the amount of time the material was subjected to PWHT after the qualified cycle has been deducted. To qualify the materials for PWHT, the manufacturer subjects test specimens of the various components to a simulated PWHT long cycle followed by mechanical testing. This simulated qualified PWHT long cycle is then recorded on the material certificate (for both the shell and dome the simulated PWHT cycle was 198 minutes at 605°C). Simulated PWHT is done to certify that the material will be able to withstand a number of individual PWHT cycles during fabrication and repairs equivalent to this qualified long cycle with the resultant mechanical properties generally being equal to or higher than that reflected on the certificate. The Hp is used to determine whether a material still has a part of this qualified cycle left before repairs are carried out. The Hp represents the total exposure to PWHT, while the Hp_{eff} represents the total exposure to PWHT after this qualified cycle has been deducted. Since the code data books did not contain the material certificates for the shell and dome in the as-fabricated condition, the Hp_{eff}, as opposed to the Hp, will be used in this study.

4.4.1 Tension tests

Tables A.1 to A.3 in Appendix A show the tensile properties for the shell and dome in the as-received condition and after simulated PWHT. The term “as-received” refers to a moment in time (i.e. 2001) when the ash lock was scrapped due to too low predicted mechanical properties. At that time the shell had already been exposed to a total PWHT time of 11.93 hours and the dome to 7.35 hours, respectively as shown in the tables, at a holding temperature of 620°C. When deducting the qualified cycle of 198 minutes at 605°C (or equivalently, 3.62 hours at 620°C [2007Sas]) it can be seen that the shell, for example, had in fact only been exposed to an effective PWHT time of 8.31 hours at 620°C.

The results showed that actual measured tensile properties for the shell and dome samples, in the as-received condition as well as after additional simulated PWHT cycles, were generally much higher than what was predicted (calculated) using the graphical prediction model derived from test results by Hattingh [1987Hat, 2009Met2]. Tension test results of specimens cut from the external surface, internal surface and middle of the plate thickness, are indicated in the tables. Tensile properties were comparable through the thickness of the plate, with values in the middle of the plate generally slightly lower (between 0 to 5%) than at the surfaces due to longer heat retention at mid-thickness of the plate and thus slower cooling after heat treatment. Note that tensile properties could not be predicted for the weld due to absence of a model for welded samples (see Appendix A table A.3).

Tension test results for the shell and dome materials and the shell-to-dome weld were plotted against the Hp_{eff} (refer to figures 4.1 to 4.3). Curves for the measured UTS and YS of samples taken from the external and internal surfaces, and the middle of the plate, with increasing Hp_{eff} are shown. The predicted UTS and YS (see red and blue lines) are also indicated [1987Hat].

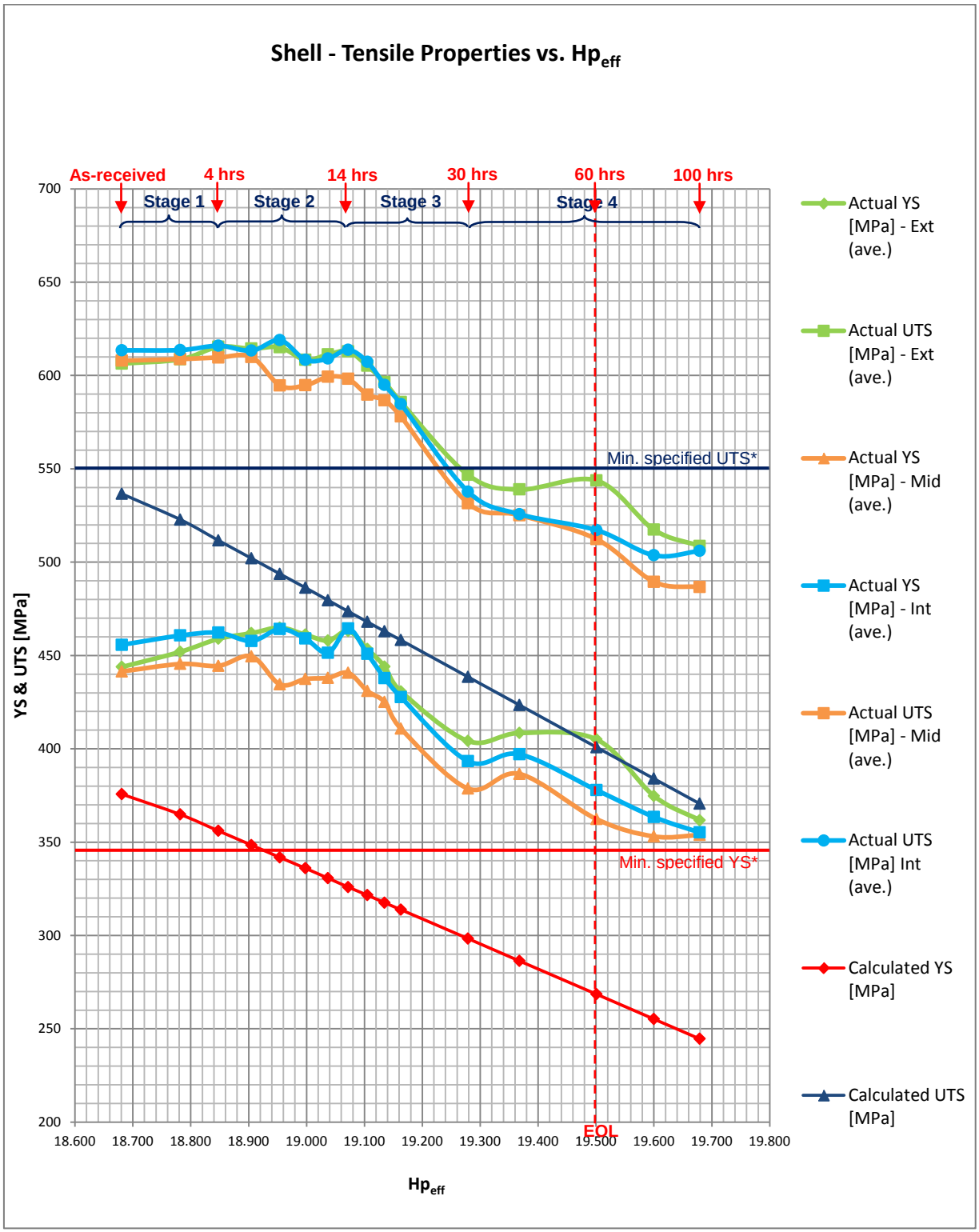

Figure 4.1: Tensile properties vs. Hp_{eff} on shell samples in as-received condition and after additional PWHT. Calculated UTS and YS are also indicated [1987Hat]. *Minimum specified properties for ASME SA-302 Grade B [2013As1].

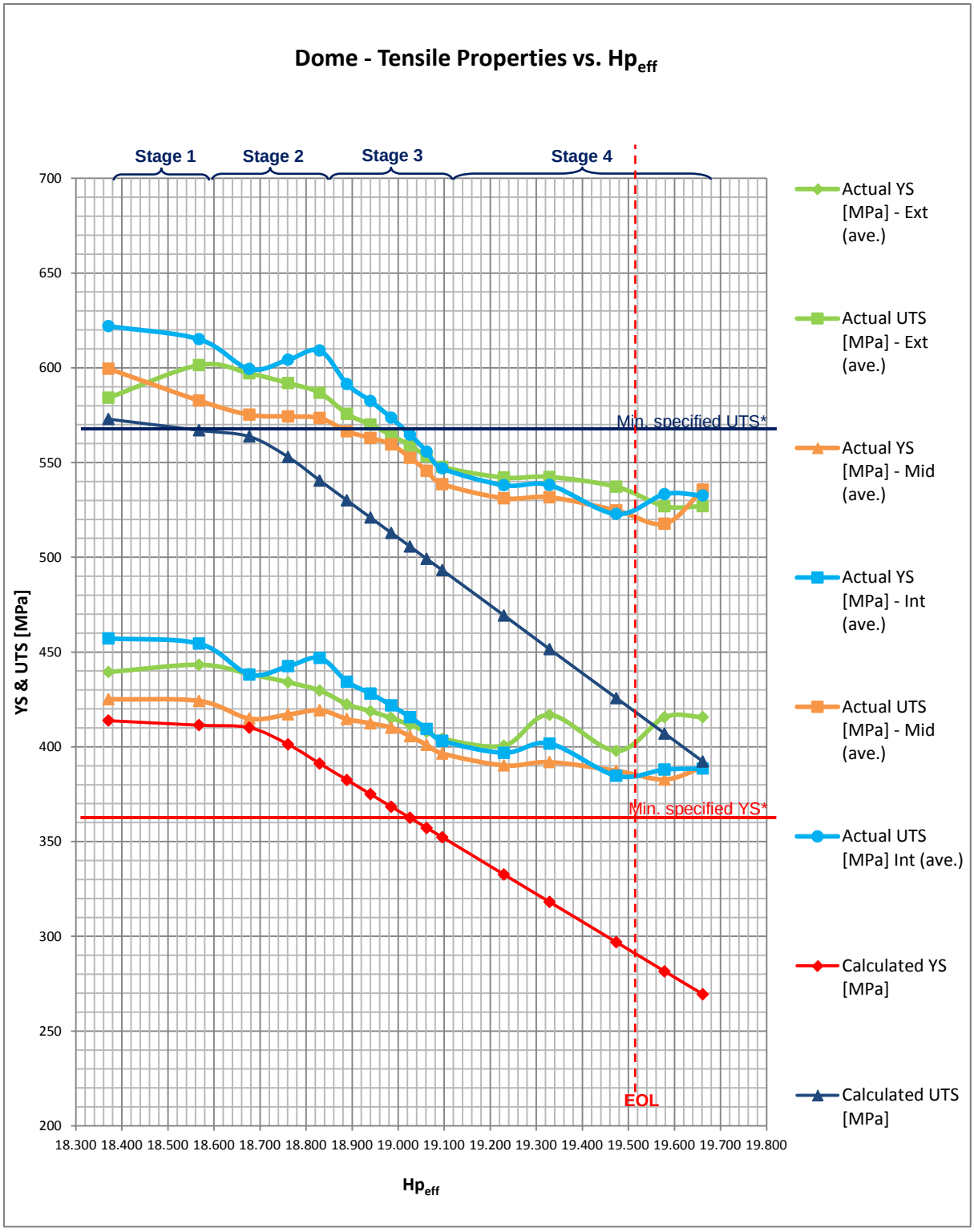

Figure 4.2: Tensile properties vs. Hp_{eff} on dome samples in as-received condition and after additional PWHT. Calculated UTS and YS are also indicated [1987Hat]. *Minimum specified properties for ASME SA-302 Grade B [2013As1].

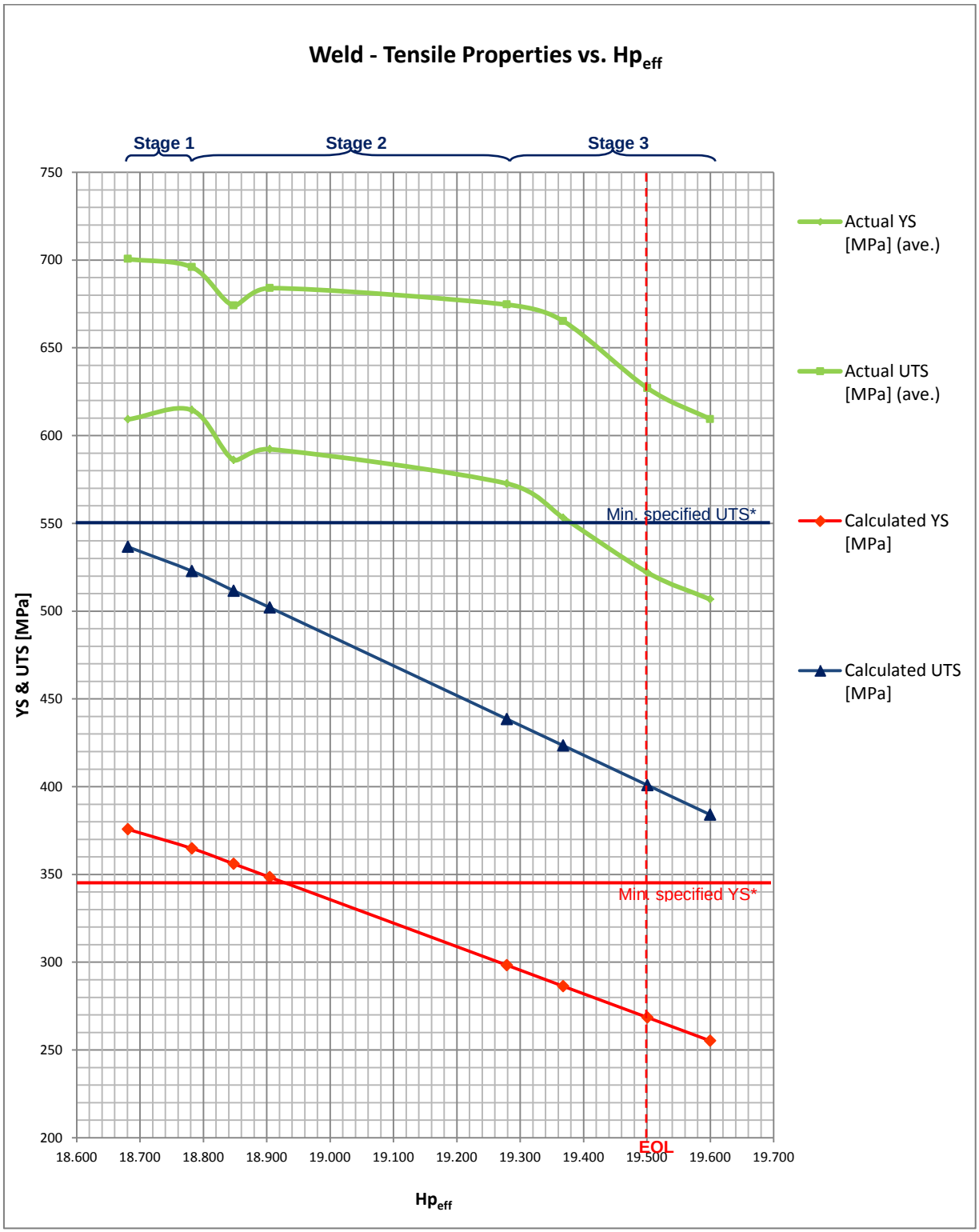

Figure 4.3: Tensile properties vs. Hp_{eff} on shell-to-dome weld samples in as-received condition and after additional PWHT. Calculated UTS and YS are also indicated [1987Hat]. *Minimum specified properties for ASME SA-302 Grade B [2013As1].

The graphs show 4 distinct stages in mechanical tensile property evolution with increasing simulated PWHT:

- **Stage 1: Slight* increase in tensile properties for the shell, dome and weld with increasing simulated PWHT.**

  This stage already started at initial fabrication (1980) when the first PWHT was performed. Tests have confirmed that when the ash lock was scrapped in 2001, due to apparent end of life (as-received condition), tensile properties for the shell and dome had already evolved some distance into stage 1, higher than minimum ASME required values [2013As1], higher than the predicted values [1987Hat] and still generally increasing with increasing Hp_{eff}.

  *The slopes for the shell, dome and weld sample curves in this stage were calculated using the formula m = Δy / Δx and are as follows:

	Shell	Dome	Weld
YS:	+49	+0	+52
UTS:	+26	-11	-46

- **Stage 2: Slight* decrease in tensile properties for the shell, dome and weld with increasing simulated PWHT.**

  During this stage there is a gradual general decrease in UTS and YS with increasing Hp_{eff}.

  *The slopes for the shell, dome and weld sample curves in this stage were calculated using the formula m = Δy / Δx and are as follows:

	Shell	Dome	Weld
YS:	+4	-33	-84
UTS:	-24	-38	-43

- **Stage 3: Rapid* decrease in tensile properties for the shell, dome and weld with increasing simulated PWHT.**

  At an Hp_{eff} of 19.072 for the shell, 18.830 for the dome and 19.279 for the shell-to-dome weld a rapid decrease in tensile properties occurred.

  *The slopes for the shell, dome and weld sample curves in this stage were calculated using the formula m = Δy / Δx and are as follows:

	Shell	Dome	Weld
YS:	-309	-115	-206
UTS:	-336	-171	-203

- **Stage 4: Stabilisation* of tensile properties for the shell and dome (decrease at a reduced rate) with increasing simulated PWHT.**

  During this stage the rate of decrease in YS and UTS is much lower than in stage 3. This stage was absent for the shell-to-dome weld tension tests.

  *The slopes for the shell, dome and weld sample curves in this stage were calculated using the formula $m = \Delta y / \Delta x$ and are as follows:

	Shell	Dome	Weld
YS:	-88	-6	n/a
UTS:	-96	-22	n/a

The graphs show that tensile properties for the shell and dome only dropped below the minimum ASME required values after 30 hours (Hp_{eff} = 19.279) of additional simulated PWHT for the shell and 20 hours (Hp_{eff} = 19.096) for the dome, respectively (at the end of stage 3).

At an Hp_{eff} of ~19.5 (i.e. 19.501 for the shell and 19.474 for the dome) tensile properties were below the minimum ASME requirements [2013As1], but may still be high enough to pass a fitness-for-service (FFS) evaluation [2007Ap2]. Mechanical design engineers at Sasol Group Technology department have confirmed (verbally) that, from their experience, should the tensile properties of the shell, dome and cone decrease to values 15% below the minimum specified ASME requirement due to repeated PWHT, the ash lock should still pass a FFS evaluation. The vertical lines in the graphs with the abbreviation “EOL”, indicating potential “end of life”, are discussed later in this chapter (see “Charpy impact tests” section).

4.4.2 Hardness tests

Tables A.4 to A.6 in Appendix A show that hardness values for the shell and dome generally decreased with increasing Hp_{eff}. Hardness was inconsistent through the thickness of the shell and dome material. Brinell hardness measurements compared well with Vickers hardness measurements for the shell as per SA-370 Table 3 [2013As2], but for the dome Brinell hardness was overall lower than the Vickers hardness values. Hardness obtained with the portable hardness tester were scattered in some instances for both the shell and dome. MicroDur MIC20 portable Vickers hardness measurements were taken on a cross-section of the shell-to-dome weld (no Brinell or Vickers hardness tests were performed on the welds).

Hardness values for the shell, dome and shell-to-dome weld were plotted against Hp_{eff} (refer to figures 4.4 to 4.6). The stages from figures 4.1 to 4.3, as obtained via tension testing, are also indicated on these graphs for comparison purposes. The graphs show that hardness did not exactly follow the same trends per stage as with the tensile properties. There was, however, an overall general downward trend with increasing Hp_{eff} and, especially for the shell, a sharp decrease in hardness during stage 3 with stabilisation of hardness values occurring in stage 4. These trends were not very prominent in the graphs for the dome and weld.

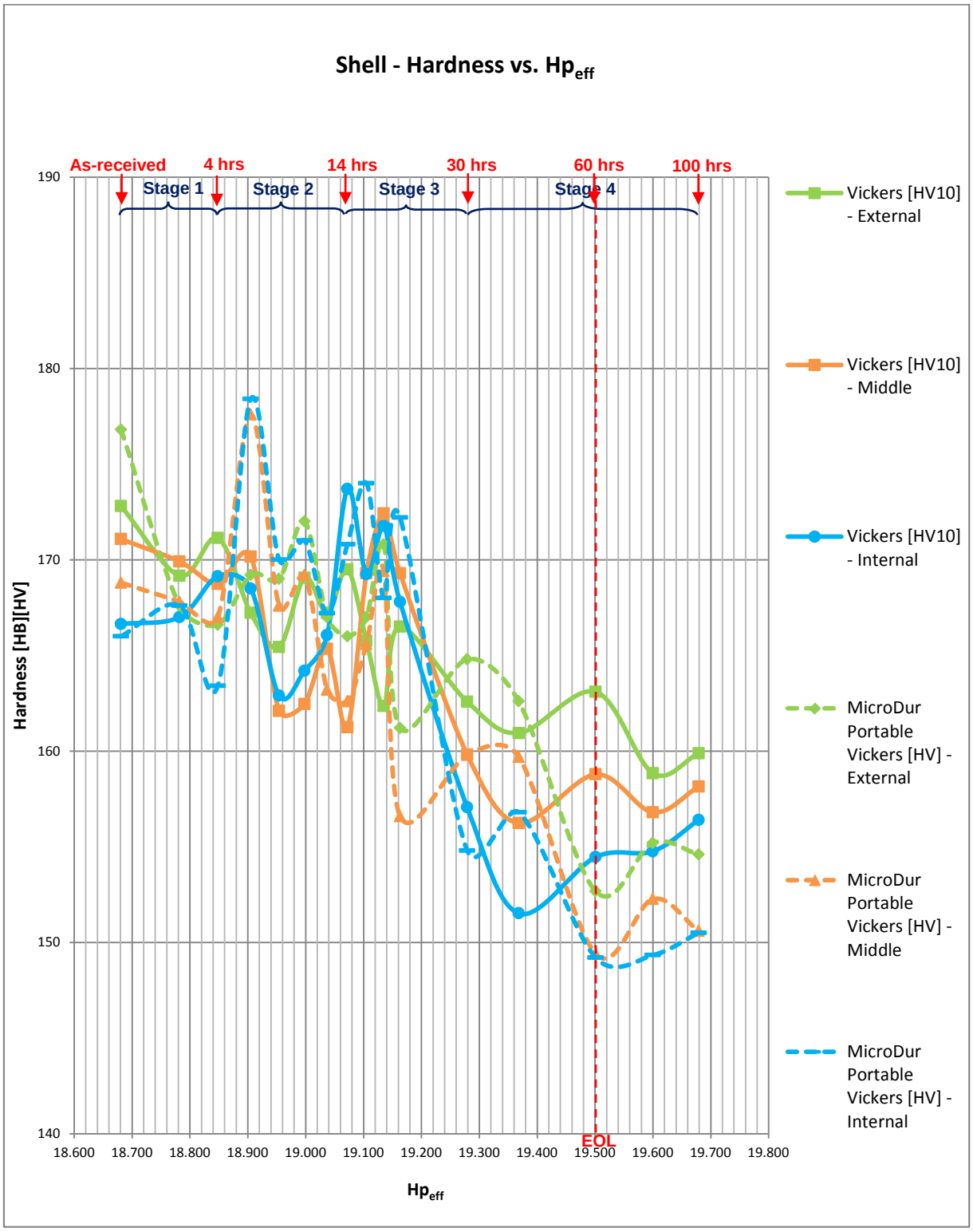

Figure 4.4: Hardness vs. Hp$_{eff}$ on shell samples in as-received condition and after additional PWHT.

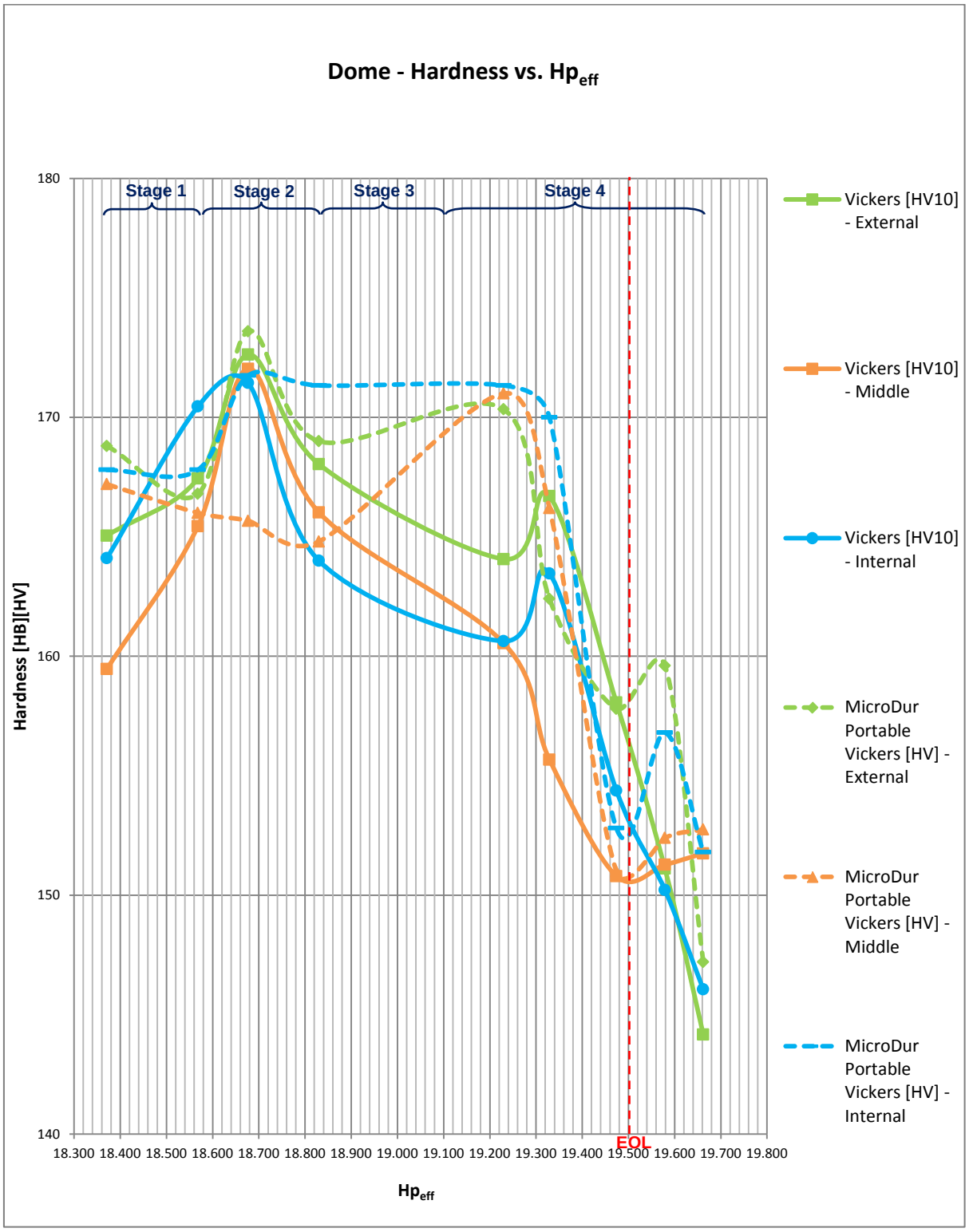

Figure 4.5: Hardness vs. Hp_{eff} on dome samples in as-received condition and after additional PWHT.

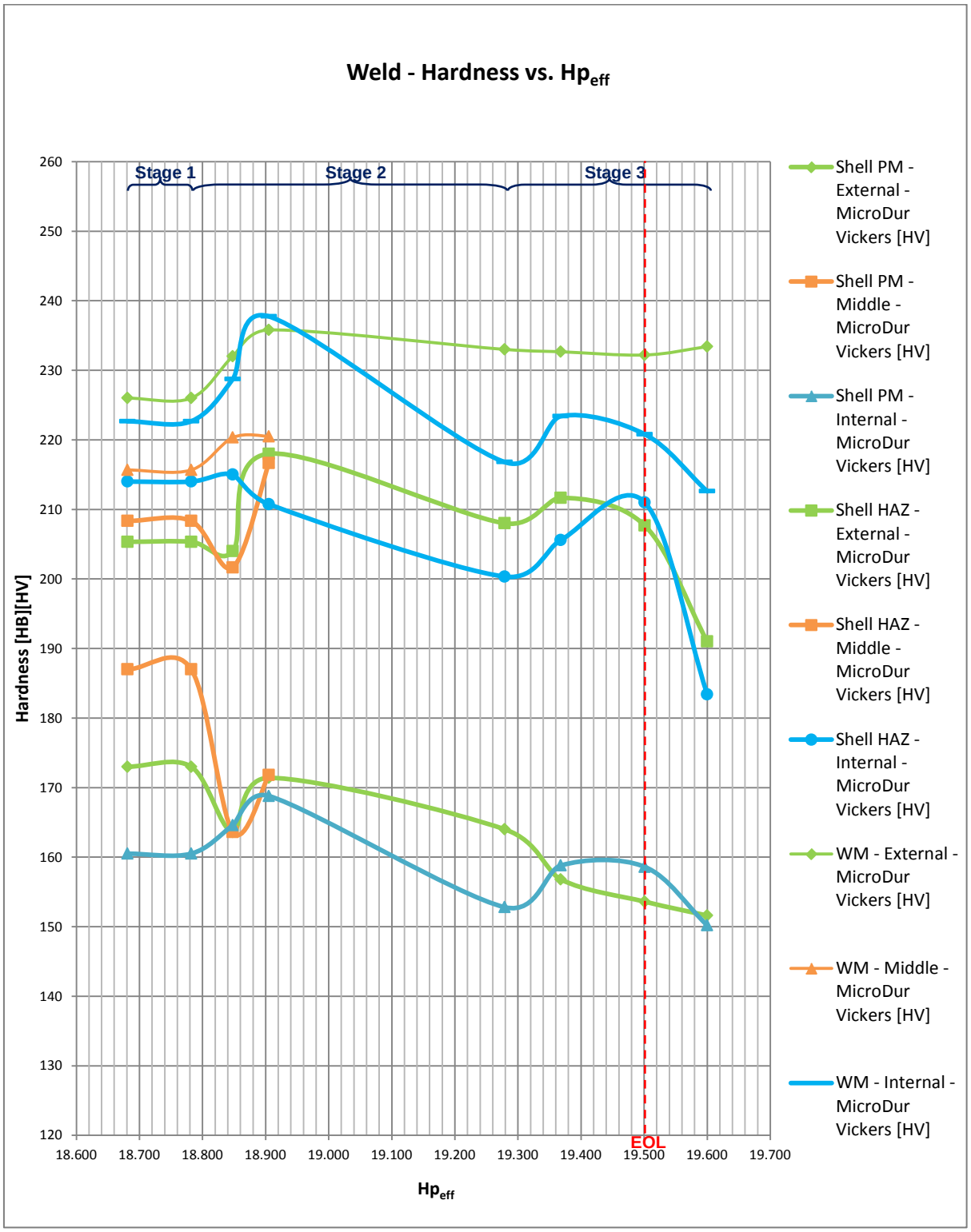

Figure 4.6: Hardness vs. Hp_{eff} on shell-to-dome weld samples in as-received condition and after additional PWHT.

4.4.3 Charpy impact tests

Impact toughness for the shell, dome and shell-to-dome weld samples are shown in tables A.7 to A.9 of Appendix A. Impact testing was performed at 0°C as per material certificates. Impact toughness for the shell and dome was above the minimum required values of 35 Joules average and 24 Joules minimum [2003Sas] during the largest part of the Hp_{eff} range. After 60 hours of additional PWHT (Hp_{eff} ~ 19.5) impact toughness for both the shell and dome and shell-to-dome weld was still within requirements [2003Sas]. Impact toughness for the shell and dome after 100 hours of additional PWHT (Hp_{eff} ~ 19.67) was below the minimum required values [2003Sas], while impact toughness for the shell-to-dome weld (Appendix A table A.9) showed an overall increase with increasing Hp_{eff}. Impact toughness was also generally comparable through the thickness of the plate.

Figures 4.7 to 4.9 show a trend of impact toughness (energy absorbed) vs. Hp_{eff}. The stages from figures 4.1 to 4.3, as obtained via tension testing, are also indicated on these graphs for comparison purposes. Values during stages 1 and 2 were very scattered for the shell and dome, but showed an overall downward trend in impact toughness with increasing Hp_{eff}. During the final stage (stage 4) at a certain point between 60 and 100 hours of additional PWHT impact toughness on both the shell and dome samples decreased to values below the specified minimum of 35 Joules average [2003Sas]. From the graphs it can be seen that at an Hp_{eff} of ~19.5 (60 hours additional PWHT) impact toughness for the shell and dome are still above the minimum specified. This Hp_{eff} value can, thus, be considered a safe cut-off point as tests have shown that mechanical properties and microstructure up to this point are acceptable provided that tensile properties pass a FFS evaluation (figures 4.1 to 4.9). This point is indicated as a dashed vertical line with the letters “EOL”, potentially indicating end of life of the ash lock. Note this point is also indicated on figures 4.1 to 4.9 for comparison purposes. This phenomenon was not observed on the weld samples for which, on the contrary, an increase in impact toughness was observed (see figure 4.9).

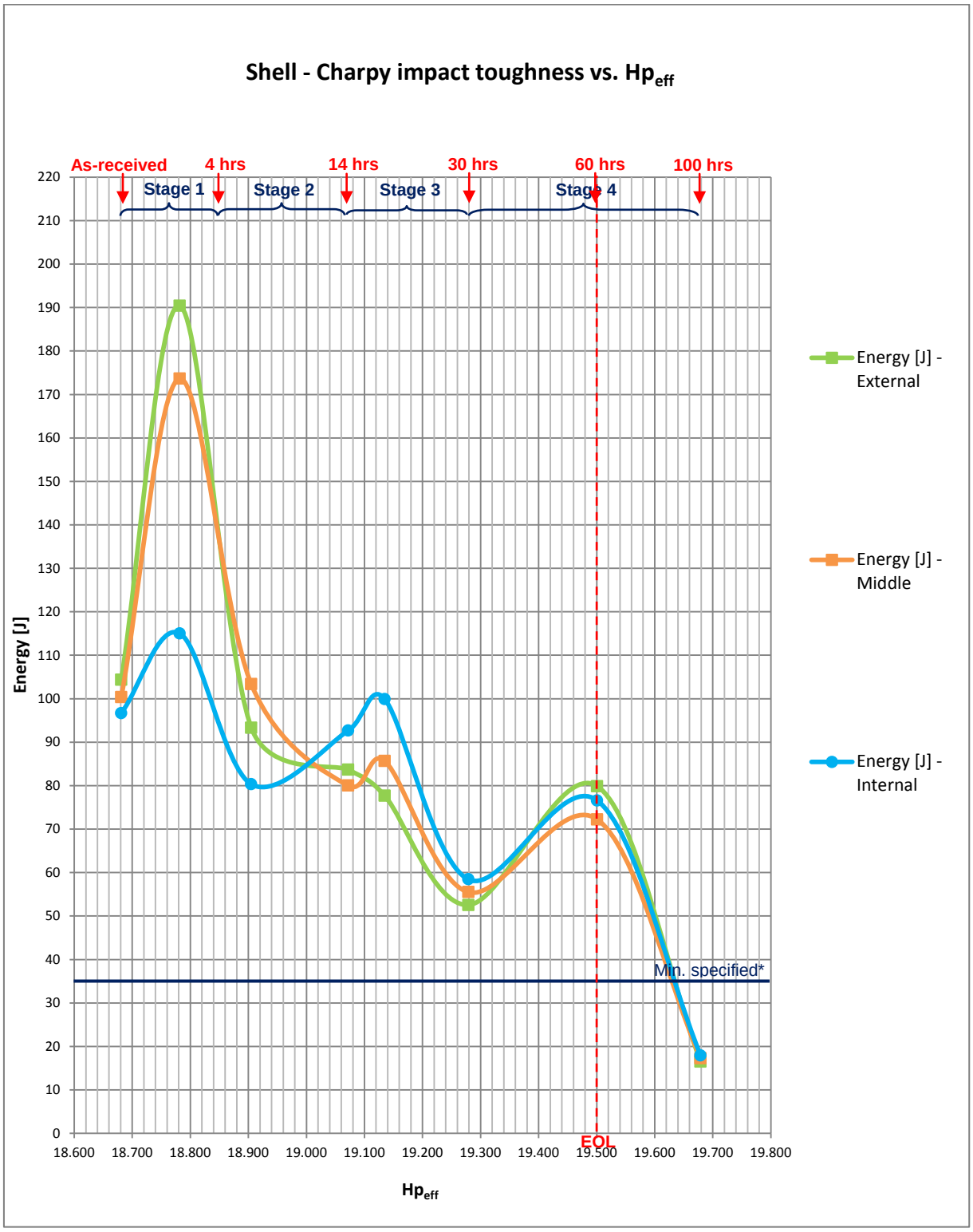

Figure 4.7: Charpy impact toughness vs. Hp_{eff} on shell samples in as-received condition and after additional PWHT. *Minimum specified impact toughness for this material [2003Sas].

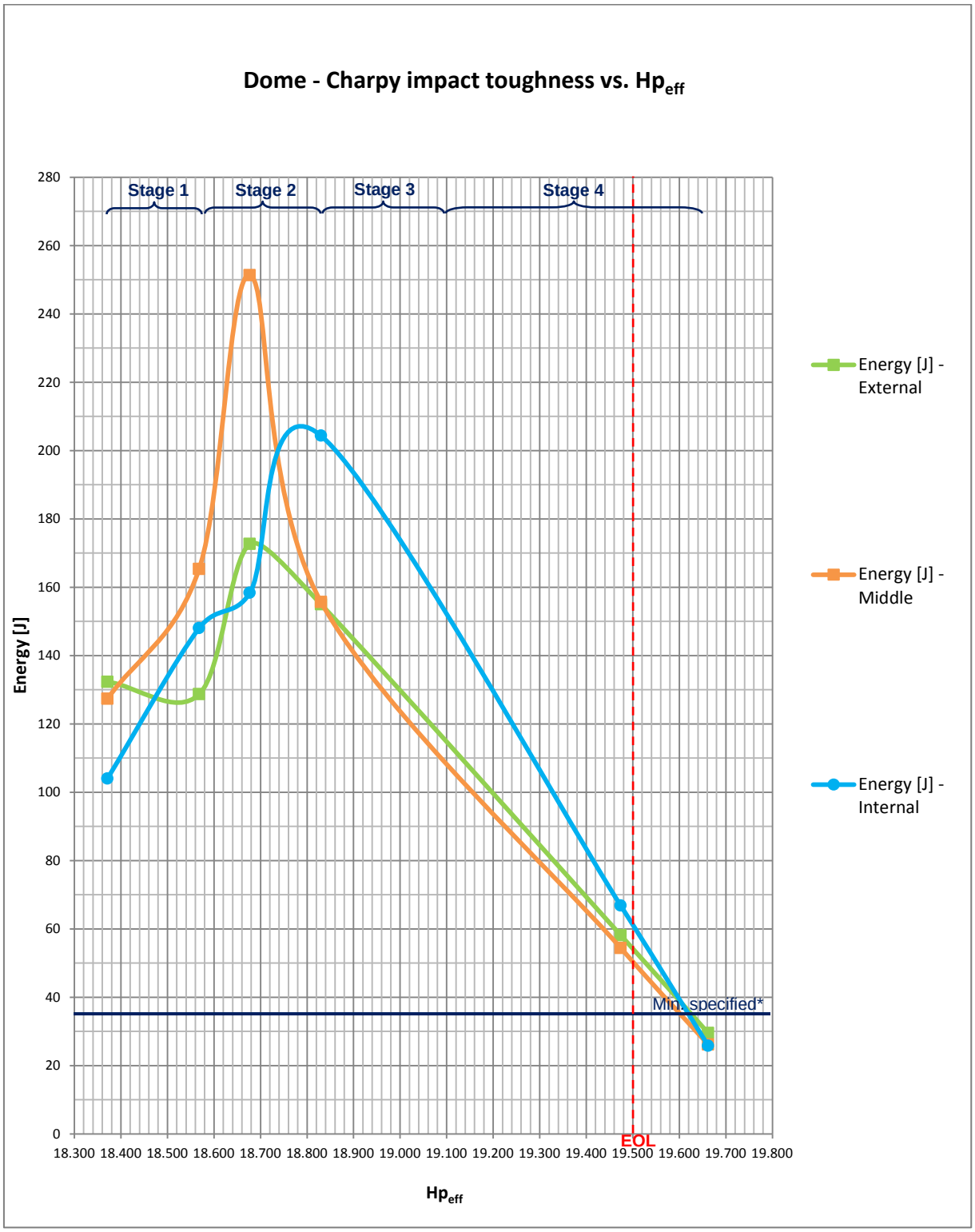

Figure 4.8: Charpy impact toughness vs. Hp_{eff} on dome samples in as-received condition and after additional PWHT. *Minimum specified impact toughness for this material [2003Sas].

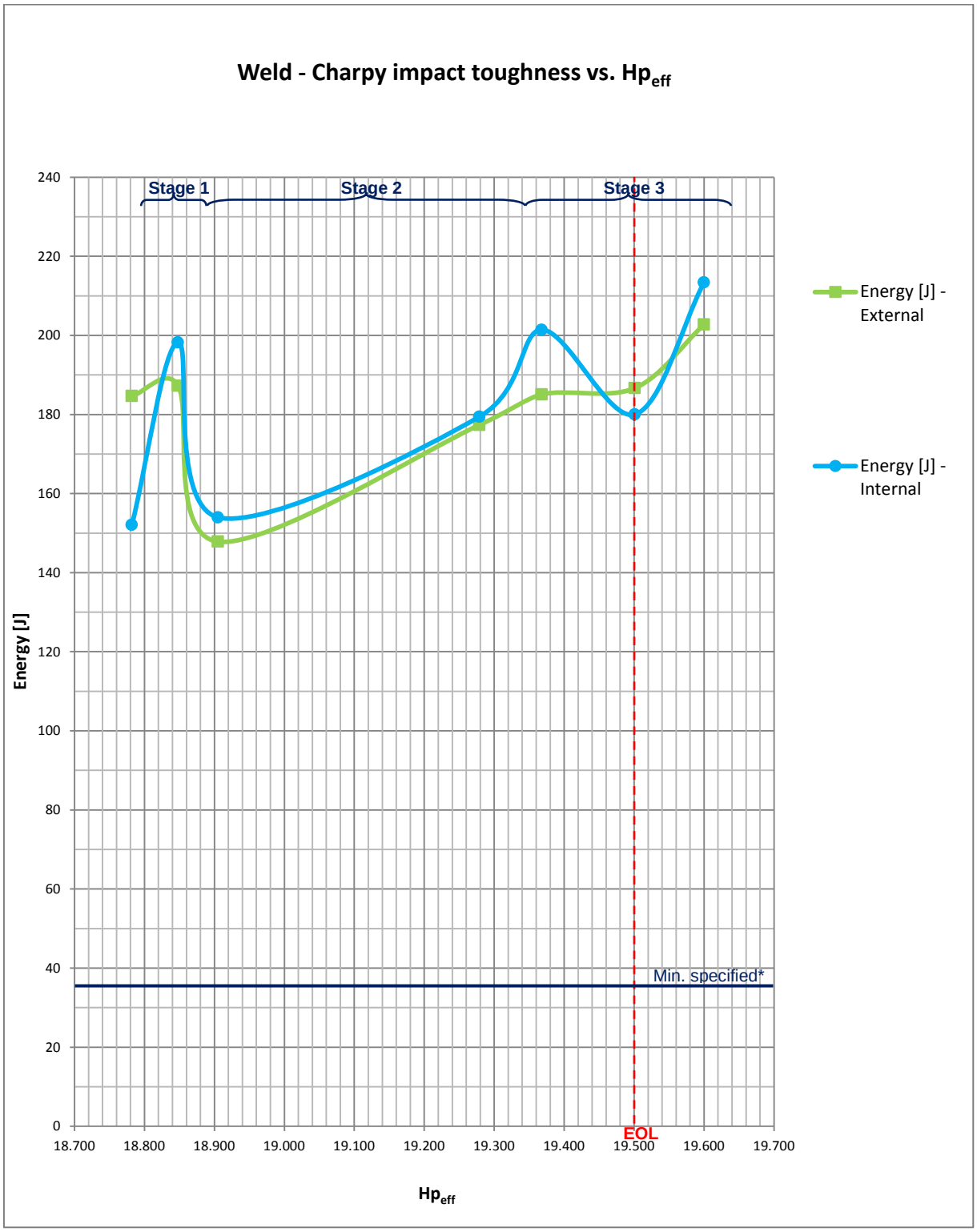

Figure 4.9: Charpy impact toughness vs. Hp_{eff} on shell-to-dome weld samples in as-received condition and after additional PWHT. *Minimum specified impact toughness for this material [2003Sas].

4.4.4 Ductile to brittle transition temperature (DBTT) curve

To determine whether impact toughness would be a governing factor after prolonged PWHT exposure of the ash locks above Hp_{eff} of ~19.5, it was decided to do additional impact tests on samples of the shell subjected to 100 hours of additional simulated PWHT (Hp_{eff} = 19.679), but at higher temperatures than the previous test temperature of 0°C. Test temperatures for these tests were 0°C, 10°C, 20°C, 30°C, 40°C, 50°C, 60°C, 70°C and 80°C. The test results were used to construct a DBTT (ductile to brittle transition temperature) curve (see figure 4.10). Energy absorbed during the test was plotted against test temperature.

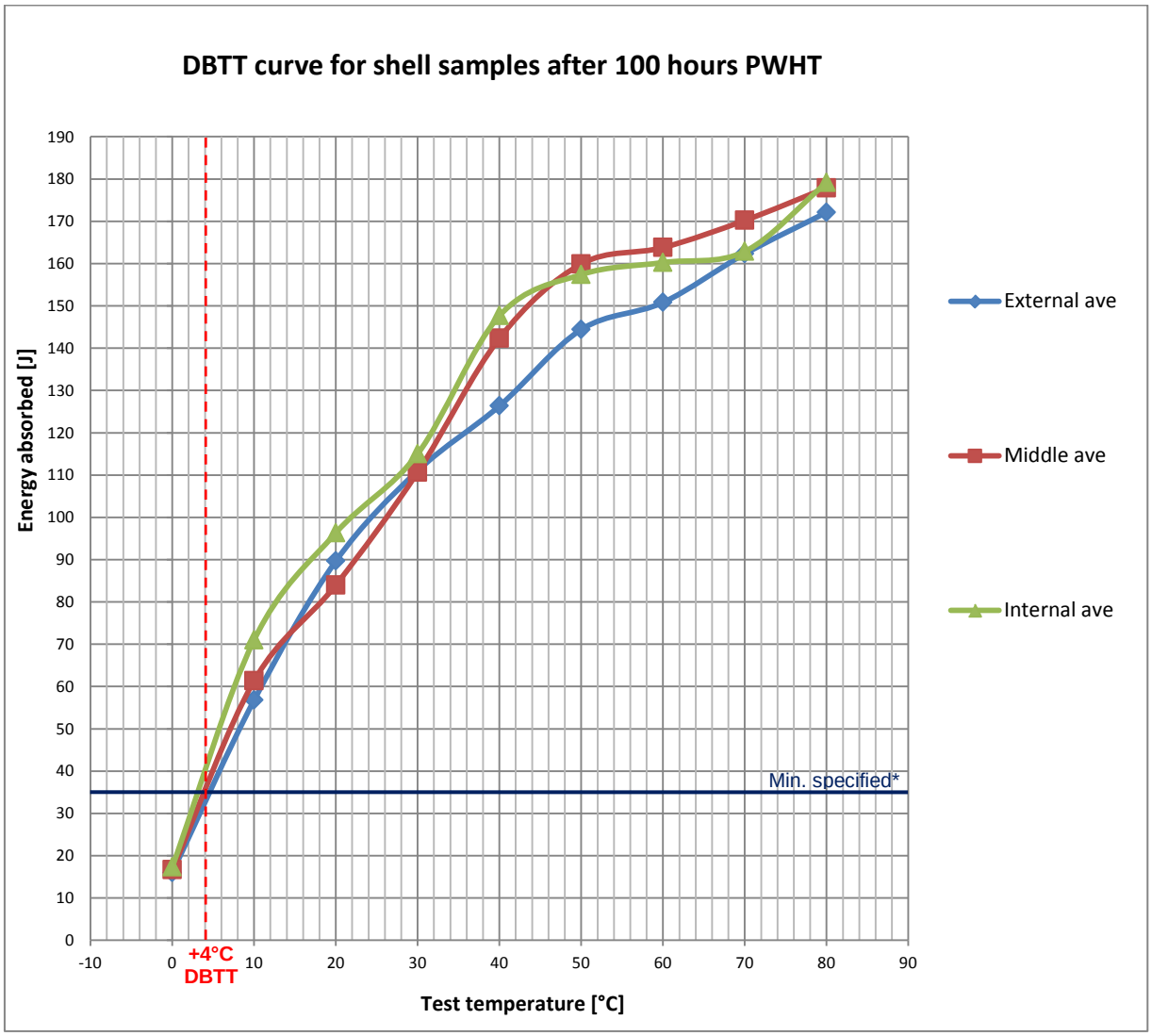

Figure 4.10: DBTT curve for shell samples after additional 100 hours PWHT. *Minimum specified impact toughness for this material [2003Sas].

The DBTT can be obtained from the graph by drawing a vertical line through the point where the curves intersect with the horizontal line that indicates the minimum specified energy absorbed [2003Sas] and then read off the temperature from the X-axis. Exposure to a temperature lower than the DBTT is generally expected to result in brittle fracture upon impact and is, thus, not advised. Operation at a temperature higher than the DBTT is preferred as material should behave more ductile upon impact and should provide improved resistance to fracture.

For the specimens removed from the external surface of the shell plate the DBTT can be read off as +5°C, while for the internal surface the DBTT is +3°C and for the specimens removed from the middle of the shell plate the DBTT is +4°C (average DBTT is +4°C). The upper shelf energy can be read from the graph as approximately 150 Joules at a upper transition temperature of 42°C and the lower shelf energy about 10 Joules at a lower transition temperature of 0°C [1988Die]. The percentage shear (ductile) fracture measured on the fracture surface of the impact test specimen tested at both 0°C and 10°C was 20%, implying that fracture between 0°C to 10°C would be predominantly brittle. The percentage shear fracture on the specimens tested at between 20°C and 40°C was measured as between 20 - 30%, implying that fracture would be mixed mode (both ductile and brittle, however slightly more brittle). At a test temperature of 50°C the percentage shear fracture was between 30 - 60%, i.e. mixed mode with an approximately 50/50 ratio between ductile and brittle fracture. The percentage shear fracture on the specimen tested at 80°C was 85% indicating predominantly ductile fracture behaviour above this temperature.

The test results on the shell samples can be considered representative of the dome and cone components as well, since the shell, dome and cone are made from the same type of material with similar initial heat treatment condition, microstructure, and comparable degree of degradation of properties with increasing PWHT.

The fracture surfaces of the shell impact test specimens heat treated at 100 hours additional PWHT and tested at 0°C showed the same level of shear fracture appearance than the specimens heat treated at 60 hours and tested at 0°C, i.e. 20% shear fracture. However, the lateral expansion at 100 hours was significantly lower at 0.26 mm average compared to 1.26 mm average at 60 hours, indicating a significant drop in ductility between 60 and 100 hours.

4.5 Metallographic examination

A metallographic examination using bright field optical microscopy was performed on the samples of the shell and dome removed from the external and internal surfaces and the middle of the plate after each heat treatment cycle (see figures 4.11 to 4.21). Figures 4.11 and 4.12 (as-received and 2 hours additional PWHT, respectively) show fine precipates (see arrows) on the grain boundaries, but also intragranular in the ferrite. These precipitates were confirmed via the SEM (see figures 4.22 to 4.24) and EDX to be rich in molybdenum, and therefore typically molybdenum carbides (Mo_2C) formed due to secondary hardening [1962Cla] during the first stage of PWHT exposure (refer to stage 1 in figures 4.1 and 4.2). Incipient (stage B [1961Tof]) spheroidisation of the cementite in the pearlite phase also started to emerge during stage 1 (see figure 4.11).

Figures 4.13 and 4.14 (4 hours and 8 hours additional PWHT, respectively) show that with further heat treatment these molybdenum carbides started to overage resulting in slow coarsening of the carbides (see arrows). This, together with more advanced (stage C [1961Tof]) spheroidisation of the cementite phase, consequently resulted in a decrease in tensile properties (stage 2) [1986Spa]. At this stage spheroidisation of the cementite phase became more advanced.

With more heat treatment (14 hours and 20 hours additional PWHT, respectively) other larger alloy carbides, possibly Mo_3C and M_6C carbides, precipitated on the grain boundaries (see figures 4.15 and 4.16). Significant coarsening of the Mo_2C carbides, formation of large Mo_3C and possibly M_6C carbides, transformation from cementite (Fe_3C) to Mo_2C in the pearlite phases, together with an increase in the level of spheroidisation (stage C/D [1961Tof]) of the cementite, resulted in a rapid decrease in tensile properties with increasing Hp_{eff} (stage 3) [1986Spa].

Eventually after prolonged heat treatments of 30 hours and 40 hours additional PWHT, respectively, stabilisation of tensile properties (stage 4) was reached, i.e. a decrease in tensile properties at a reduced rate. This was a result of reaching complete (stage D

[1961Tof]) spheroidisation and no further coarsening of molybdenum carbides occurred (figures 4.17 and 4.18).

After extended PWHT exposure beyond this point (60, 80 and 100 hours additional PWHT, respectively) a marked increase in the size of the Mo_3C carbides was noted (figures 4.19 to 4.21). The increase in size of these carbides was observed via the ETD and BSED of the SEM (see figures 4.22 to 4.24). The photos show complete spheroidisation and large carbides mainly on the grain boundaries, but also intragranular. The carbides are substantially larger after 100 hours of PWHT as compared to 60 hours. EDX analysis confirmed that these large carbides were rich in molybdenum and typically Mo_3C as per literature [1962Cla]. The sudden drop in impact toughness at Hp_{eff} 19.679 for the shell and Hp_{eff} 19.662 for the dome as seen in figures 4.7 and 4.8 can be directly ascribed to the large size of these carbides [1986Spa]. The threshold size of carbides that would result in the drop in impact toughness could not be confirmed from literature. However, the sizes of these carbides at 100 hours of additional PWHT ranged from 800 nm to 900 nm in diameteter (1 nm [nanometre] = 0.001µm [micrometre]) as compared to 400 nm to 500 nm at 60 hours. In the as-received condition the size of these carbides measured only 200 nm to 300 nm in diameteter.

For the shell-to-dome weld during stage 1 (see figures 4.25 and 4.26) fine molybdenum carbide precipitates were noted on the grain boundaries, within the ferrite grains of the parent metal, in the HAZ and weld metal. Incipient spheroidisation (stage B [1961Tof]) of the cementite phase in the parent metal occurred. Figure 4.27 shows coarsening of the carbides and spheroidisation becoming more advanced (stage C spheroidisation [1961Tof]) during stage 2 of simulated PWHT exposure. During stage 3 (figures 4.28 to 4.30) further coarsening of the Mo_2C carbides, formation of large Mo_3C and M_6C carbides, etc. together with an increase in the level of spheroidisation (stage C/D [1961Tof]) of the cementite, resulted in a rapid decrease in tensile properties (figure 4.3) [1986Spa]. In contrast, an increase in ductility and impact toughness with increasing Hp_{eff} occurred (see figure 4.9). Fine-grained ferrite (see light areas indicated by yellow arrows in figures 4.28 to 4.29) along prior austenite grain boundaries was found in the intercritically reheated coarse-grained heat affected zone (ICRCG HAZ) with large carbides noted in the sub-critical heat affected zone (SCHAZ) [2014Hu, 2010Wei]. Stage 4 (stabilisation of tensile properties) was absent during tension testing of the weld metal samples; however, virtually complete (stage D/E

[1961Tof]) spheroidisation and no significant further coarsening of molybdenum carbides was noticed in the microstructures (figures 4.28 to 4.29).

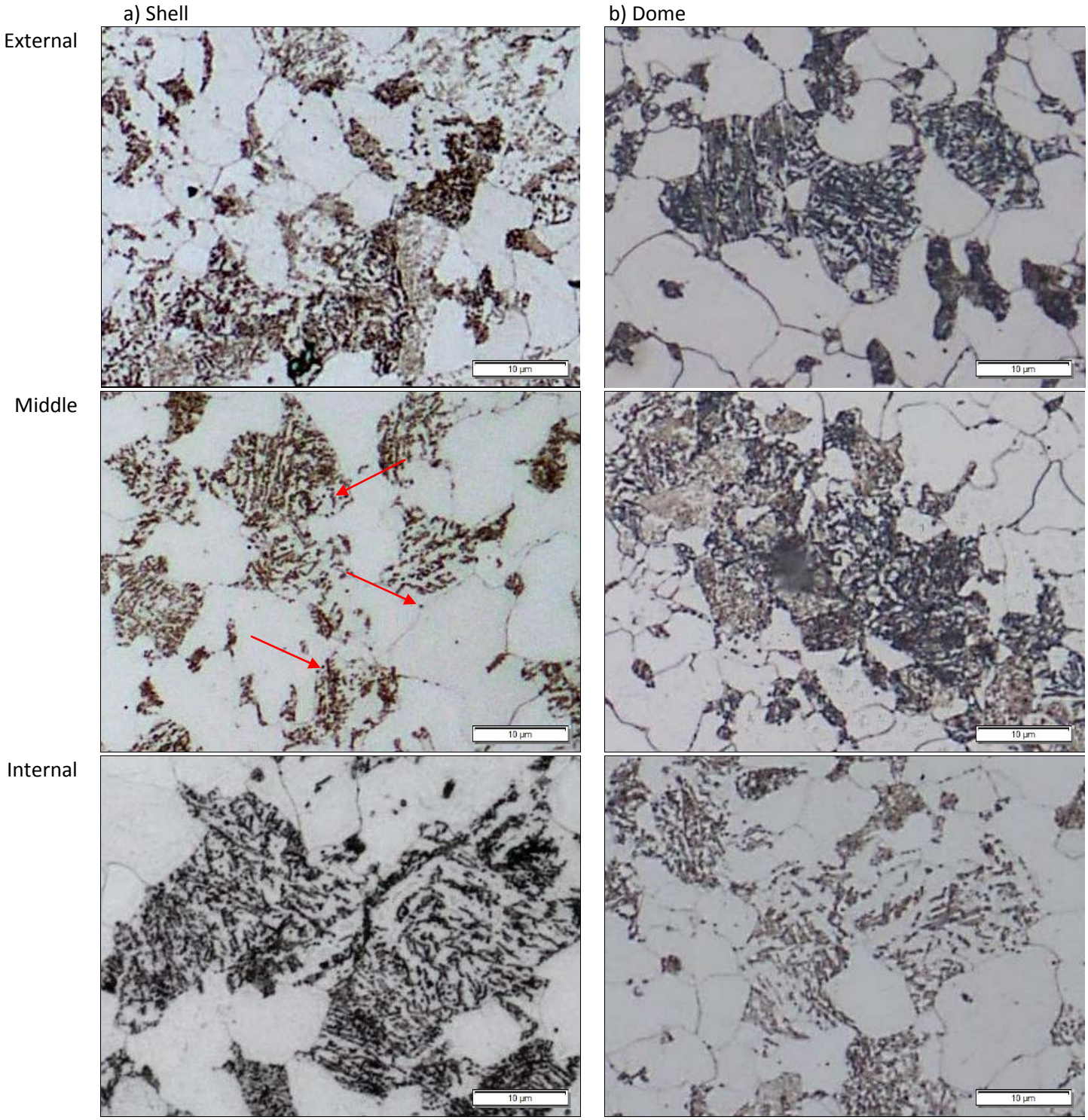

Figure 4.11: Photomicrograph of a cross-section through the (a) shell and (b) dome samples in the as-received condition: External surface (top photos), Middle (middle photos) and Internal surface (bottom photos)[1000x, 5% Nital].

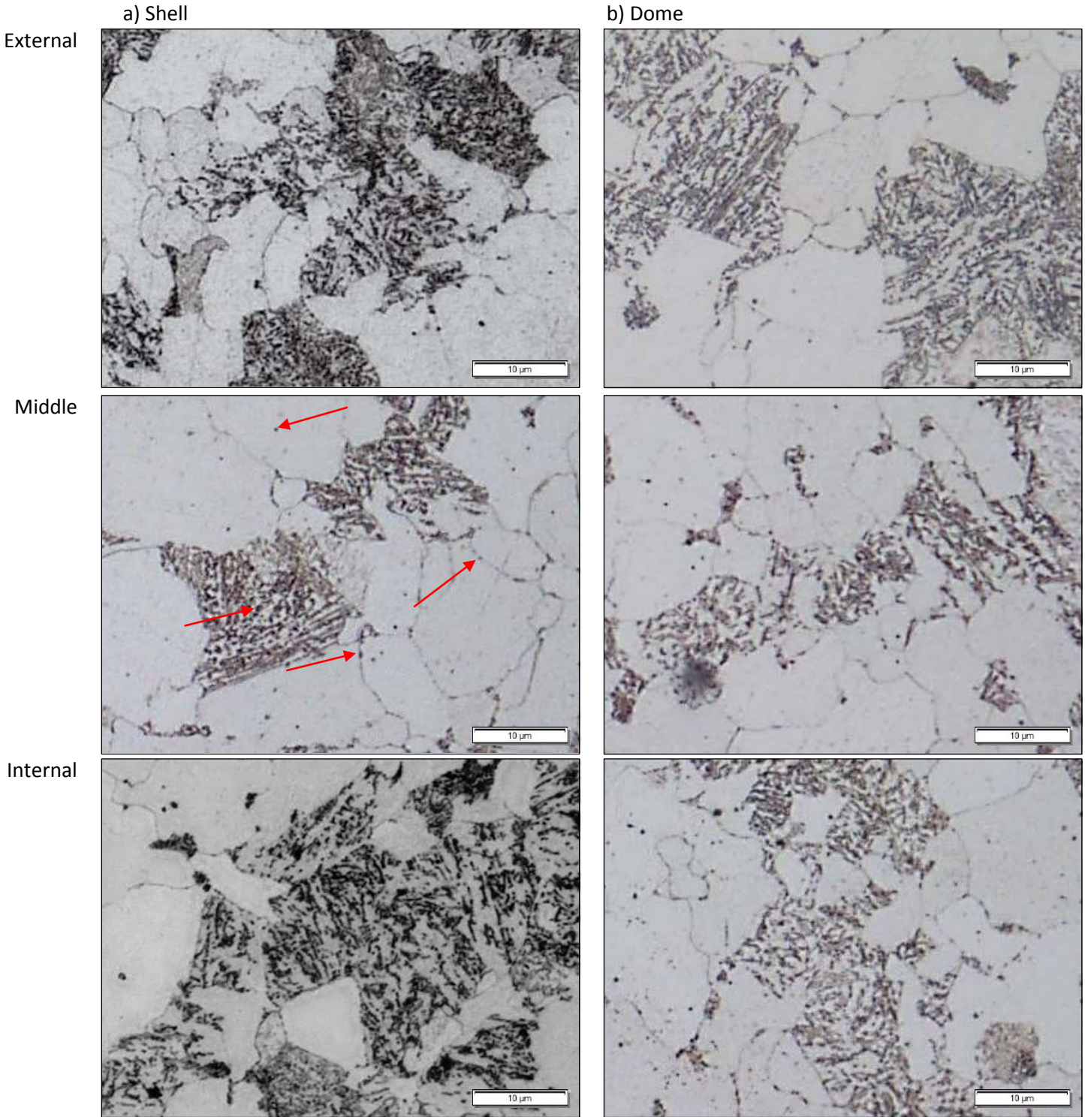

Figure 4.12: Photomicrograph of a cross-section through the (a) shell and (b) dome samples after an additional 2 hours simulated PWHT: External surface (top photos), Middle (middle photos) and Internal surface (bottom photos)[1000x, 5% Nital].

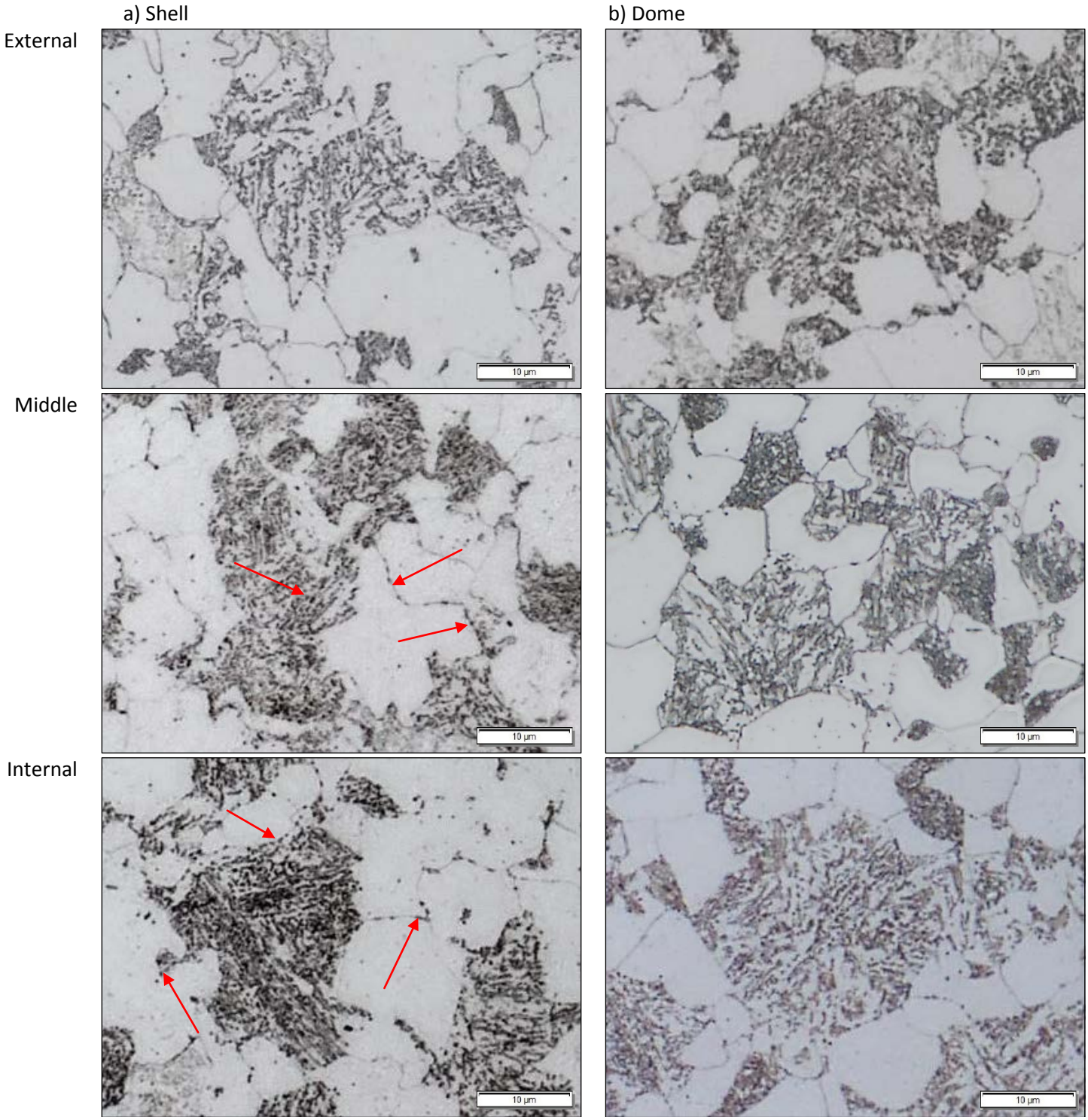

Figure 4.13: Photomicrograph of a cross-section through the (a) shell and (b) dome samples after an additional 4 hours simulated PWHT: External surface (top photos), Middle (middle photos) and Internal surface (bottom photos)[1000x, 5% Nital].

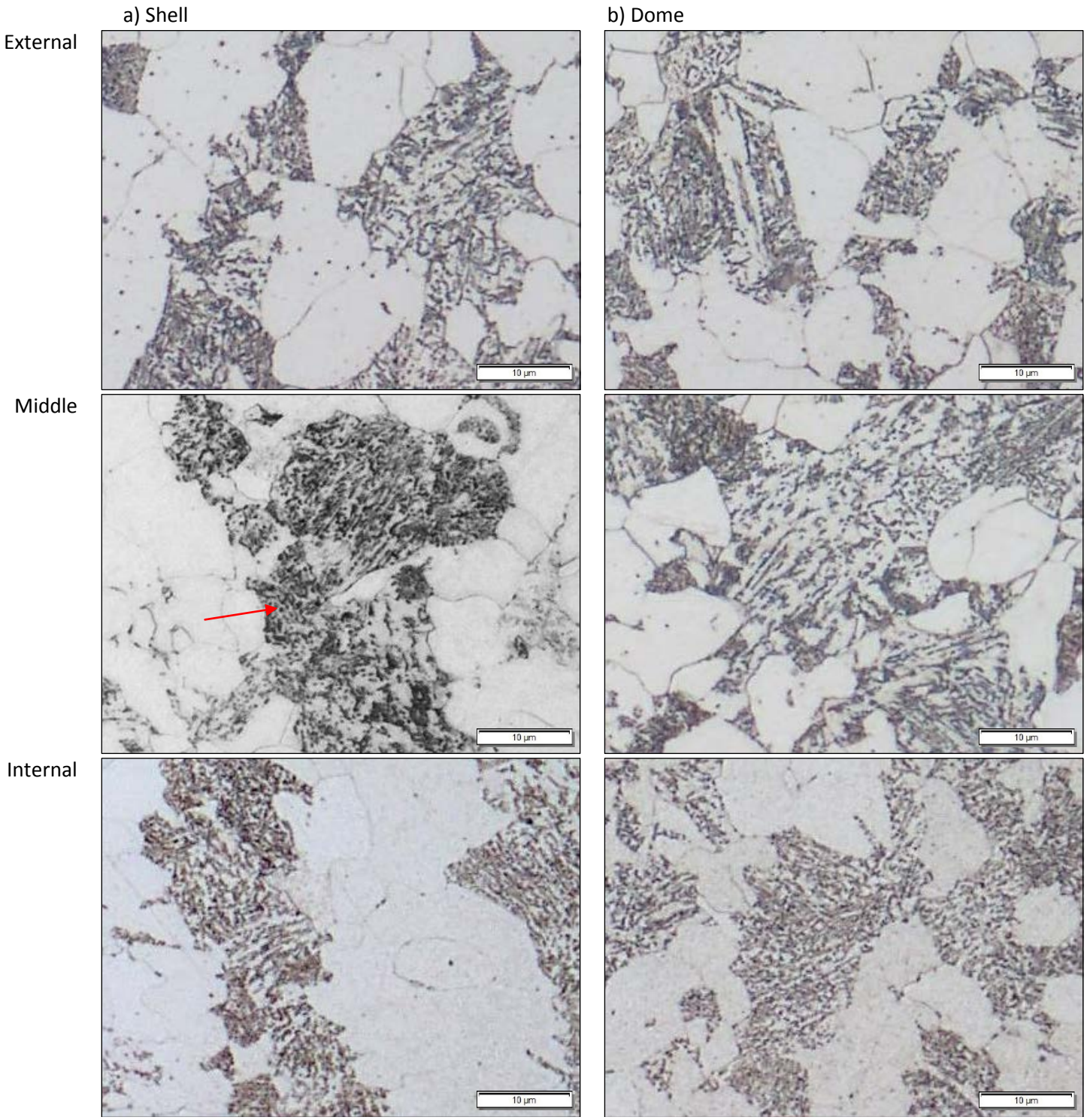

Figure 4.14: Photomicrograph of a cross-section through the (a) shell and (b) dome samples after an additional 8 hours simulated PWHT: External surface (top photos), Middle (middle photos) and Internal surface (bottom photos)[1000x, 5% Nital].

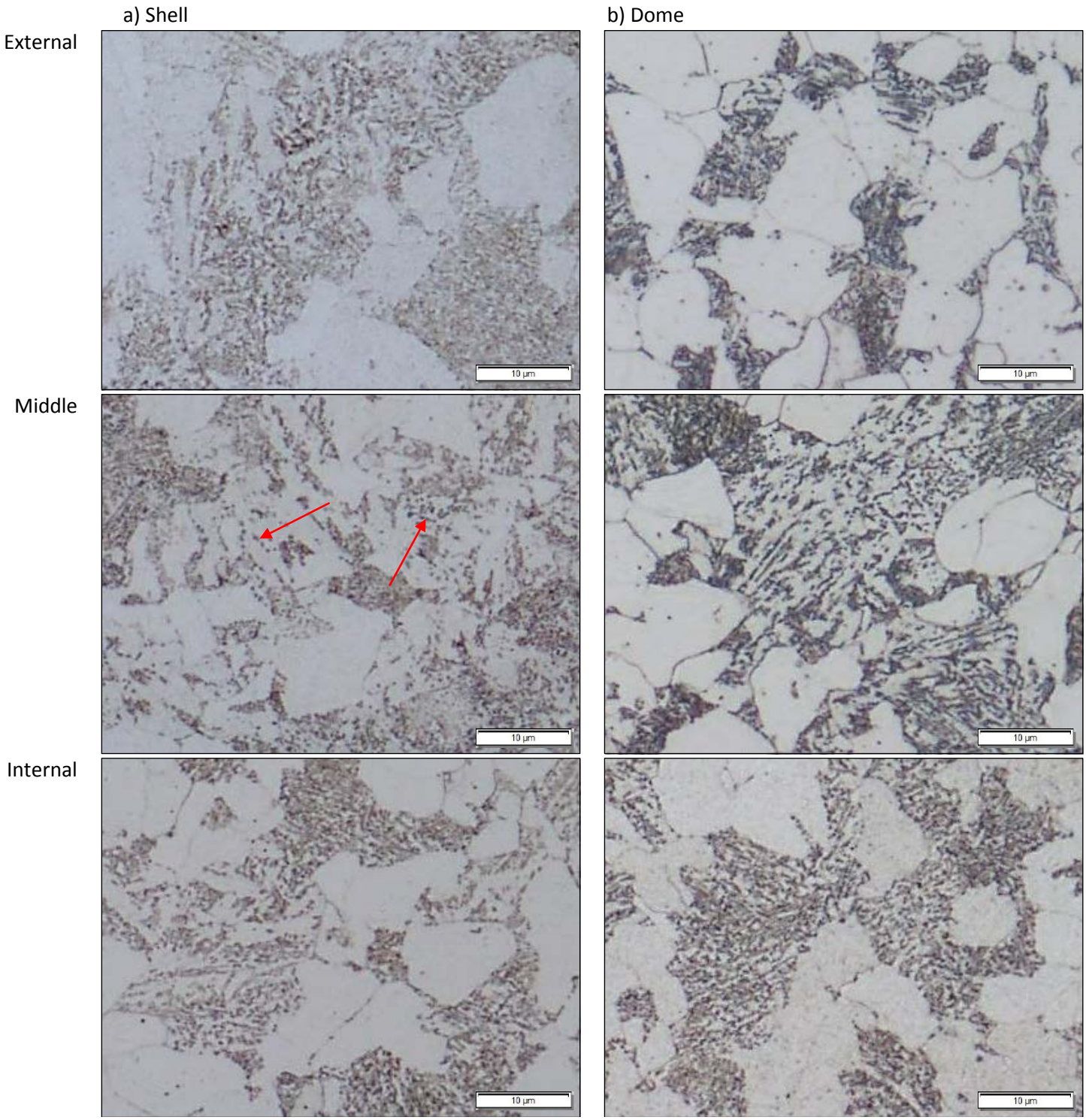

Figure 4.15: Photomicrograph of a cross-section through the (a) shell and (b) dome samples after an additional 14 hours simulated PWHT: External surface (top photos), Middle (middle photos) and Internal surface (bottom photos)[1000x, 5% Nital].

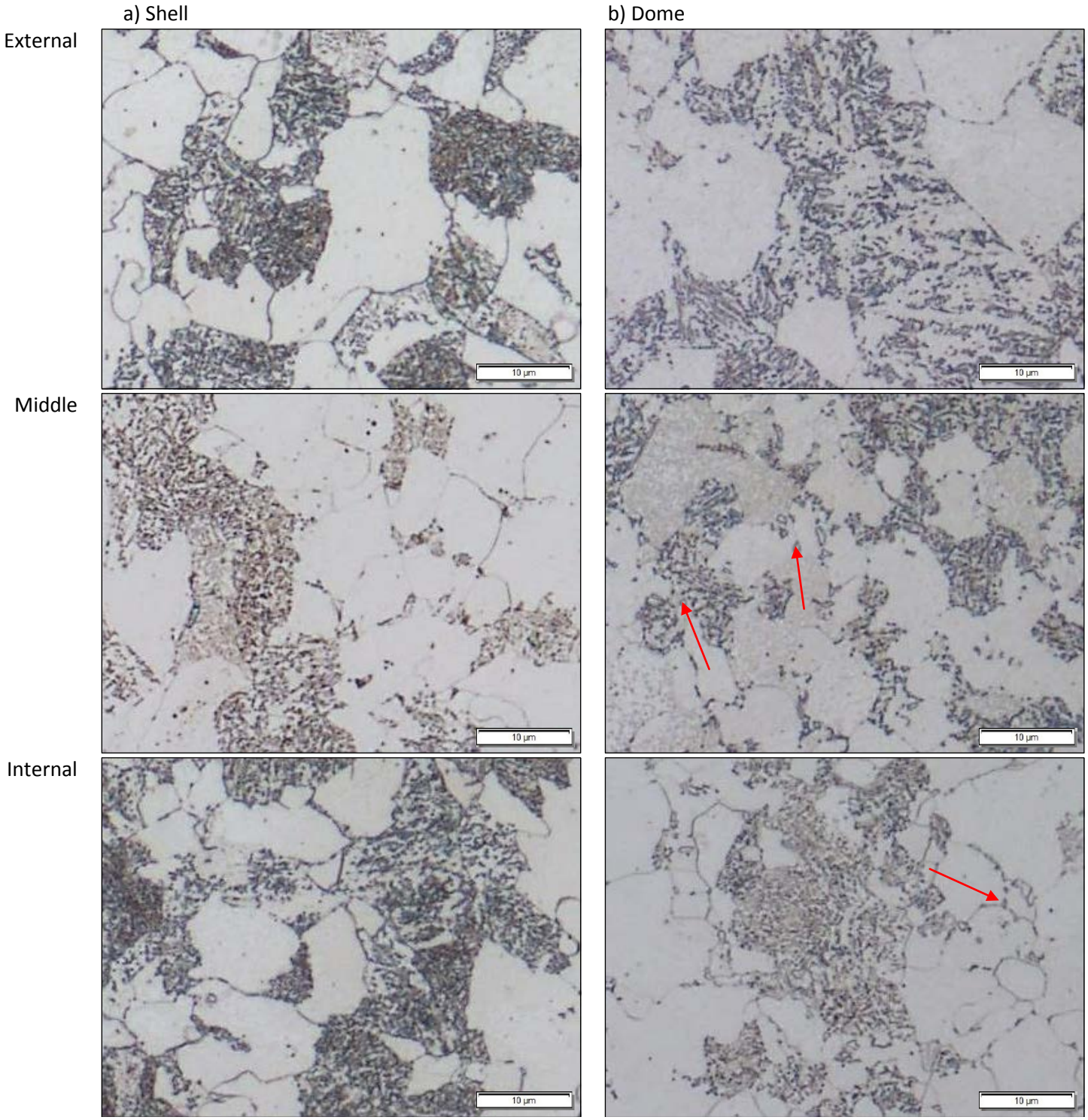

Figure 4.16: Photomicrograph of a cross-section through the (a) shell and (b) dome samples after an additional 20 hours simulated PWHT: External surface (top photos), Middle (middle photos) and Internal surface (bottom photos)[1000x, 5% Nital].

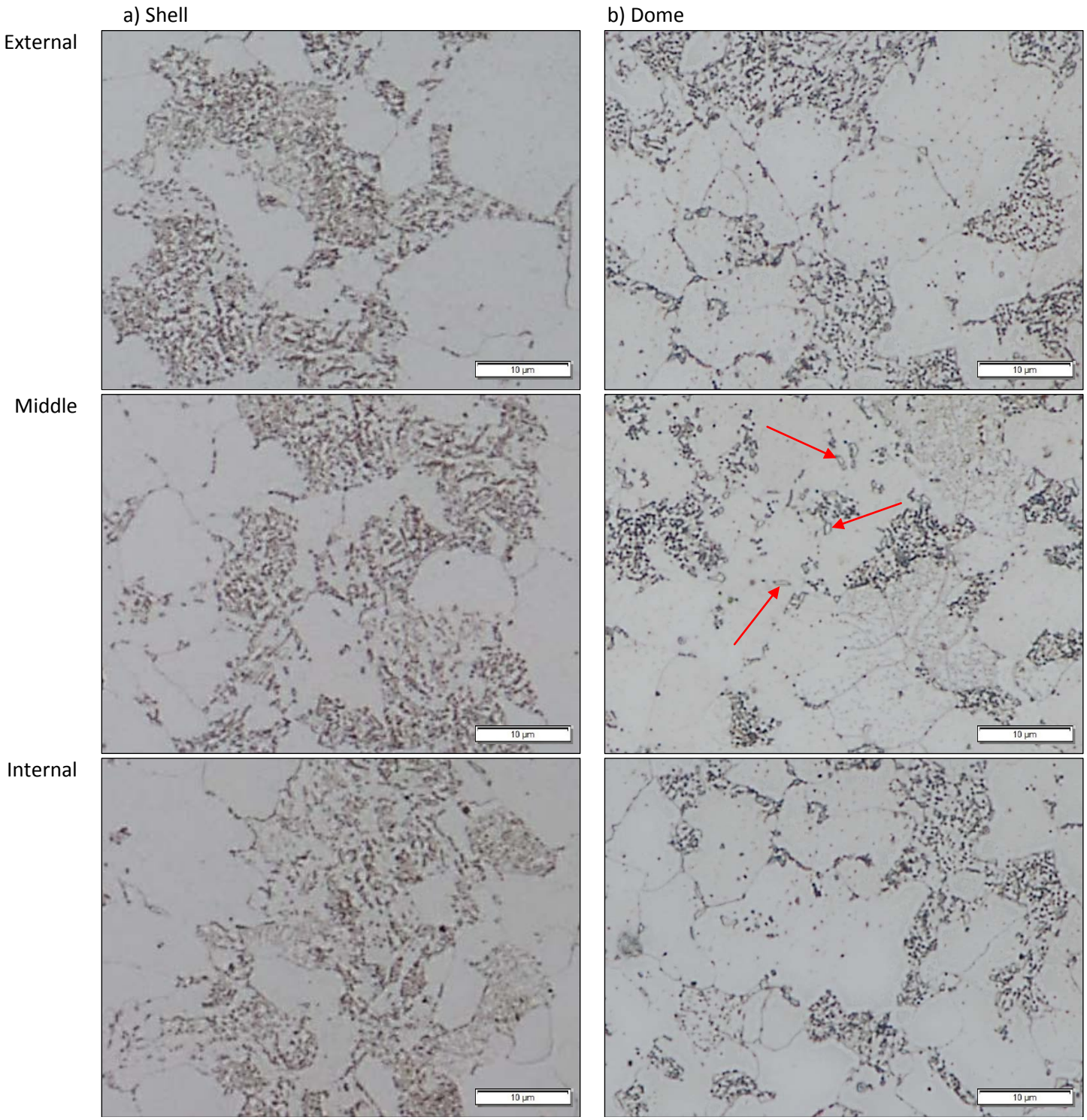

Figure 4.17: Photomicrograph of a cross-section through the (a) shell and (b) dome samples after an additional 30 hours simulated PWHT: External surface (top photos), Middle (middle photos) and Internal surface (bottom photos)[1000x, 5% Nital].

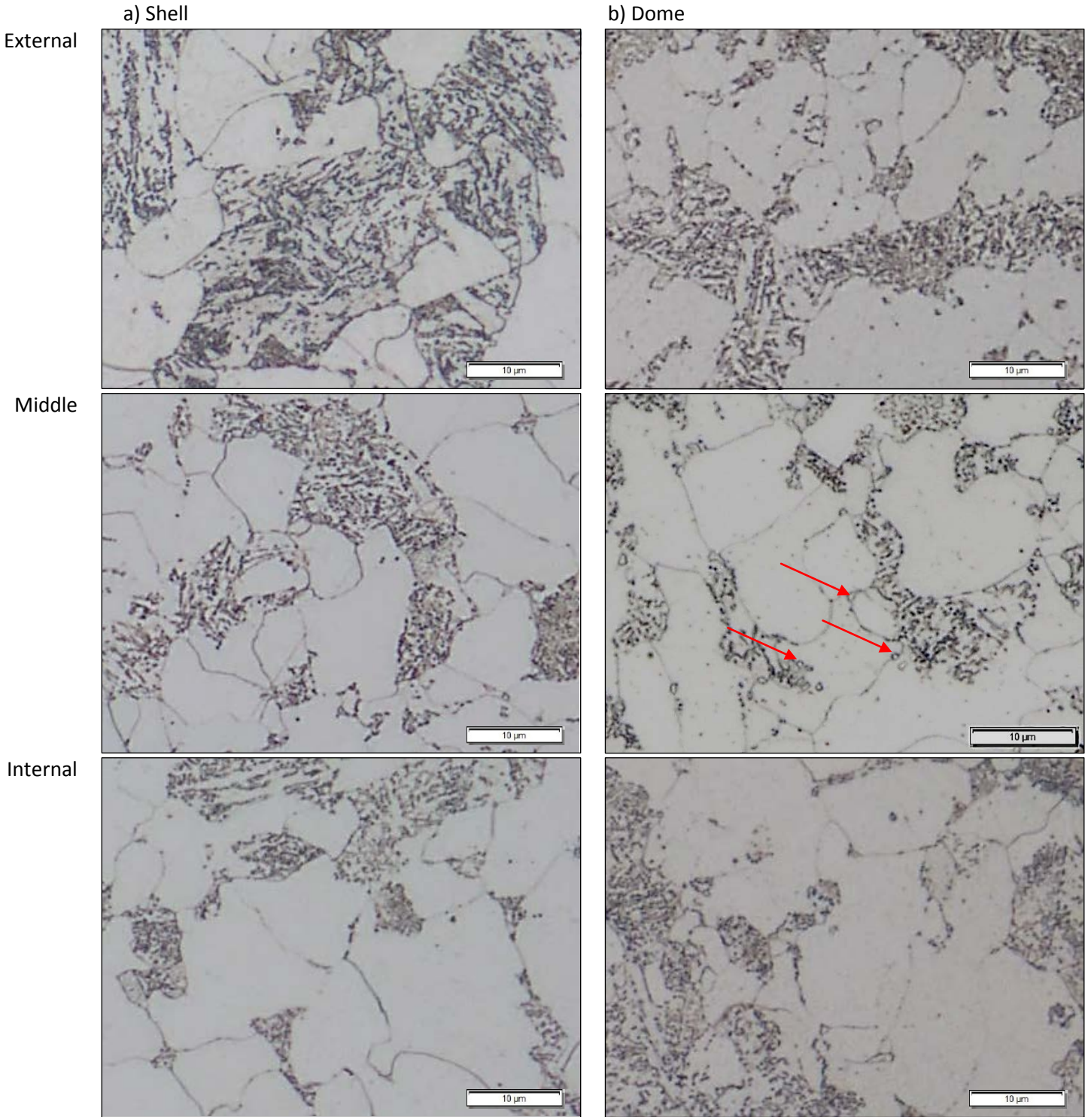

Figure 4.18: Photomicrograph of a cross-section through the (a) shell and (b) dome samples after an additional 40 hours simulated PWHT: External surface (top photos), Middle (middle photos) and Internal surface (bottom photos)[1000x, 5% Nital].

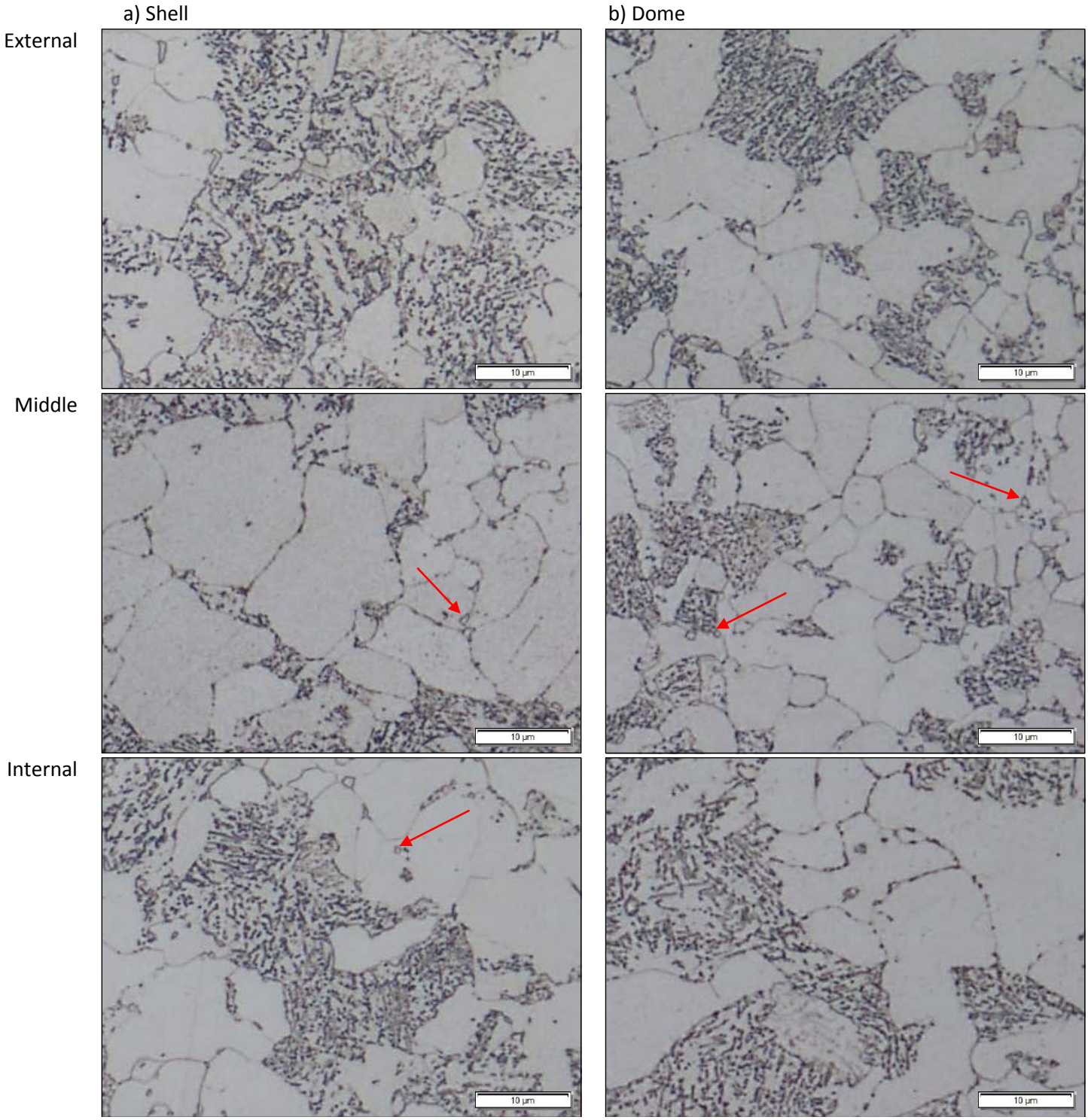

Figure 4.19: Photomicrograph of a cross-section through the (a) shell and (b) dome samples after an additional 60 hours simulated PWHT: External surface (top photos), Middle (middle photos) and Internal surface (bottom photos)[1000x, 5% Nital].

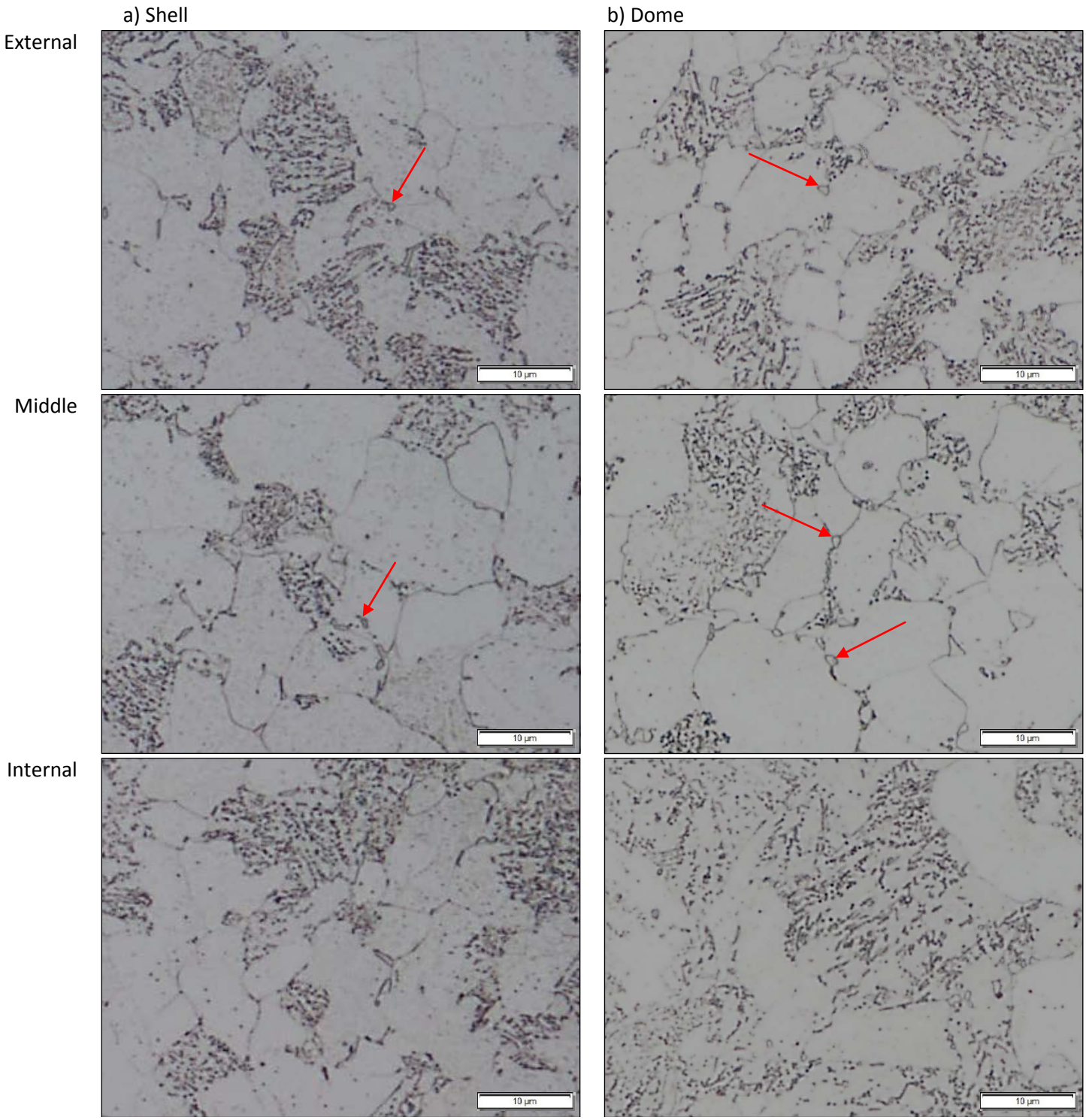

Figure 4.20: Photomicrograph of a cross-section through the (a) shell and (b) dome samples after an additional 80 hours simulated PWHT: External surface (top photos), Middle (middle photos) and Internal surface (bottom photos)[1000x, 5% Nital].

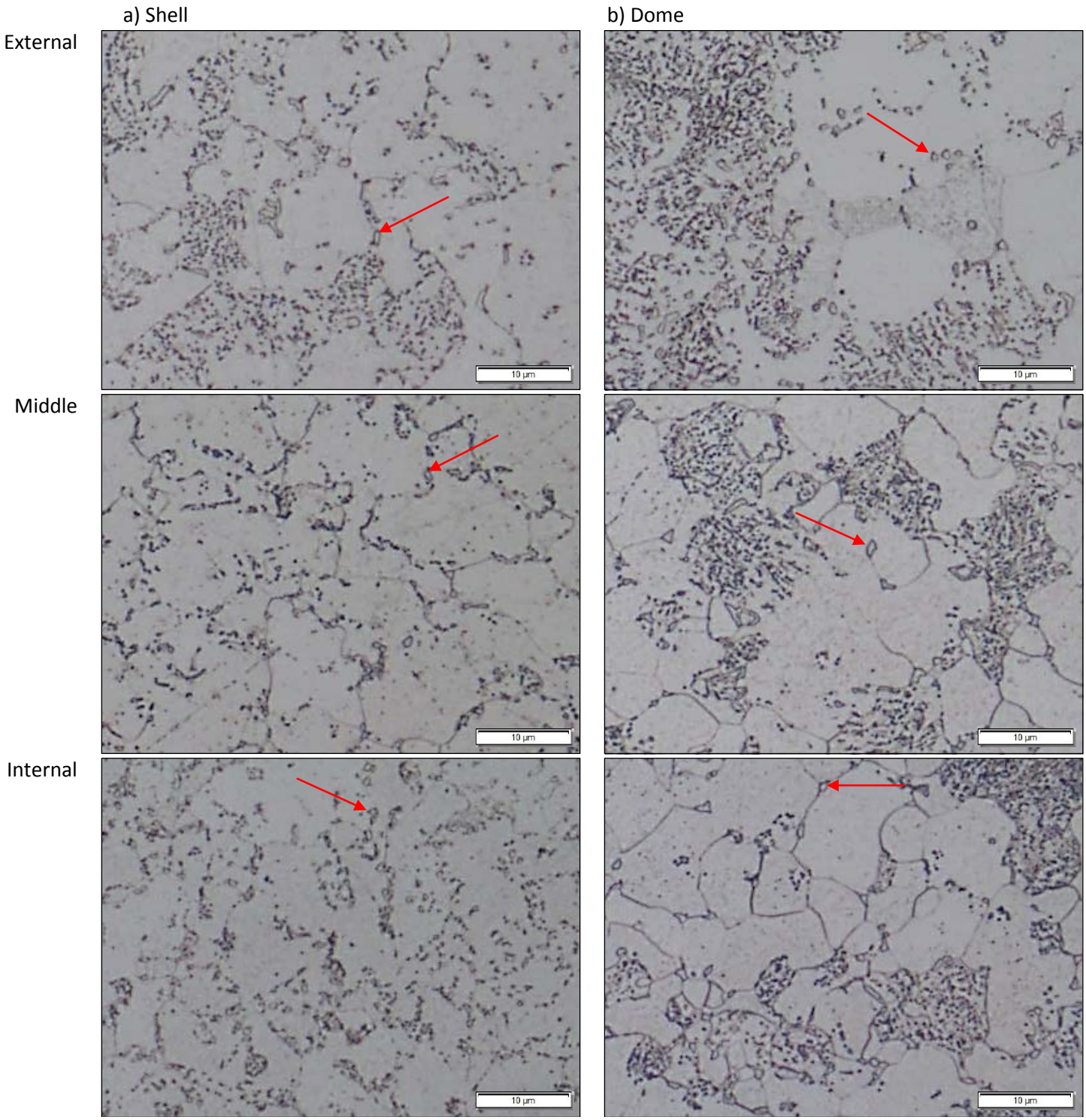

Figure 4.21: Photomicrograph of a cross-section through the (a) shell and (b) dome samples after an additional 100 hours simulated PWHT: External surface (top photos), Middle (middle photos) and Internal surface (bottom photos)[1000x, 5% Nital].

a) As-received

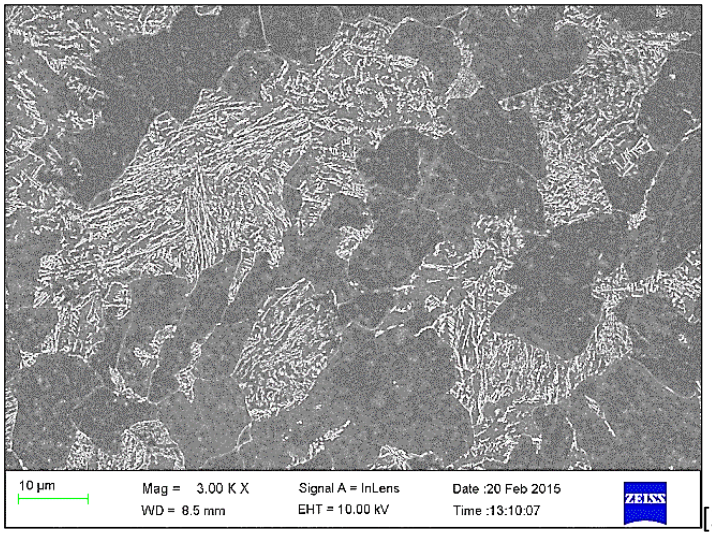

[3000x, 5% Nital]

b) 60 hours

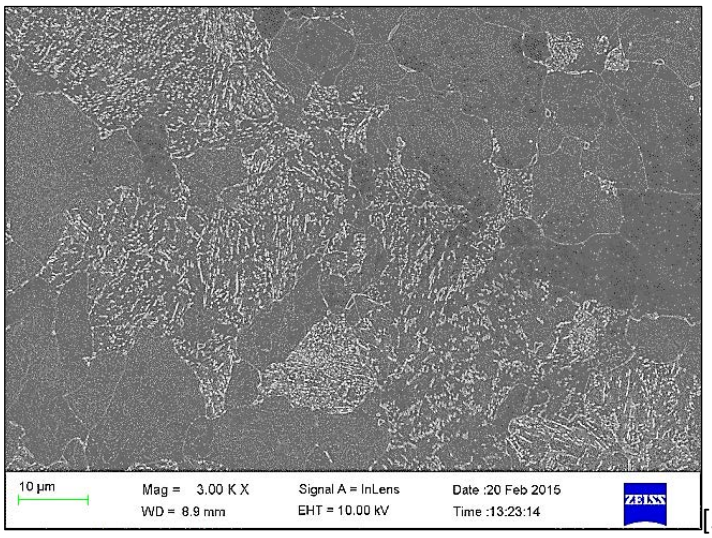

[3000x, 5% Nital]

c) 100 hours

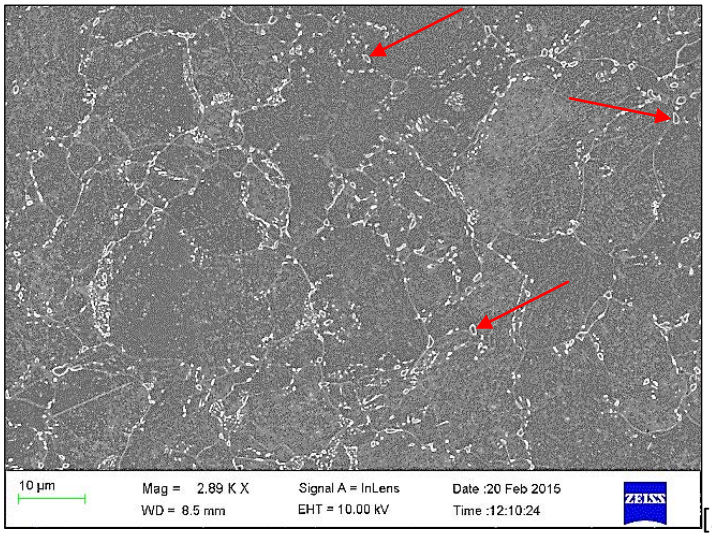

[2890x, 5% Nital]

Figure 4.22: SEM micrographs of shell samples in the as-received condition, and after an additional 60 and 100 hours simulated PWHT, respectively. Increased spheroidisation, carbide precipitation on the grain boundaries and growth in carbide size with increasing PWHT time can be seen [3000x, 5% Nital].

a) As-received

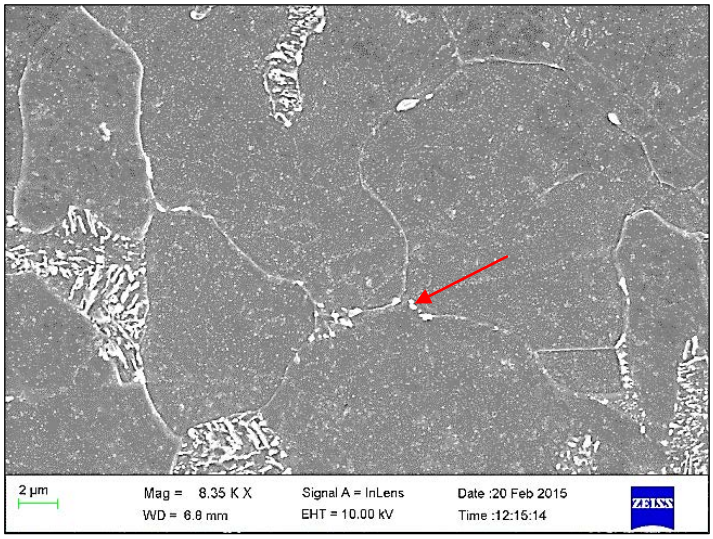

[8350x, 5% Nital]

b) 60 hours

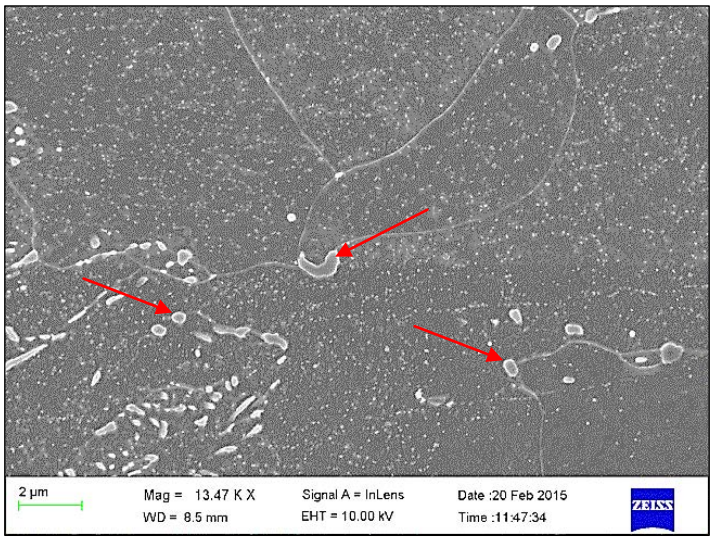

[13470x, 5% Nital]

c) 100 hours

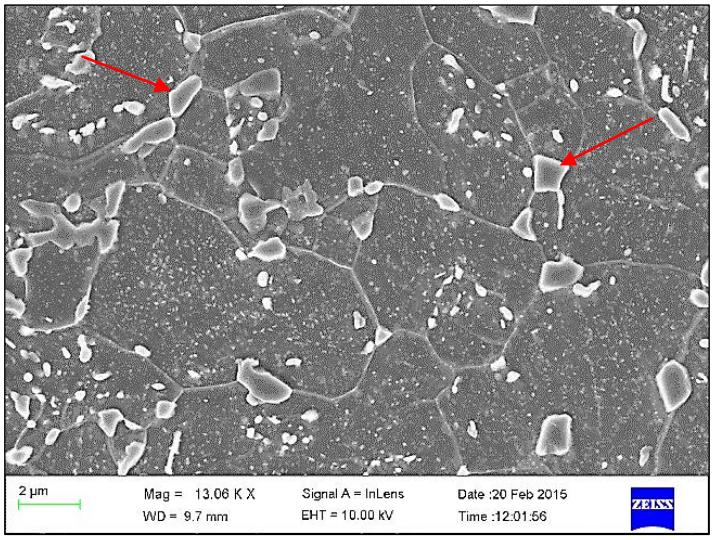

[13060x, 5% Nital]

Figure 4.23: Higher magnification SEM micrographs of samples shown in figure 4.22. Growth in carbide size with increasing PWHT time is evident especially when comparing (b) and (c) [8350x, 13000x, 5% Nital].

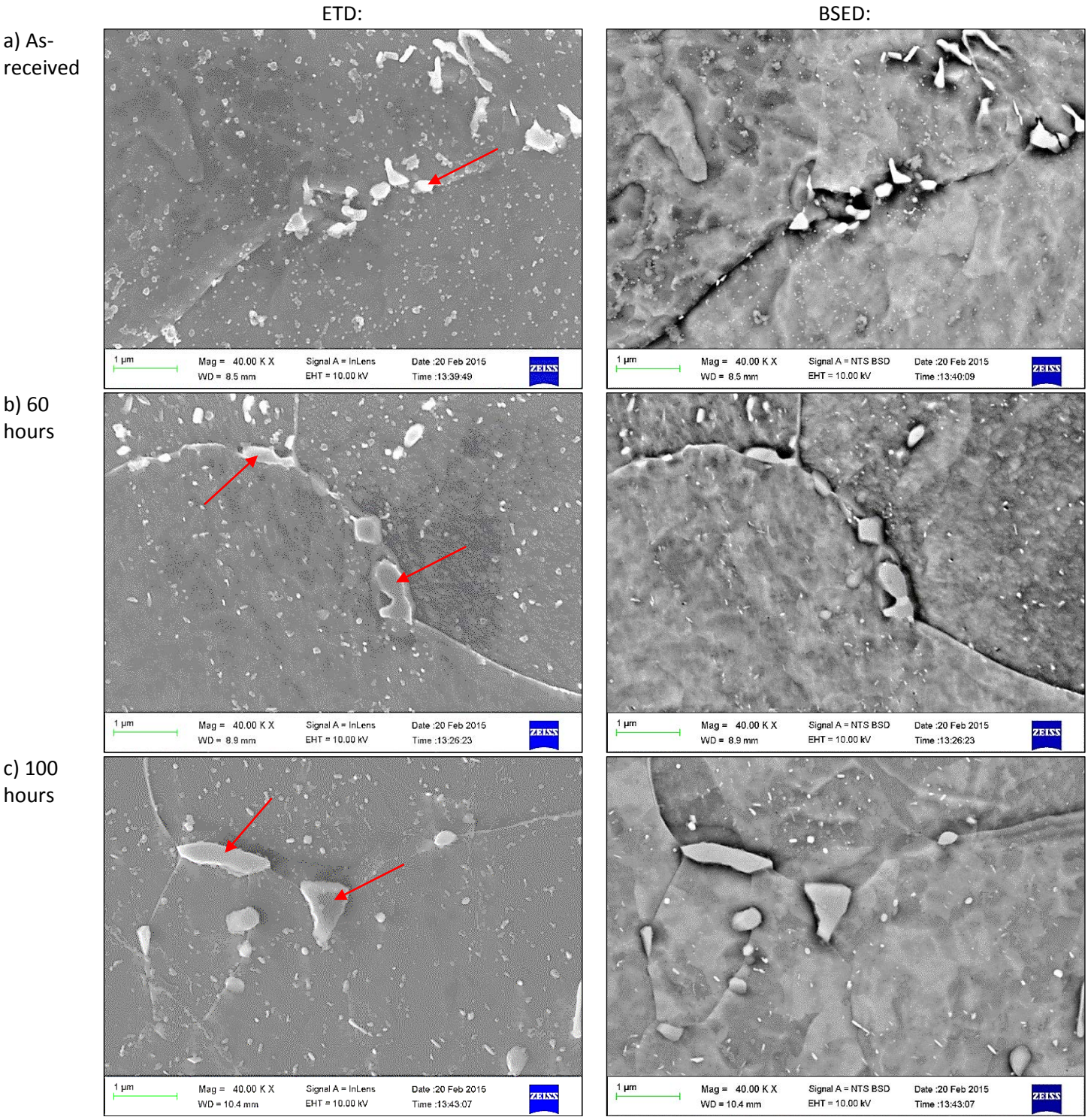

Figure 4.24: High magnification SEM micrographs of samples shown in figure 4.22. Large carbides on the grain boundaries and growth in carbide size with increasing PWHT time are evident [40000x, 5% Nital].

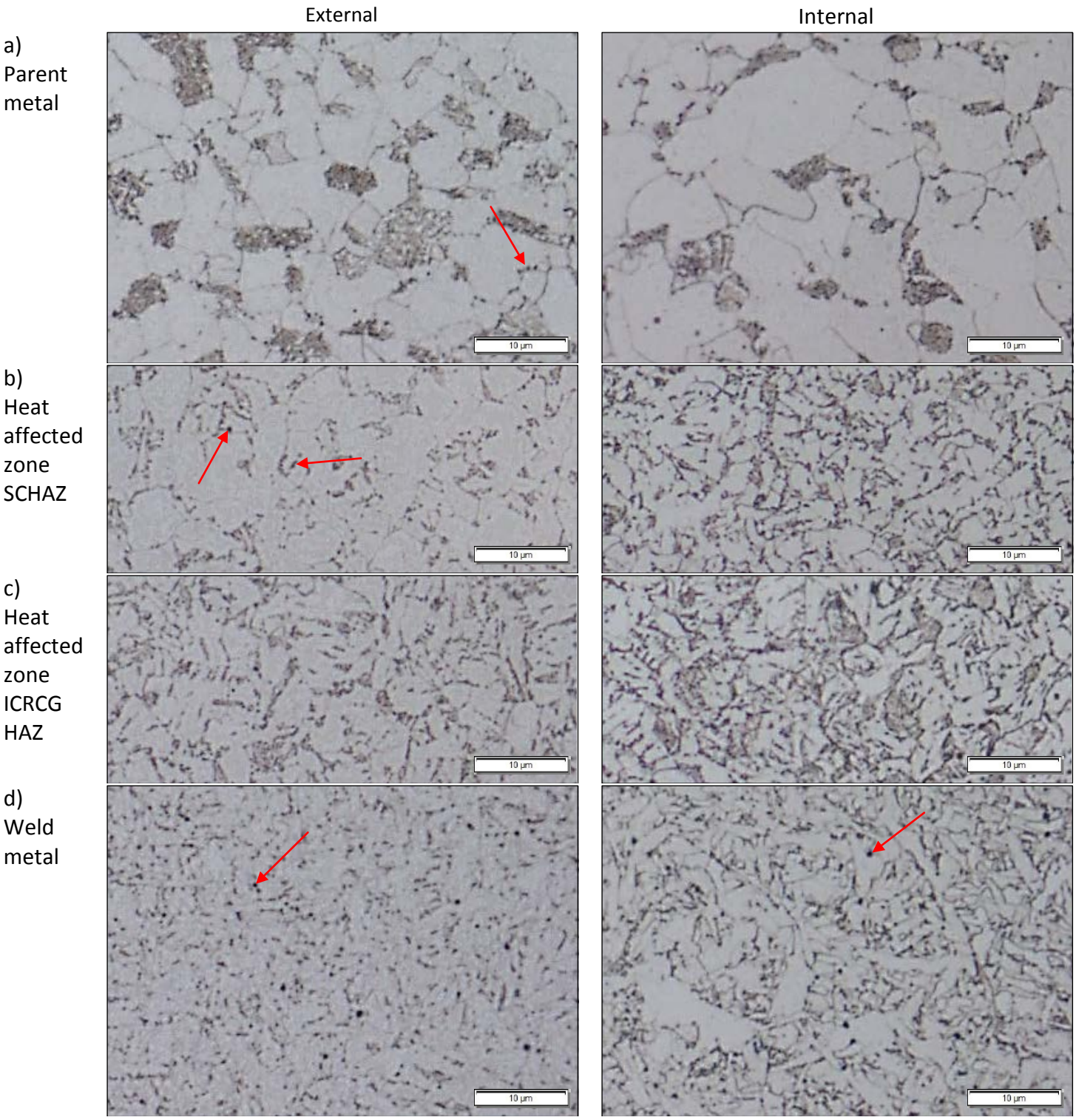

Figure 4.25: Photomicrograph of a cross-section through the shell-to-dome weld samples showing the (a) parent metal, (b) heat affected zone and (c) weld metal in the as-received condition: External surface (left) and internal surface (right)[1000x, 5% Nital].

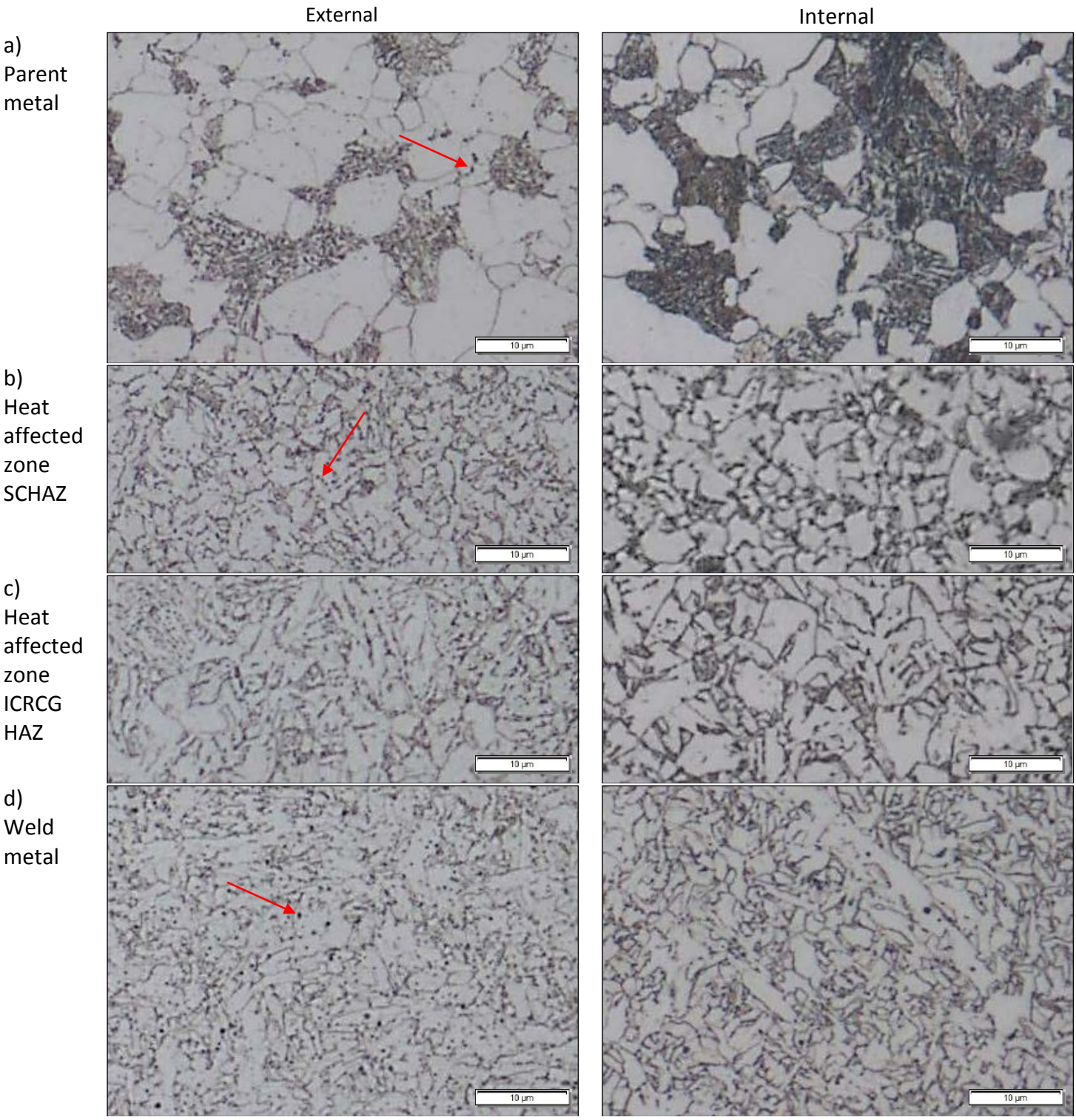

Figure 4.26: Photomicrograph of a cross-section through the shell-to-dome weld samples showing the (a) parent metal, (b) heat affected zone and (c) weld metal after an additional 2 hours simulated PWHT: External surface (left) and internal surface (right)[1000x, 5% Nital].

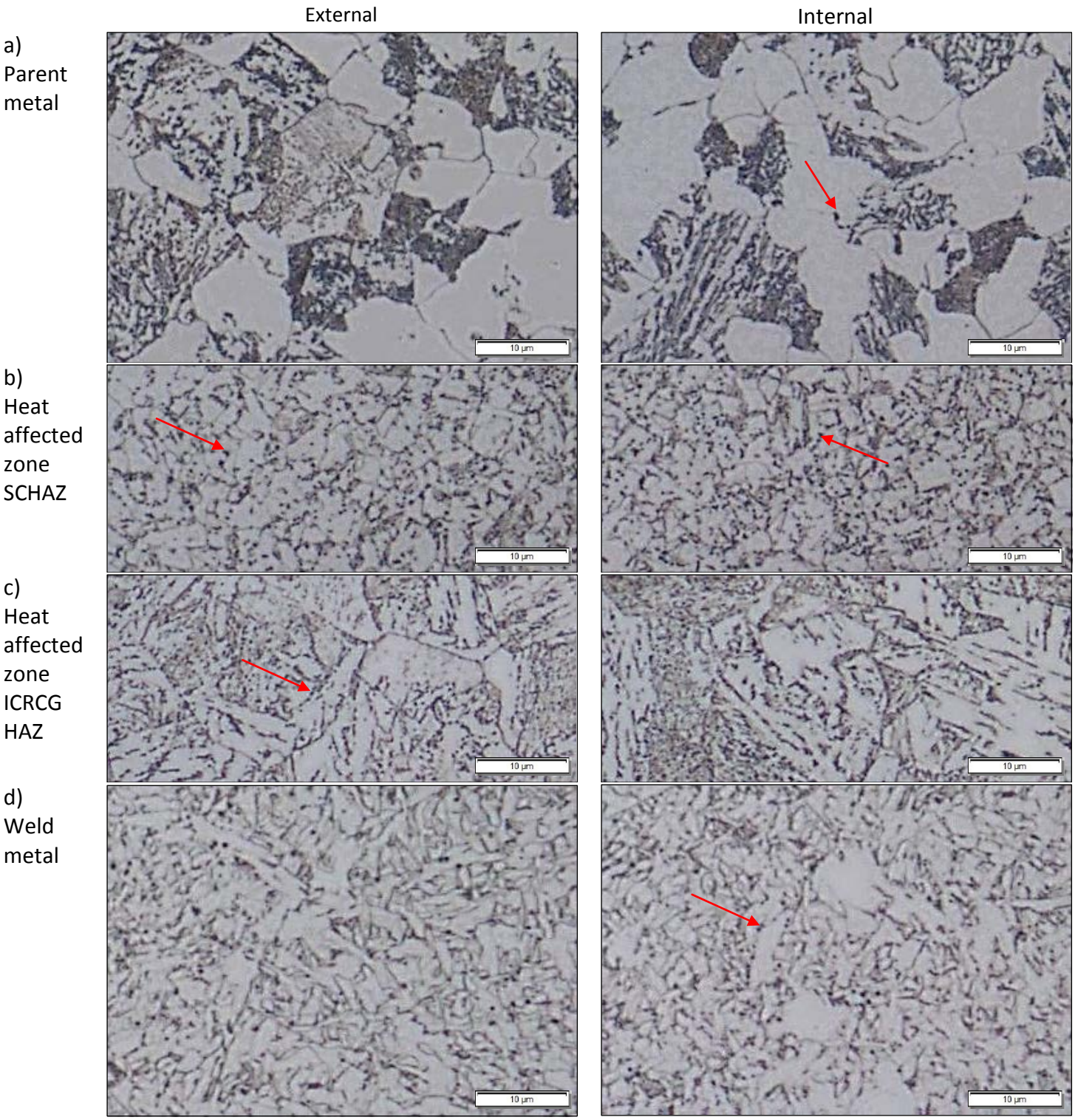

Figure 4.27: Photomicrograph of a cross-section through the shell-to-dome weld samples showing the (a) parent metal, (b) heat affected zone and (c) weld metal after an additional 6 hours simulated PWHT: External surface (left) and internal surface (right)[1000x, 5% Nital].

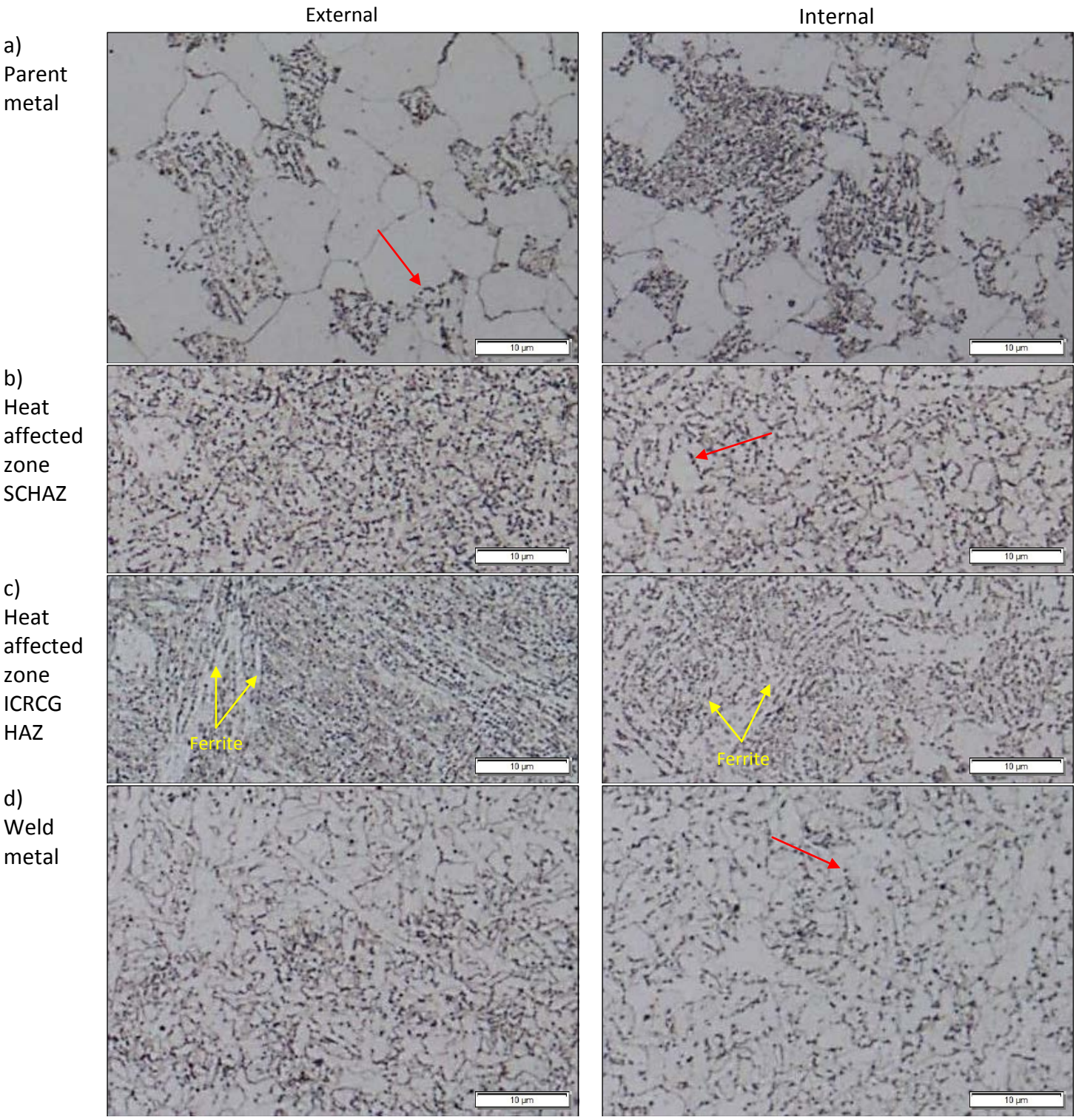

Figure 4.28: Photomicrograph of a cross-section through the shell-to-dome weld samples showing the (a) parent metal, (b) heat affected zone and (c) weld metal after an additional 30 hours simulated PWHT: External surface (left) and internal surface (right)[1000x, 5% Nital].

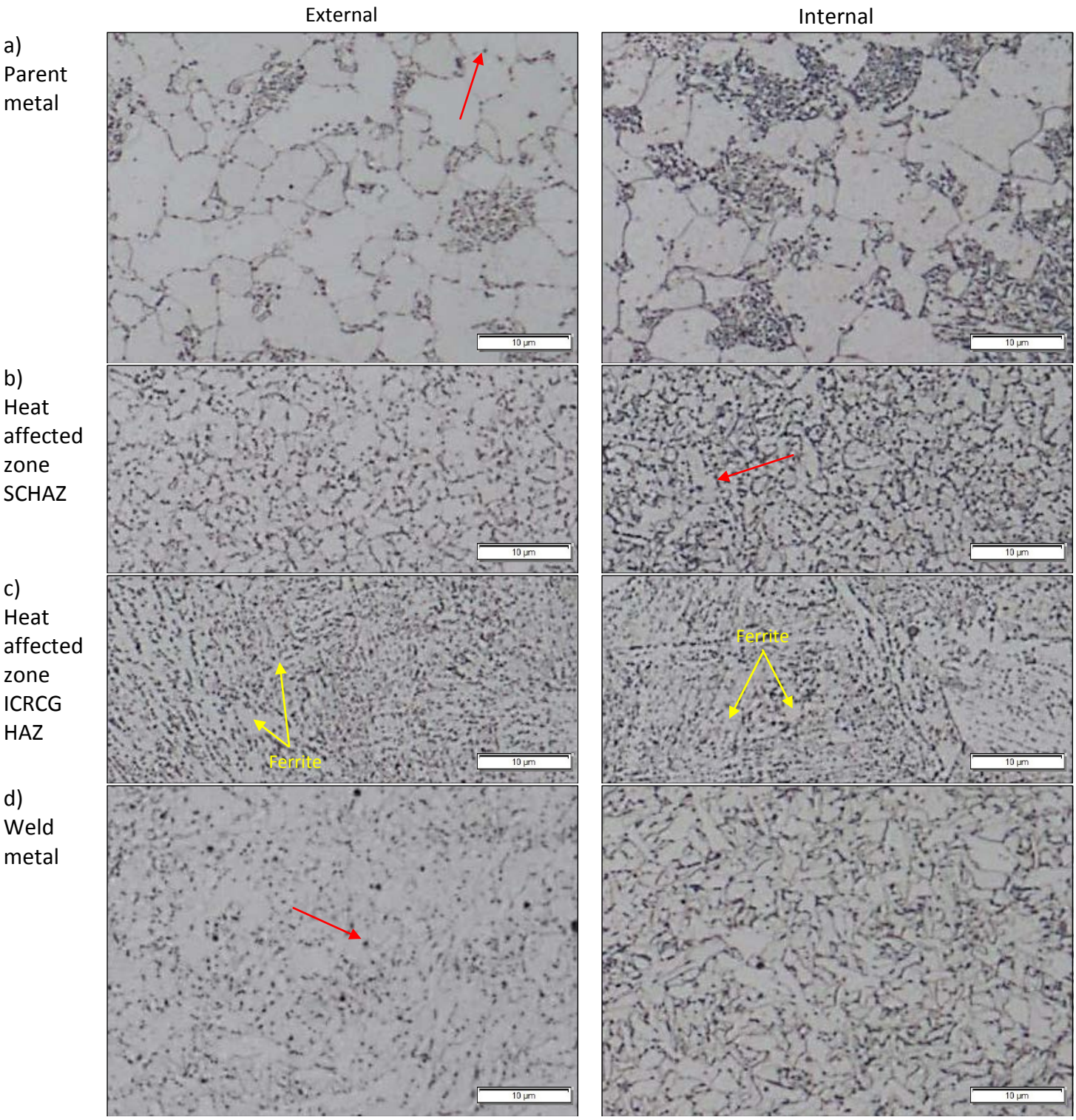

Figure 4.29: Photomicrograph of a cross-section through the shell-to-dome weld samples showing the (a) parent metal, (b) heat affected zone and (c) weld metal after an additional 60 hours simulated PWHT: External surface (left) and internal surface (right)[1000x, 5% Nital].

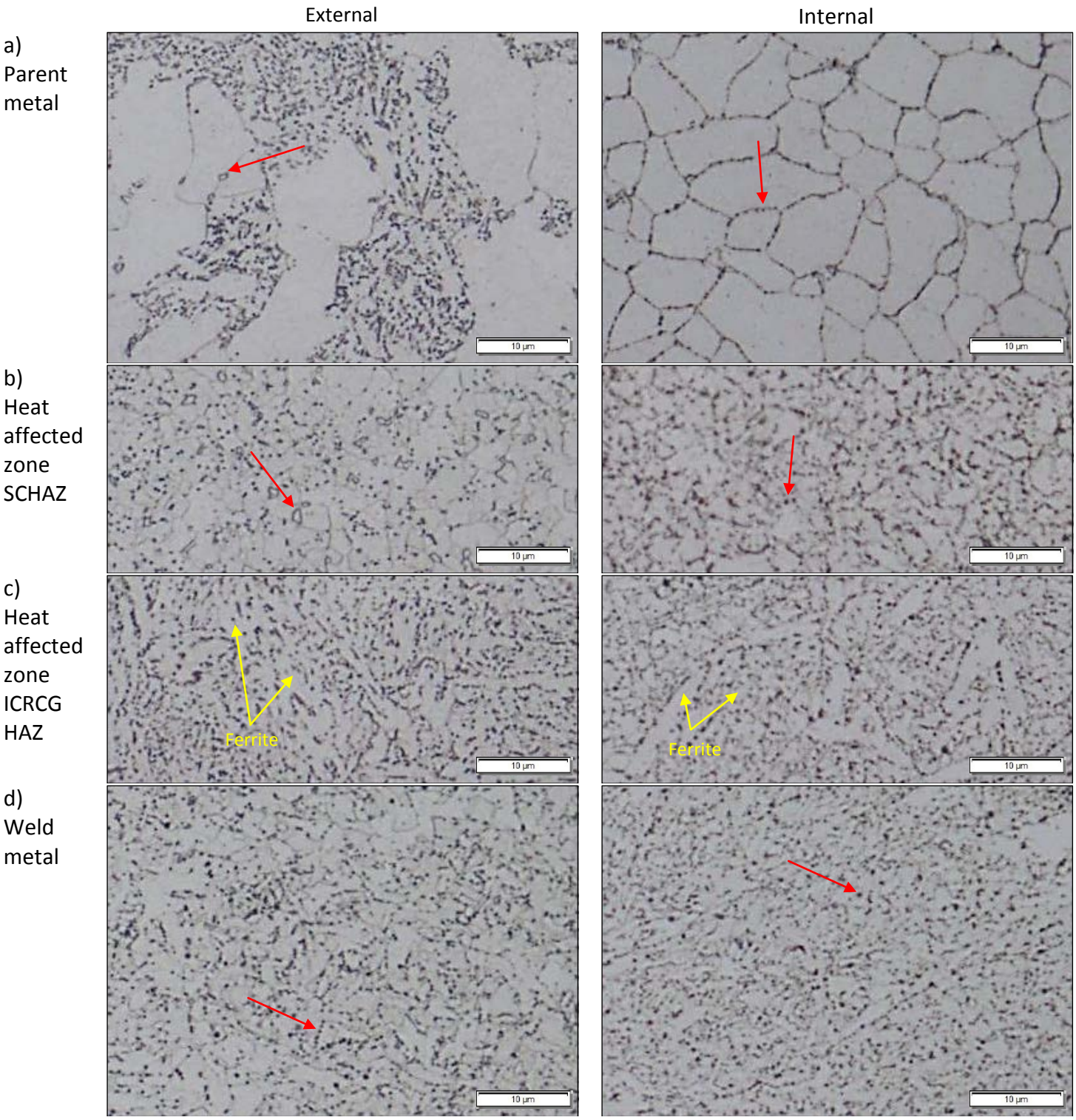

Figure 4.30: Photomicrograph of a cross-section through the shell-to-dome weld samples showing the (a) parent metal, (b) heat affected zone and (c) weld metal after an additional 80 hours simulated PWHT: External surface (left) and internal surface (right)[1000x, 5% Nital].

4.6 Graphical prediction model

The tension test results and graphical prediction model derived from Hattingh's work [1987Hat] are displayed in figures 4.31 and 4.32, respectively. Figure 4.32 shows the

percentage change in tensile properties vs. Hp for A302 Grade B material and the corresponding formulas derived from these curves. These are the formulas that have been used in the past to predict tensile properties of the shell, dome and cone of the ash locks after PWHT. The formulas were valid for an Hp range of 17.93 to 19.36.

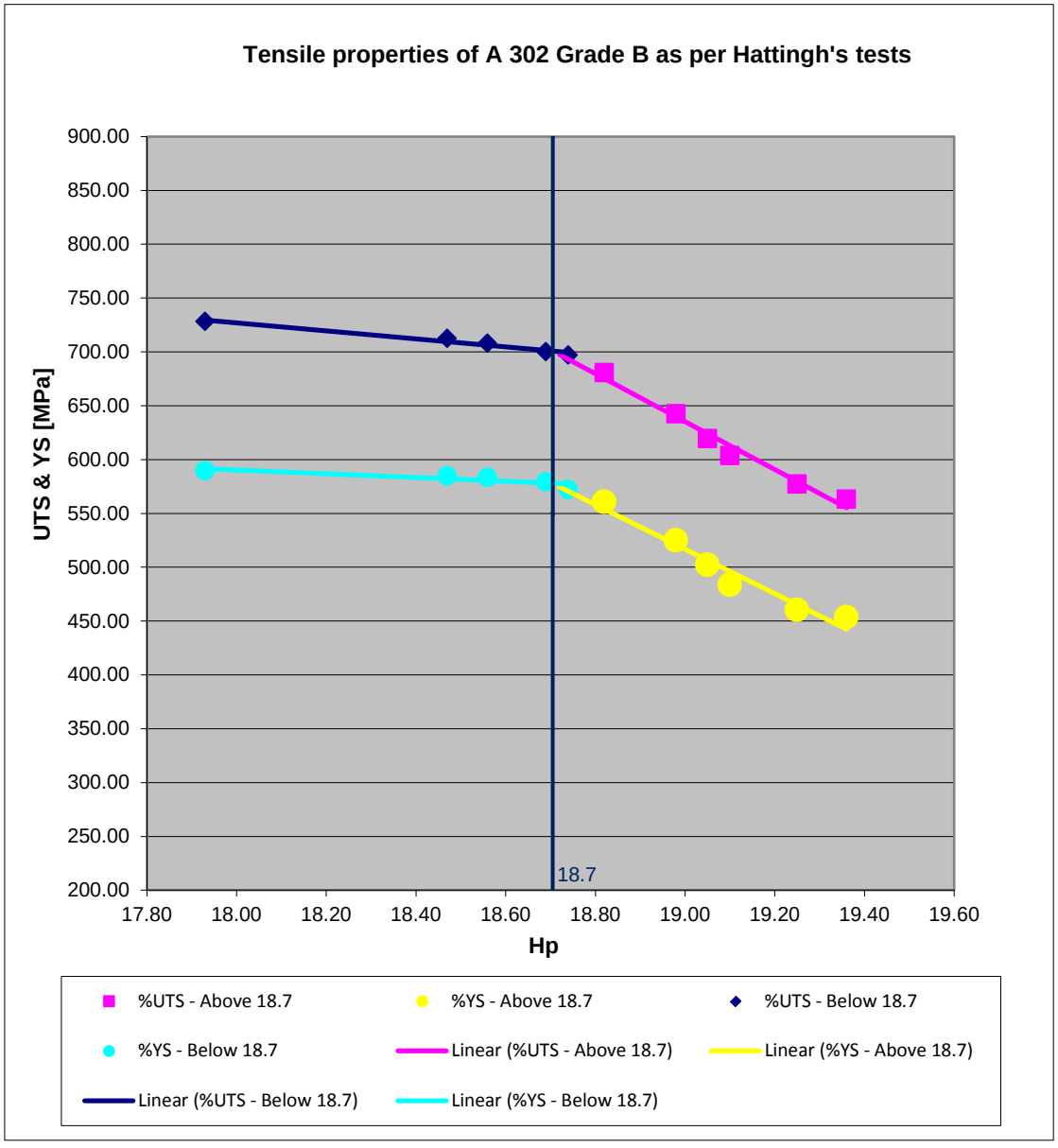

Figure 4.31: Tensile properties vs. Hp on A 302 Grade B material as tested by Hattingh [1987Hat].

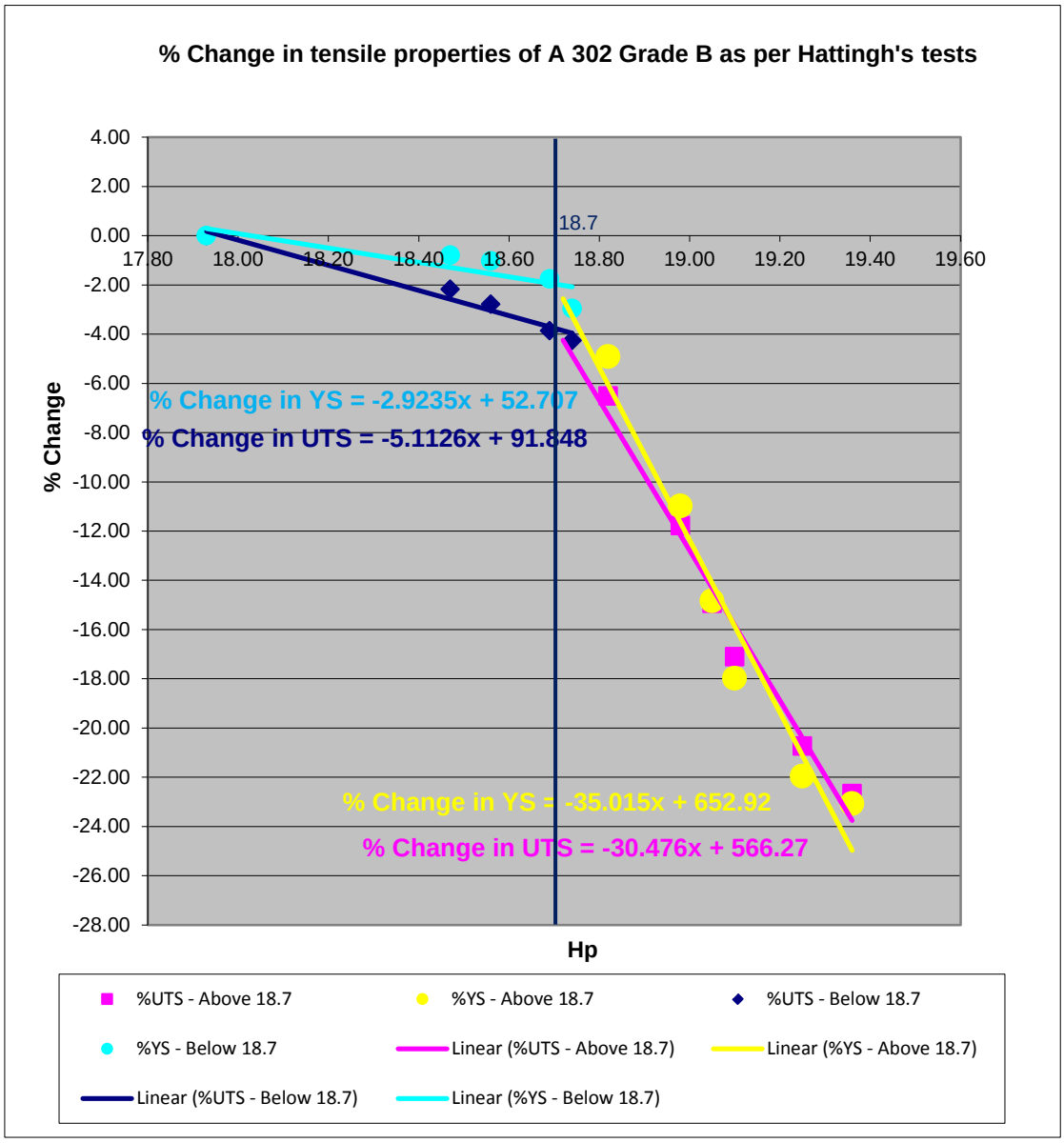

Figure 4.32: % Change in tensile properties vs. Hp on A 302 Grade B material as tested by Hattingh [1987Hat].

Linear regression was applied to the data points, as opposed to polynomial regression. The reason for this was simplicity when performing the calculations as well as to be conservative where ever the maximum Hp of 19.36 was exceeded and a polynomial regression could wrongfully predict an increase in properties. The graph shows that at an Hp of 18.7 a sharp decrease in properties was evident (see Chapter 2 figure 2.1) leading to a different set of formulas to be used at Hp values higher than 18.7.

A new graphical prediction model was derived from tension test results obtained in the current study (refer to figures 4.1 and 4.2). Figures 4.33 and 4.34 show the percentage change in UTS and YS vs. Hp_{eff} for the A 302 Grade B shell and dome materials.

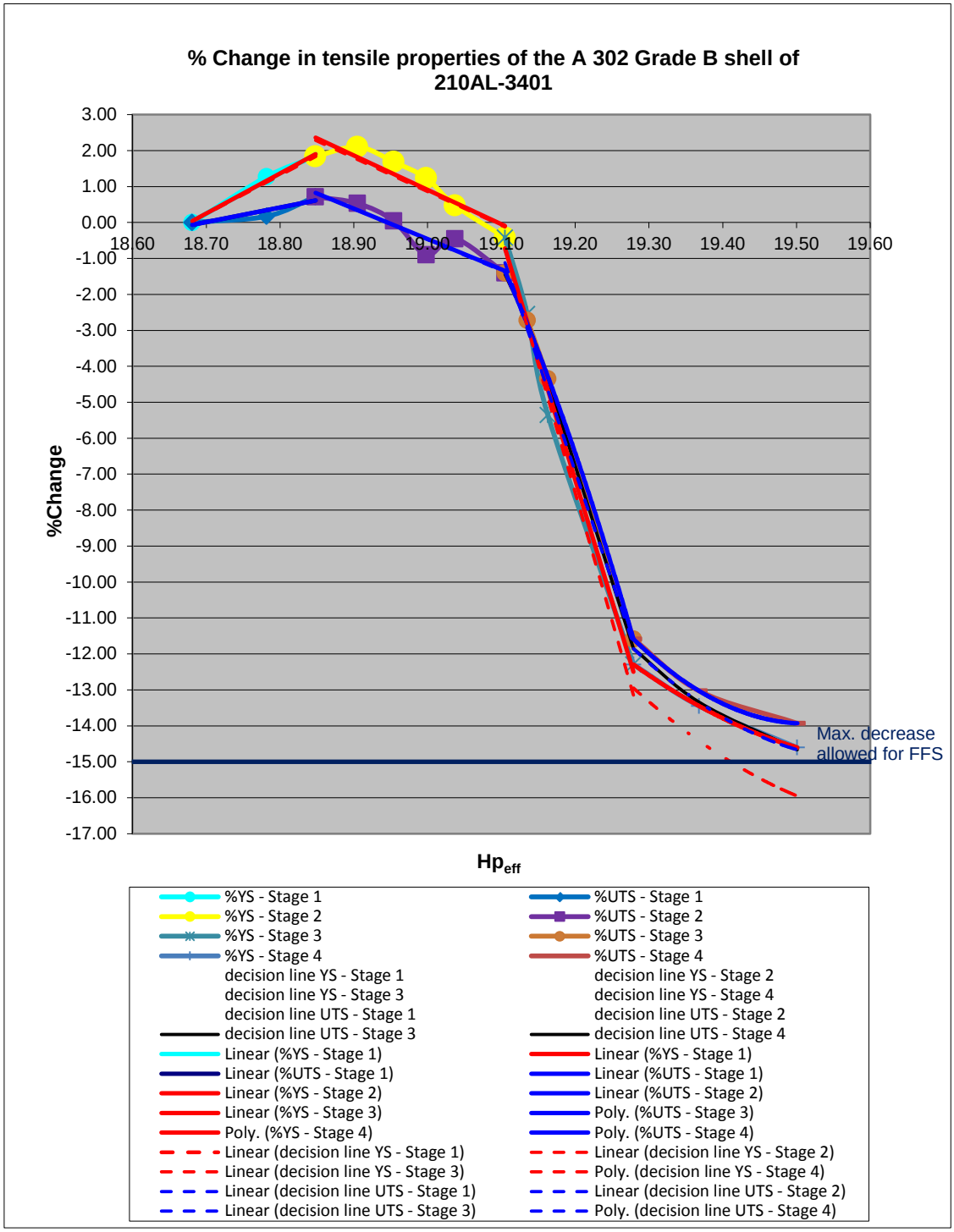

Figure 4.33: % Change in tensile properties vs. Hp_{eff} on A 302 Grade B shell material of 210AL-3401. These curves can be used for predicting tensile properties for the bottom cone as well.

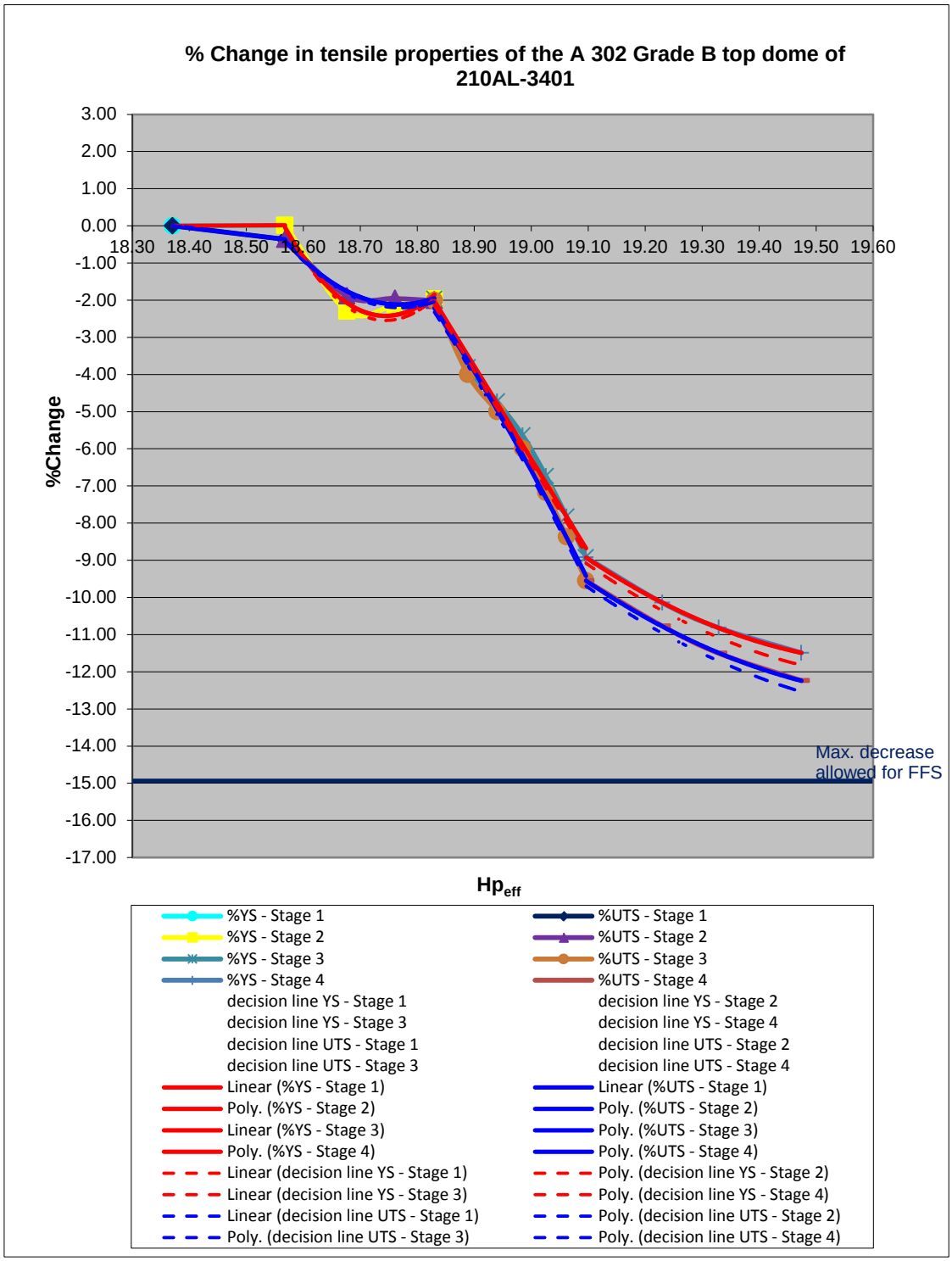

Figure 4.34: % Change in tensile properties vs. Hp_{eff} on A 302 Grade B dome material of 210AL-3401.

To achieve a mathematical model, as opposed to a graphical prediction model, a statistical fitting was applied to the test results. A safety margin of between approximately 2 to 10% below the actual values were obtained using a statistical 2 standard deviations (2σ) fitting. This 2σ fitting was plotted on the graph as a decision line for replacement of ash locks (see red and blue dashed lines). The cut-off line at a value of 15% below minimum required

ASME value, above which the component is expected to pass a FFS evaluation, is also indicated. The intersection of the decision line with the cut-off line implies that at an Hp_{eff} of ~19.40 replacement of an ash lock becomes relevant. The mathematical formulas for these curves, i.e. a set of linear ($y = mx + c$) and polynomial ($y = ax^2 + bx + c$) equations for each specific Hp_{eff} range, are shown in table 4.5 below. These formulas can be used for calculating the decrease in UTS and YS of the shell, bottom cone and top dome components of the ash lock. The formulas are valid for an Hp range of 18.681 to 19.679 for the shell and bottom cone, and 18.371 to 19.662 for the top dome.

Table 4.5: Formulas for new mathematical model derived from tension test results on 210AL-3401.

Component		**Hp_{eff} range**			
Shell and bottom cone		**18.681 - 18.848**	**18.848 - 19.105**	**19.105 - 19.279**	**19.279 - 19.679**
Actual	%Change in YS	11.132 Hp_{eff} - 207.92	-9.5697 Hp_{eff} + 182.73	-67.664 Hp_{eff} + 1292	19.338 Hp_{eff}^2 - 760.35 Hp_{eff} + 7458.7
	%Change in UTS	4.0797 Hp_{eff} - 76.28	-8.4495 Hp_{eff} + 160.08	-72.552 Hp_{eff}^2 + 2726.1 Hp_{eff} - 25602	42.484 Hp_{eff}^2 - 1658.1 Hp_{eff} + 16164
2σ	%Change in YS	10.681 Hp_{eff} - 199.5	-9.3734 Hp_{eff} + 178.96	-71.4 Hp_{eff} + 1363.4	22.388 Hp_{eff}^2 - 881.73 Hp_{eff} + 8664.9
fitting	%Change in UTS	4.0423 Hp_{eff} - 75.581	-8.5573 Hp_{eff} + 162.12	-61.036 Hp_{eff} + 1165	30.495 Hp_{eff}^2 - 1195.3 Hp_{eff} + 11697
Top dome		**18.371 - 18.568**	**18.568 - 18.830**	**18.830 - 19.096**	**19.096 - 19.662**
Actual	%Change in YS	0.0704 Hp_{eff} - 1.2935	76.767 Hp_{eff}^2 - 2877.9 Hp_{eff} + 26969	-25.037 Hp_{eff} + 469.43	9.3756 Hp_{eff}^2 - 368.41 Hp_{eff} + 3607.3
	%Change in UTS	-1.8485 Hp_{eff} + 33.958	43.124 Hp_{eff}^2 - 1618.7 Hp_{eff} + 15187	-14.135 Hp_{eff}^2 + 508.97 Hp_{eff} - 4574.3	8.4266 Hp_{eff}^2 - 332.13 Hp_{eff} + 3260.1
2σ	%Change in YS	0.0664 Hp_{eff} - 1.2202	80.441 Hp_{eff}^2 - 3015.6 Hp_{eff} + 28260	-25.146 Hp_{eff} + 471.36	9.2032 Hp_{eff}^2 - 362.23 Hp_{eff} + 3552
fitting	%Change in UTS	-1.9303 Hp_{eff} + 35.462	43.938 Hp_{eff}^2 - 1649.4 Hp_{eff} + 15477	-13.489 Hp_{eff}^2 + 484.41 Hp_{eff} - 4340.8	7.8732 Hp_{eff}^2 - 311.19 Hp_{eff} + 3061.8

Absence of a statistical confidence level in Hattingh's model can also be considered a further weakness in that model when compared to the new mathematical model. Testing the accuracy of the new proposed model can be performed by allocating certain ash locks for monitoring purposes. During future GO's cutting of samples from these ash locks (and doing window repairs) can be done and destructive testing performed for the purpose of monitoring the accuracy of the model.

4.7 Conclusion

Results of mechanical tests on samples from the shell and dome and shell-to-dome circumferential weld of the test ash lock 210AL-3401, in the as-received condition as well as after being subjected to a series of simulated PWHT cycles, have shown a general downward trend in mechanical properties with increasing PWHT. The test values are generally higher than what was predicted using Hattingh's model and above acceptable limits after extended PWHT, with the exception of impact strength. A new mathematical model was constructed to be used to predict future tensile properties of the ash locks after PWHT. Test results will be discussed in the next chapter (see Chapter 5 "Discussion").

CHAPTER 5: DISCUSSION

5.1 Introduction

Shell, dome and shell-to-dome weld samples removed from the test ash lock 210AL-3401 were exposed to several additional PWHT cycles with holding times ranging from 2 hours to 100 hours. These samples were subjected to mechanical testing (tension -, hardness - and impact testing) to determine the effect of extended PWHT on the mechanical properties. This was done to verify the validity of the graphical prediction model that was derived previously based on test results from Hattingh's work [1987Hat] and used to predict mechanical tensile properties for the ash locks after being subjected to PWHT [2009Me1, 2009Me2]. This model was suspected to have been too conservative and that the actual properties of the ash locks after PWHT could be higher than the predicted values leading to ash locks being scrapped prematurely.

5.2 Mechanical test results

5.2.1 Tension test results

Tension test results for the shell and dome materials and the shell-to-dome weld in the as-received condition and after additional simulated PWHT were higher than what was predicted using the graphical prediction model derived from test results by Hattingh [1987Hat, 2009Met2]. The results showed 4 distinct stages in mechanical tensile property evolution with an increasing Hp_{eff} (i.e. increasing simulated PWHT).

Stage 1 showed a slight increase in tensile properties for the shell, dome and shell-to-dome weld with increasing simulated PWHT. This stage already started at initial fabrication of the ash lock when the first PWHT was performed (±1980). Test have confirmed that at the time the ash lock was scrapped in 2001 due to apparent end of life (as-received condition), it had already evolved quite a distance into stage 1 with tensile properties for the shell and dome higher than minimum ASME required values [2013As1] and higher than the predicted values [1987Hat] and in fact still increasing with increasing Hp_{eff}.

Stage 2 showed a slight decrease in tensile properties (UTS and YS) for the shell, dome and shell-to-dome weld with increasing Hp_{eff}.

Stage 3 showed a rapid decrease in tensile properties for the shell, dome and shell-to-dome weld with increasing Hp_{eff}. This occurred at an Hp_{eff} of 19.072 for the shell, 18.830 for the dome and 19.279 for the shell-to-dome weld.

During stage 4 stabilisation of tensile properties for the shell and dome (decrease at a reduced rate) occurred with increasing Hp_{eff}. During this stage the rate of decrease in UTS and YS is much lower. This stage was absent for the shell-to-dome weld tension tests.

Hattingh also found these similar 4 stages in his work [1987Hat]. An initial increase in tensile properties as well as hardness occurred after the first couple of PWHT cycles, followed by a significant drop in properties after a number of PWHT cycles. Eventually the decrease in properties was significantly lower and tended to flatten with increasing PWHT.

5.2.2 Hardness test results

Hardness values for the shell and dome were found to generally decrease with increasing Hp_{eff}. There was, however, a sharp decrease in hardness during stage 3 with stabilisation of hardness values occurring during stage 4. This was also confirmed in Hattingh's work [1987Hat].

5.2.3 Charpy impact test results

Impact toughness for the shell and dome was above the minimum required values of 35 Joules average and 24 Joules minimum [2003Sas] during the largest part of the Hp_{eff} range (stages 1 to 4). Test temperature was 0°C as per material certificates. During stage 1 an increase in impact toughness was noted with a sharp decrease noted during stage 3 and stabilisation during stage 4. Impact toughness for the shell and dome after 100 hours of additional PWHT was below the minimum required values. Hattingh found similar results in his work [1987Hat]. This phenomenon was not observed on the weld samples for which, on the contrary, an overal increase in impact toughness was observed.

Hu, Hu, Du, Wang et al. [2014Hu] also found that impact toughness of the HAZ after a number of PWHT cycles increased. Wei, Shang and Wu [2010Wei] investigated grain refinement in the coarse-grained region of the HAZ in low-carbon steel and found that with increasing PWHT the grain size became smaller leading to an increase in toughness. None of these researchers, however, studied the effects of several PWHT cycles.

5.2.4 Ductile to brittle transition temperature (DBTT) curve

Test results have shown that tensile properties for the test ash lock after 100 hours of additional PWHT exposure (Hp_{eff} = 19.679) were below minimum ASME requirements [2013As1], but may still be high enough to pass a FFS evaluation [2007Ap2]. A decrease in impact toughness below the minimum required value [2003Sas], however, occurred at an Hp_{eff} value of 19.679 for the shell and 19.662 for the dome when tested at 0°C. This was directlly ascribed to the marked increase in size of the very brittle molybdenum carbides phases (Mo_2C, Mo_3C and M_6C).

To confirm whether impact toughness would be the governing factor on future integrity of the ash locks, a DBTT curve was constructed by conducting Charpy V-notch impact testing at temperatures varying from 0°C to 80°C on samples of the shell that were subjected to an additional 100 hours of PWHT. This was done to determine the DBTT, i.e. the temperature below which failure is expected to behave predominantly brittle. It was found that the impact toughness increased with increasing test temperature with an upper shelf energy of approximately 150 Joules at a upper transition temperature of 42°C and the lower shelf energy approximately 10J at a lower transition temperature of 0°C. The average DBTT for the external -, internal surface and middle of the plate was determined from the graph as +4°C. This is the point where absorbed energy during impact testing was exactly equal to the minimum specified 35 Joules [2003Sas]. The percentage shear (ductile) fracture on the fracture surface of the impact test specimen tested at both 0°C and 10°C was measured as 20%, implying that fracture at +4°C would be predominantly brittle, yet above the minimum specified 35 Joules [2003Sas].

Hattingh [1987Hat] also found that the DBTT of samples exposed to numerous PWHT cycles decreased compared to the DBTT in the as-received condition, indicating an increase in ductility with increasing Hp. A significant upwards shift in uppershelf energy with increasing Hp was noticed in Hattingh's work, which was attributed to an increased toughness of the material.

Using this DBTT graph the impact toughness of the shell and dome at the currently specified hydrostatic pressure test temperature of +16°C for the ash locks will be between 75 - 90 Joules, which is above the minimum specified 35 Joules [2003Sas]. The percentage shear (ductile) fracture on the fracture surface of the impact test specimen tested at both 10°C and 20°C was, however, measured as 20%, implying that fracture at +16°C would be predominantly brittle. The percentage shear fracture on the specimens tested at between 20°C and 40°C was measured as between 20 - 30%, implying that fracture would be mixed mode (both ductile and brittle, however slightly more brittle). At a test temperature of 50°C the percentage shear fracture was between 30 - 60%, i.e. mixed mode with an approximately 50/50 ratio between ductile and brittle fracture. The percentage shear fracture measured on the fracture surface of the impact test specimen tested at 80°C was 85%, implying that fracture at normal operating temperatures between 360 and 400°C is expected to be predominantly ductile. At normal operating temperatures the material is, therefore, not expected to be susceptible to brittle fracture.

5.3 Metallographic examination

5.3.1 Parent metal

Metallographic examination showed that during stage 1 microstructures of the shell and dome samples showed fine precipates on the grain boundaries, but also intragranular in the ferrite. These precipitates were confirmed via the SEM and EDX to be rich in molybdenum, and therefore typically molybdenum carbides (Mo_2C) formed due to secondary hardening. Hattingh also noted that after the first PWHT cycle a network of fine molybdenum carbide precipitates (Mo_2C) was observed in the microstructure, a precipitation hardening effect known as secondary hardening [1987Hat].

After further heat treatment (stage 2) overaging of the molybdenum carbides occurred, which resulted in slow coarsening of the carbides. This, together with more advanced (stage C [1961Tof]) spheroidisation of the cementite phase, consequently resulted in a decrease in tensile properties. Clark and Varney found that secondary hardening results in an initial increase in mechanical tensile properties after which, with further heat treatment, the effect gradually dissappears as the Mo_2C coarsens [1962Cla].

During stage 3 large alloy carbides, possibly Mo_3C and M_6C carbides, have precipitated on the grain boundaries. Coarsening of the Mo_2C carbides, formation of large Mo_3C and possibly M_6C carbides, transformation from cementite (Fe_3C) to Mo_2C in the pearlite phases, together with an increase in the level of spheroidisation (stage C/D [1961Tof]) of the cementite, have resulted in a rapid decrease in tensile properties with increasing Hp_{eff}. Hattingh found after more PWHT cycles at a certain point a sharp drop in tensile properties was observed due to coarsening of the Mo_2C, formation of M_6C carbides, transformation from Fe_3C to Mo_2C in the pearlite phases, and spheroidisation of the cementite phase [1987Hat].

After prolonged heat treatment of 30 hours additional PWHT on the shell and 20 hours on the dome, stabilisation of tensile properties (stage 4) was reached, i.e. a decrease in tensile properties at a reduced rate. This was a result of reaching complete (stage D [1961Tof]) spheroidisation and no further coarsening of molybdenum carbides occurred. Hattingh also

found that after a certain number of cycles spheroidisation was virtually complete and the decrease in tensile properties became lower [1987Hat].

After extended PWHT (>60 hours additional PWHT) a marked increase in the size of the Mo_3C carbides was noted, which grew even bigger after 100 hours additional PWHT. These phases were confirmed via the ETD and BSED of the SEM and the EDX to be molybdenum-rich and, therefore, typically Mo_3C [1962Cla]. The sudden drop in impact toughness at Hp_{eff} 19.679 for the shell and Hp_{eff} 19.662 for the dome can be directly ascribed to the large size of these carbides [1986Spa, 2001deB].

5.3.2 Welded samples

For the welded samples during stage 1 a network of fine molybdenum carbide precipitates was noted on the grain boundaries, within the ferrite grains of the parent metal, in the HAZ and weld metal, i.e. secondary hardnening. Coarsening of the carbides and spheroidisation become more advanced (stage C spheroidisation [1961Tof]) during stage 2. With further heat treatment (stage 3) fine-grained ferrite along prior austenite grain boundaries was found in the ICRCG HAZ with large carbides noted in the SCHAZ. Stage 4 (stabilisation of tensile properties) was absent during tension testing of the weld metal samples; however, virtually complete (stage D/E [1961Tof]) spheroidisation and no significant further coarsening of molybdenum carbides were noted.

Hu, Du, Wang et al. [2014Hu] found that after PWHT precipitates formed in the weld metal providing potential nucleation sites for ferrite. This led to extraordinary refinement of martensite/austenite (M/A) constituents and consequent decrease in hardness and increase in toughness.

5.4 Significance of test results from this study

5.4.1 Comparison with Hattingh's test results

The results of this investigation showed that the actual tensile properties of the shell and dome of ash lock 210AL-3401 at various Hp_{eff} values were significantly higher (as much as 10%) than what was predicted using the model that was based on Hattingh's work [1987Hat, 2009Met2]. The decrease in properties after PWHT was much more pronounced with Hattingh's tests (based on a thinner test plate which matched composition) than what was found with the actual ash lock tests. Tests performed by Verhoef [2002Ver] on the bottom cone of ash lock 210AL-3401 also showed that the actual mechanical properties of the cone parent material after being heat treated for 14 hours at 615°C were higher than the estimated values [1987Hat]. Based on the tension test results obtained in this study it can be concluded that the graphical prediction model [1987Hat] used to predict mechanical tensile properties for the shell and dome of the ash lock in its current (as-received) condition, as well as after additional simulated PWHT, was over-conservative. The reason for these deviations is mainly related to different initial heat treatment conditions. The material used in Hattingh's tests was normalised, quenched and tempered (temperature and time not known), while the material of the shell, dome and cone of ash lock 210AL-3401 was normalised (910°C for 145 minutes) and tempered (650°C for 155 minutes), as was confirmed from the code data book. This resulted in different initial mechanical properties and different microstructures, i.e. martensite, bainite, ferrite and pearlite for Hattingh's test material vs. ferrite and pearlite for the actual ash lock test material. This, consequently, resulted in a difference in secondary hardening behaviour and resistance of the material to overaging, ultimately resulting in a slower rate of degradation of tensile properties, during PWHT. This phenomenon was also observed by Brooks [1996Bro].

Chemical compositions of the various batches of the test ash lock and Hattingh's samples were very similar apart from a higher manganese, sulphur and phosphorous contents in the ash lock materials compared to Hattingh's batch. Manganese and phosphorous contents were slightly higher than the specified limits. Although manganese is a weak carbide former, found in solid solution in cementite and not in a separate carbide phase, the presence of manganese could have strengthened the cementite resulting in a larger

resistance to overaging. The slightly higher than specified phosphorous content is not seen as a concern. At most this would have resulted in a slightly higher UTS, YS and hardness, improved machinability and a slight decrease in toughness and ductility [2007Key]. No significant effect was, however, noted on the actual mechanical properties.

5.4.2 UTS vs. hardness

No direct correlation could be confirmed between UTS and hardness obtained during the tests other than an overall decrease in both UTS and hardness with increasing Hp_{eff}. Hardness was inconsistent with increasing Hp_{eff} and did not follow the same trend as the UTS, i.e. no inital increase in hardness was observed in stage 1 and no significant decrease in hardness occurred in stage 2. No consistent rapid decrease in hardness was noted in stage 3. Hardness values during stage 4 was also inconsistent. Hardness showed a general downward trend through stages 1 to 4 with increasing Hp_{eff}.

UTS in the middle of the plate thickness was generally slightly lower (between 0 to 5%) than at the external and internal surfaces where UTS was comparable. The lower UTS values in the middle of the plate could be attributed to slower cooling rates due to longer heat retention in the middle of the plate resulting in more spheroidisation. Metallographic examination of the samples taken from the middle of the plate and the surfaces did, however, not indicate a significant difference in the level of spheroidisation in the microstructure. Impact toughness in the middle of the plate compared well with that at the surfaces, but also showed a general downward trend with increasing Hp_{eff}.

Canonico and Berggren [1971Can] also found a variation in mechanical tensile properties through the thickness of the plate after PWHT with higher UTS measured at the surface than at mid-section. The UTS of welded samples was, however, found to be uniform through the thickness with similar strength measured at the surface than at mid-section.

Hardness throughout the thickness of the plate was inconsistent and scattered. Surface hardness measurements can, therefore, not be considered representative of the hardness in the middle of the plate and can, thus, not be used to reliably determine the estimated UTS in the middle of the plate using SA-370 conversion methods [2013As2].

For instance, from figure 4.4 it can be seen that at an Hp_{eff} of 19.501 the hardness measured with a MIC20 portable Vickers hardness tester at the internal and external surfaces of the shell varied between 149.2 and 158.8HV. This correlated to an estimated UTS range of 495 - 550MPa (average 522MPa) using SA-370 Table 3. The measured UTS at Hp_{eff} 19.501 is, however, shown in figure 4.1 as between 517 - 537MPa (average 527MPa) at the surfaces, i.e. an error margin of only ~0.95%, and 522.8MPa in the middle of the plate, i.e. an error margin of only ~0.15%.

However, using the same principal to obtain the estimated UTS in the middle of the plate at an Hp_{eff} of 19.279 results in quite a different outcome. Portable Vickers hardness measurements at the surfaces varied between 154.8 and 164.8HV, correlating to an estimated UTS range of 522.5 - 565MPa (average 543MPa) using SA-370 Table 3. The measured UTS at Hp_{eff} 19.279 is, however, shown in figure 4.1 as between 531 - 546MPa (average 542MPa) at the surfaces, i.e. an error margin of ~0.18%, but 531.6MPa in the middle of the plate, i.e. an error margin of ~2.10%! Relying on portable hardness testing could, therefore, lead to either premature scrapping of an ash lock if estimated UTS from hardness measurements is too low, or, worse, a safety risk if actual UTS values are lower as compared to estimated UTS from hardness measurements.

5.4.3 Status of other installed ash locks

Since the same graphical prediction model [1987Hat, 2009Met2] was used to predict mechanical tensile properties for all originally fabricated ash locks it is possible that the actual mechanical tensile properties for these ash locks may also be higher than what was predicted.

It was confirmed from studying the code data books that the initial heat treatment condition (i.e. normalised and tempered) as per material certificates of the shell, dome and

cone of the other originally installed ash locks on the plant are comparable to that of the test ash lock 210AL-3401 (see Appendix B table B.1 for a list of ash locks, their initial heat treatment condition, initial mechanical properties and chemical composition).

Table B.1 shows that initial mechanical properties for the ash locks differ substantially (up to 60% range between the lowest and highest UTS values). This can be ascribed to various factors, such as slight differences in chemical composition, grain shape and size, different initial heat treatment temperatures and times and method of manufacturing. The ash locks all come from different batches, therefore, these variables are expected to vary. The shell, dome and cone were, however, also from different batches with different initial mechanical properties, but the tests have shown that the microstructure behaviour and the degree of change in mechanical properties with increasing Hp_{eff} for these components were comparable.

The outcome of the tests in this study can, therefore, be considered representative of the originally installed ash locks. The new mathematical model can, thus, be used for future predictions of the tensile properties of the shell, dome and cone of these ash locks. Note, this model should only be used for the originally installed ash locks shown in Appendix B table B.1. For any ash lock installed at a later stage the initial heat treatment condition should first be determined from the code data books before deciding whether the outcome of the tests in this study applies to that ash lock. In cases where these conditions are not met it is recommended to use the current model that was based on Hattingh's work [1987Hat, 2009Met2], or, alternatively, to perform destructive testing similar to what was done in this study on samples of that specific ash lock.

5.4.4 Replication

Microstructural examination via replication using an optical microscope at magnification 1000x or at higher magnifications using the SEM may be used to determine the stage of PWHT exposure (stages 1 to 4 in figure 4.1), the level of spheroidisation and the presence and size of molybdenum carbides. However, to obtain the exact Hp_{eff} in that specific stage may not be accurate due to the large span of each stage and little notable metallographic

changes throughout each specific stage. Also, EDX analysis to confirm molybdenum in the carbides cannot be performed on a replica as it is only an imprint of the microstructure.

5.5 Conclusion

From this study it can be confirmed that the graphical prediction model, that was based on Hattingh's work and used to predict mechanical tensile properties for the ash locks after being subjected to PWHT, was too conservative. Actual tensile properties of the test ash lock in the as-received condition and after PWHT were higher than the predicted values. The A 302 Grade B material of the ash lock shell and dome was shown to have a limited life (Hp_{eff} ~19.5), which is governed by both tensile properties and impact toughness. When this point is reached tensile properties are required to pass a FFS evaluation [2007Ap2]. To ensure sufficient impact toughness between Hp_{eff} ~19.5 and Hp_{eff} ~19.67, metal temperature for the ash locks during plant commissioning, decommissioning and hydrostatic pressure testing should be kept above +20°C before pressure is applied to avoid brittle fracture. It must be noted that the minimum metal temperature for the ash lock is also dependent on test results for the forged materials of the nozzles, dip pipe and internals of the ash lock. Testing of the forgings did not form part of this project.

CHAPTER 6: CONCLUSIONS

6.1. Research objectives

The hypothesis is that resulting from the adoption of an overly conservative life limit approach, ash locks at Sasol are being prematurely scrapped due to too low predicted tensile properties.

Objectives to test this hypothesis were as follows (from Chapter 1 paragraph 1.4):

a. Determine the mechanical properties (tensile -, hardness -, impact properties) and microstructure of the ASTM A 302 Grade B shell and top dome components and the shell-to-dome weld of the test ash lock 210AL-3401 in the as-received condition.
b. Determine the effect of several repeated PWHT cycles on the mechanical properties and microstructure of the ASTM A 302 Grade B materials and whether the mechanical properties will reach a minimum limiting value beyond which no further degradation occurs.
c. Investigate whether there is a correlation between hardness and ultimate tensile strength (UTS) of the material and whether surface hardness measurements before and after PWHT can accurately predict the through-thickness UTS of the ash lock material.

From the findings of this investigation the following conclusions to the research objectives can be made:

a. Tensile -, hardness -, and impact properties of the ASTM A 302 Grade B shell and top dome components and the shell-to-dome weld of test ash lock 210AL-3401 in the as-received condition were determined and found to be much higher than what was predicted using a graphical prediction model that was based on Hattingh's test results [1987Hat, 2009Met2]. The microstructure of the test ash lock was confirmed to be ferrite/pearlite typical of normalised and tempered material, as compared to Hattingh's material that was martensite/bainite/ferrite/pearlite typical of normalised, quenched and tempered material.

b. With several repeated PWHT cycles it was determined that the rate of decrease in tensile properties with increasing Hp_{eff} was lower than predicted [1987Hat]. It was also discovered that mechanical tensile properties and hardness will reach a minimum limiting value beyond which degradation in properties occurs at a much slower rate. Impact toughness was found to decrease gradually and then drop significantly at a certain point (Hp_{eff} 19.679 for the shell and 19.662 for the dome). DBTT tests showed that the impact toughness is above minimum specified limits [2003Sas] at a DBTT of +4°C. Visual appearance of the fracture surface, however, showed that fracture mode at this temperature was predominantly brittle. It is advised, based on DBTT tests, that between an Hp_{eff} value of ~19.5 and ~19.67 the metal temperature of the ash lock during commissioning, decommissioning and hydrostatic pressure test of the ash lock should be maintained above +20°C.

c. It was found that there is no direct correlation between UTS and hardness of the material before and after PWHT. There is an overall decrease in both UTS and hardness with increasing Hp_{eff}. Hardness was inconsistent with increasing Hp_{eff} and did not follow the same trends as the UTS. Hardness throughout the thickness of the plate was also inconsistent whereas UTS in the middle was generally slightly lower than at the surfaces. Surface hardness measurements can, therefore, not be considered representative of the hardness in the middle of the plate and can, thus, also not be used to determine the estimated UTS in the middle of the plate using SA-370 conversion methods [2013As2].

The hypothesis that ash locks at Sasol are being prematurely scrapped due to too low predicted tensile properties was, thus, proven to be true.

6.2. Research questions

As a result of achieving the above-mentioned objectives the following research questions were posed:

a. Can microstructural examination (i.e. replication) be performed to accurately determine the mechanical properties of the ash locks after PWHT? This was suggested by Hattingh [1987Hat] as a practical means during GO's to determine the

mechanical properties of the components of the ash lock to confirm whether it can undergo any further PWHT.

b. Can the results obtained from mechanical testing on this ash lock, 210AL-3401, be considered representative of the other ash locks still in service?

c. Can a new graphical prediction model be derived from these test results or should the current model be optimised to more accurately predict the mechanical tensile properties after repeated PWHT on the other ash locks still in service?

From the findings of this investigation the following answers to the research questions can be given:

a. Microstructural examination via replication cannot be used to determine mechanical properties. It may, however, be used to determine the stage of PWHT exposure (stages 1 to 4 in figure 4.1) using an optical microscope at magnification 1000x, or even higher magnifications using the SEM, to determine the level of spheroidisation and to detect the presence and size of molybdenum carbides. However, to obtain the exact position (Hp_{eff}) in that specific stage may not be accurate due to the large span of each stage and little notable metallographic changes throughout each specific stage. Also, bear in mind that EDX analysis to confirm molybdenum content in the carbides cannot be performed on a replica as it is only an imprint of the microstructure.

b. The results obtained from tests on this ash lock, 210AL-3401, can be considered representative of the other originally installed ash locks still in service, since those ash locks were manufactured from the same grade of material and have been subjected to a similar initial heat treatment (refer to Appendix B table B.1). Initial UTS for the ash locks differ significantly probably resulting from the manufacturing processes used. The minimum UTS per ash lock will, therefore, need to be considered when predicting properties for that ash lock.

c. A new mathematical model (figure 4.34) was derived from the tests on ash lock 210AL-3401. This model can be used to predict tensile properties of individual originally installed ash locks after PWHT, since those ash locks were manufactured from the same grade of material and have been subjected to a similar initial heat treatment. For ash locks installed at a later stage the initial heat treatment condition

should first be determined from the code data books before deciding whether the new model can be applied.

6.3. Limitations of the study

All tension tests in the study were performed at room temperature. No elevated temperature tension tests could be performed due to a limited number of samples that could be cut from the shell and dome. It was considered more important that a sufficient number of test specimens are made available for tension testing at room temperature. This is not seen as a concern as the minimum requirements in ASME [2013As1] for this material are given at room temperature. Elevated temperature tension tests would have been very informative, but can be considered an optional extra.

The integrity of the forged components (nozzles, dip pipe and internals) was not tested in this study as the study was aimed at testing only the ASTM A 302 Grade B material of the shell, top dome and bottom cone. The pressure envelope of a typical ash lock consists mainly of the shell, dome and cone, all of which are made from ASTM A 302 Grade B material. Only the top and bottom nozzle and dip pipe, as well as non-pressure bearing internals, are made from ASTM A 182 Grade F1 forged material. Testing of the forgings did not form part of this project. However, calculations have shown that predicted properties of the forged components [2009Me1, 2009Me2], based on previous repeated PWHT tests on this type of material, were generally higher than what was predicted for the shell, dome and cone. It is, therefore, expected that a similar study on the ASTM A 182 Grade F1 forged material of the ash locks will yield positive results.

CHAPTER 7: REFERENCES

[1945Hol] J.H. Hollomon and L.D. Jaffe, Time-Temperature Relations In Tempering Steel, Technical Publication No. 1831, Metals Technology, American Institute of Mining and Metallurgical Engineers, USA, (1945).

[1996Bro] C. Brooks, Principles of the heat treatment of plain carbon and low alloy steels, ASM International, p158 (1996).

[1947Hol] J.H. Hollomon and L.D. Jaffe, Ferrous Metallurgical Design, John Wiley and Sons Inc., p245, (1947).

[1944Fle] S.G. Fletcher and M. Cohen, Trans.ASM, Vol.32, p333, (1944).

[1984Kra] G. Krauss, A.R. Marder AR and J.I. Goldstein, Phase Transformations in Ferrous Alloys, The Metallurgical Society, Warrendale, PA, (1984).

[1945Ho2] J.H. Hollomon and L.D. Jaffe, Trans AIME, Vol. 162, p223, (1945).

[1969Spei] G.R. Speich, Trans AIME, Vol. 245, p2553, (1969).

[1952Lar] F.R. Larson and J. Miller, A Time-Temperature Relationship For Rupture And Creep Stresses, Trans.ASME, (1952).

[1961Tof] L.H. Toft and R.A. Marsden, The Structure And Properties Of 1%Cr-0.5%Mo Steel After Service In CEGB Power Stations, Materials Division, Central Electrical Research Laboratories, Special Report 70, Iron and Steel Institute, London, (1961).

[1962Cla] D.S. Clark and W.R. Varney, Physical Metallurgy for Engineers, D. Van Norstand Company, New York, p132-185, (1962).

[1971Can] D.A. Canonico and R.G. Berggren, Tensile And Impact Properties Of Thick-Section Plate And Weldments, Oak Ridge National Laboratory, Oak Ridge, Tennessee, USA, (1971).

[1972Toy] T. Toyooka and K. Terai, On the effects of post weld heat treatment, 53rd Annual AWS Meeting held in Detroit, Michigan, USA, Welding Research Supplement, p247, (1972)

[1980As1] ASME II-A Specification SA-302, Specification For Pressure Vessel Plates, Alloy Steel, Manganese-Molybdenum And Manganese-Molybdenum-Nickel, American Society for Mechanical Engineers, (1980).

[1980As2] ASME II-A Specification SA-370, Test methods and definitions for mechanical testing of steel products, American Society for Mechanical Engineers, (1980).

[1980As3] ASME VIII Division 1 Paragraph UCS-56, American Society for Mechanical Engineers, (1980).

[1980Sas] General arrangement drawing for ash locks 210AL-01-59, Sasol Drawing Number: SDM-210-003486, Sasol Synfuels, (1980).

[1980Ued] S. Ueda, A. Ishikawa and N. Ohashi, Relation Between Precipitation Behaviour of Mo-, V- and Nb carbides and Yield Strength in Normalised and Tempered Steel, Trans. Iron & Steel, Japan, p.759-767, (1980).

[1981Gil] J.G. Gillissie, National Board Classic Series, Category: Design/Fabrication, National Board Bulletin (1981)

[1982Hon] R.W.K. Honeycombe, Steels: Microstructure and properties, Metallurgy and materials science, American Society for Metals, (1982)

[1983Neu] B. Neubauer and U. Wedel, Restlife Estimation of Creeping by Means of Replicas, Advances in Life Prediction Methods, D. A. Woodford and J.R.

Whitehead Ed., American Society of Mechanical Engineers, New York, p 307-314, (1983).

[1985Sma] R.E. Smallman, Modern Physical Metallurgy, 4th edition, Butterworth-Heinemann, Saint Louis, Missouri, USA, (1985)

[1986Spa] D.J. Sparkes, Effect of Post Weld Heat Treatment on HAZ Microstructure and Toughness of Micro-Alloyed C-Mn Submerged-Arc Welds, Welding Institute Research Report 323, (1986).

[1987Hat] C. Hattingh, The Effect Of Repeated Heat Treatment On The Mechanical Properties Of ASTM A 302 Grade B (Mn-Mo) Steel And API 5L Grade B (C-Mn) Steel, Technikon Pretoria, South Africa, (1987).

[1988Die] G.E. Dieter, Mechanical Metallurgy, SI metric edition, McGraw-Hill, ISBN 0-07-100406-8 (1988).

[1995Joa] A. Joarder, Physical metallurgy of steels, National Metallurgical Laboratory, Jamshedpur, India, (1995)

[1997Tot] G.E. Totten and M.A.H. Howes, Steel Heat Treatment Handbook, CRC Press, 1st edition, p15, (1997)

[1999Guo] Congsheng Guo, Acta Metall. Sin., Vol.35(8), p865 (1999).

[2000Spa] O.D. Sparkman, Mass spectrometry desk reference, Global View Pub, Pittsburgh, USA, ISBN 0-9660813-2-3, (2000).

[2001deB] V.L. Othero de Brito, H.J.C. Voorwaald, N. das Neves and I. de S. Bott, Effects Of Post Weld Heat Treatment On A SMAW Welded ASTM A537 Pressure Vessel Steel, Journal of Materials Engineering and Performance, ASM International, Vol.10 (3), (2001).

[2002Ahm] K. Ahmed and J. Krishnan, Post-Weld Heat Treatment - Case Studies, BARC Newsletter, Centre for Design and Manufacture, Bhabha Atomic Research Centre, Mumbai, India, (2002)

[2002Ver] C. Verhoef, Results Of Mechanical Tests Performed On Samples Removed From The Cone Of Ashlock 210AL-3401, Ref. no. 138_02cv, SecMet Metallurgical Consultants, MegChem, South Africa, (2002).

[2002Ray] P.K. Ray, R.I. Ganguly and A.K. Panda, Influence of Heat Treatment Parameters on Structure and Mechanical Properties of an HSLA-100 Steel, Steel Research (Germany) Vol.73 No.8, (2002).

[2003Sas] Sasol Specification SP-110-6 Revision 2, Impact Testing Of Metallic Materials, (2003).

[2004Key] The Tempering of Martensite: Part Two, The formation of alloy carbides: secondary hardening, Key to Metals, http://steel.keytometals.com/Articles/Art128.htm (May 2004).

[2005Non] N. Wan, W. Xiong and J. Suo, Mathematical Model for Tempering Time Effect on Quenched Steel Based on Hollomon Parameter, Wuhan, China, J. Mater. Sci. Technol., Vol.21 No.6, (2005).

[2006Lee] Y.S. Leea, M.C. Kimb, B.S. Leeb and C.H. Leea, Evaluation of microstructures and mechanical properties in the HAZ of SA 508 Gr.4N Low Alloy Steel, Transactions of the Korean Nuclear Society Autumn Meeting, Gyeongju, Korea, (November 2-3, 2006).

[2006Rag] V. Raghavan, Physical Metallurgy: Principles and Practice, Second Edition, Prentice Hall of India, (2006).

[2007Ap2] API 579, Fitness-for-service, Second Edition, American Petroleum Institute, (2007).

[2007Key] Effect of Phosphorus on the Properties of Carbon Steels: Part One, Key to Metals, http://www.keytometals.com/page.aspx?ID=CheckArticle&site=kts&NM=211 (Oct 2007).

[2007Sas] Sasol Specification SP-90-17 Revision 3, Heat Treatment, (2007).

[2007Ver] J.D. Verhoeven, Steel metallurgy for the non-metallurgist, ASM International, p99-105, (2007)

[2009Api] API RP 582, Welding Guidelines for the Chemical, Oil, and Gas Industries, (2009)

[2009Jan] Z. Janjušević, Z. Gulišija, M. Mihailović and A. Patarić, The Investigation Of Applicability Of The Hollomon-Jaffe Equation On Tempering The HSLA Steel, The Institute of Technology of Nuclear and other Mineral Raw Materials, Belgrade, Serbia, Association of the Chemical Engineers AChE, Chemical Industry & Chemical Engineering Quarterly 15 (3), p131-136, (2009).

[2009Kat] S.K. Kate and H.R. Bhapkar, Basics Of Mathematics, Technical Publications, ISBN 978-81-8431-755-8, Chapter 1, (2009).

[2009Me1] R. Filmalter, Predicted Mechanical Properties For The Ash Locks At Unit 10, Ref. no. MET09.0625.00.rf, Sasol Secunda, South Africa, (2009).

[2009Me2] R. Filmalter, Predicted Mechanical Properties For The Ash Locks At Unit 210, Ref. no. MET09.0261.00.rf, Sasol Secunda, South Africa, (2009).

[2010Wei] R. Wei, C. Shang and K. Wu, Grain refinement in the coarse-grained region of the heat affected zone in low-carbon high-strength microalloyed steels, International Journal of Minerals, Metallurgy, and Materials , Vol.17 No.6, p737-741, (2010).

[2011Api] API RP 571, Damage Mechanisms, American Petroleum Institute, (2011).

[2012Hu] Z. Hu, Heat-Resistant Steels Microstructure Evolution and Life Assessment in Power Plants, School of Materials Science and Engineering, Tongji University, Shanghai, China, InTech, (2012).

[2013As1] ASME II-A Specification SA-302, Specification For Pressure Vessel Plates, Alloy Steel, Manganese-Molybdenum And Manganese-Molybdenum-Nickel, American Society for Mechanical Engineers, (2013).

[2013As2] ASME II-A Specification SA-370, Test methods and definitions for mechanical testing of steel products, American Society for Mechanical Engineers, (2013).

[2013As3] ASME VIII Division 1 Paragraph UCS-56, American Society for Mechanical Engineers, (2013).

[2013Sin] D.P. Singh, M. Sharma and J.S. Gill, Effect of Post Weld Heat Treatment on the Impact Toughness and Microstructural Property of P-91 Steel Weldment, Bhaddal Ropar Institute of Engineering and Technology & Sant Longowal Institute of Engineering and Technology, India, (2013).

[2014Hu] J. Hu, L. Du, J. Wang, H. Xie, C. Gao and R.D.K. Misra, High toughness in the intercritically reheated coarse-grained (ICRCG) heat affected zone (HAZ) of low carbon microalloyed steel, Materials Science & Engineering, Volume 590, p323 - 328, (2014).

[2014Lau] D.E. Laughlin and K. Hono, Physical Metallurgy: 3-Volume Set, Edition 5, Newnes, (2014)

[2014Moh] P. Mohseni, J.K. Solberg, M. Karlsen, O.M. Akselsen and E. Østby, Cleavage Fracture Initiation at M–A Constituents in Intercritically Coarse-Grained Heat

affected Zone of a HSLA Steel, Metallurgical and Materials Transactions, Vol.45 No.1, p384-394, (2014).

APPENDIX A

Table A.1: Mechanical tensile properties of shell of ash lock 210AL-3401 in the as-received condition as well as after simulated PWHT.

Component	Hp	Hp_{eff}	Calcula-ted YS** [MPa]	Actual YS External (ave) [MPa]	Actual YS Middle (ave) [MPa]	Actual YS Internal (ave) [MPa]	Calcula-ted UTS** [MPa]	Actual UTS External (ave) [MPa]	Actual UTS Middle (ave) [MPa]	Actual UTS Internal (ave) [MPa]
As-received [11.93 hrs total] [8.31 hrs effective*]	18.821	18.681	375.70	443.83	441.45	455.72	536.60	606.37	607.99	613.49
As-received +2 hrs [14.41 hrs total] [10.79 hrs effective]	18.895	18.782	364.80	451.97	445.44	460.69	522.80	608.64	608.77	613.63
As-received +4 hrs [16.41 hrs total] [12.79 hrs effective]	18.945	18.848	356.00	458.95	444.46	462.21	511.60	615.35	609.66	615.94
As-received +6 hrs [18.41 hrs total] [14.79 hrs effective]	18.990	18.905	348.40	461.94	449.53	457.73	502.00	614.35	609.92	613.29
As-received +8 hrs [20.41 hrs total] [16.79 hrs effective]	19.030	18.954	341.80	464.91	434.48	464.21	493.70	615.09	594.62	618.93
As-received +10 hrs [22.41 hrs total] [18.79 hrs effective]	19.066	18.998	336.00	461.12	437.40	459.03	486.30	608.33	594.73	608.38
As-received +12 hrs [24.41 hrs total] [20.79 hrs effective]	19.099	19.037	330.70	458.00	438.03	451.34	479.60	611.30	599.26	609.05
As-received +14 hrs [26.41 hrs total] [22.79 hrs effective]	19.130	19.072	325.90	463.14	440.64	464.37	473.60	612.95	598.15	613.78
As-received +16 hrs [28.41 hrs total] [24.79 hrs effective]	19.158	19.105	321.60	453.53	431.00	450.85	468.00	605.17	589.74	607.26
As-received +18 hrs [30.41 hrs total] [26.79 hrs effective]	19.184	19.135	317.50	444.01	425.03	437.83	462.90	596.39	586.71	594.97
As-received +20 hrs [32.41 hrs total]	19.209	19.163	313.80	430.74	410.78	427.63	458.20	585.71	577.99	584.68

[28.79 hrs effective]										
As-received +30 hrs [42.41 hrs total] [38.79 hrs effective]	19.313	19.279	298.30	404.16	378.66	393.31	438.50	546.71	531.57	537.77
As-received +40 hrs [52.41 hrs total] [48.79 hrs effective]	19.395	19.368	286.30	408.48	386.54	397.07	423.40	538.88	525.15	525.65
As-received +60 hrs [72.41 hrs total] [68.79 hrs effective]	19.521	19.501	268.50	405.01	362.30	377.85	400.80	543.74	512.31	517.15
As-received +80 hrs [92.41 hrs total] [88.79 hrs effective]	19.615	19.600	255.20	374.77	353.06	363.47	384.00	517.37	489.47	503.64
As-received +100 hrs [112.41 hrs total] [108.79 hrs effective]	19.691	19.679	244.60	361.74	353.83	355.16	370.60	508.67	486.63	505.99
Min. required [2013As1]:			***345***				***550-690***			

*Effective time, t_{eff}, of exposure to simulated PWHT.

**Calculated tensile properties using the graphical prediction model derived from Hattingh's tests [1987Hat, 2009Met2].

Table A.2: Mechanical tensile properties of dome of ash lock 210AL-3401 in the as-received condition as well as after simulated PWHT.

Component	Hp	Hp_{eff}	Calcula-ted YS** [MPa]	Actual YS External (ave) [MPa]	Actual YS Middle (ave) [MPa]	Actual YS Internal (ave) [MPa]	Calcula-ted UTS** [MPa]	Actual UTS External (ave) [MPa]	Actual UTS Middle (ave) [MPa]	Actual UTS Internal (ave) [MPa]
As-received [7.35 hrs total] [3.73 hrs effective*]	18.634	18.371	413.80	439.45	425.10	457.21	572.90	584.20	599.55	621.96
As-received +2 hrs [9.83 hrs total] [6.21 effective]	18.746	18.568	411.40	443.31	424.20	454.44	567	601.44	582.65	615.04
As-received +4 hrs [11.83 hrs total] [8.21 effective]	18.818	18.677	410.10	438.41	414.89	438.15	563.7	597.05	575.21	599.32
As-received +6 hrs [13.83 hrs total] [10.21 effective]	18.879	18.761	401.30	434.05	417.05	442.50	552.9	591.92	574.33	604.22
As-received +8 hrs [15.83 hrs total] [12.21 effective]	18.931	18.830	391.10	429.69	419.22	446.85	540.5	586.80	573.44	609.12
As-received +10 hrs [17.83 hrs total] [14.21 effective]	18.977	18.889	382.50	422.43	414.67	434.36	530.00	575.62	566.48	591.34
As-received +12 hrs [19.83 hrs total] [16.21 effective]	19.018	18.940	375.00	418.80	412.39	428.11	520.90	570.03	563.00	582.46
As-received +14 hrs [21.83 hrs total] [18.21 effective]	19.056	18.985	368.40	415.17	410.11	421.86	512.90	564.43	559.52	573.57
As-received +16 hrs [23.83 hrs total] [20.21 effective]	19.090	19.026	362.50	411.54	405.56	415.61	505.70	558.84	552.56	564.68
As-received +18 hrs [25.83 hrs total] [22.21 effective]	19.121	19.062	357.20	407.91	401.00	409.36	499.10	553.25	545.60	555.80
As-received +20 hrs [27.83 hrs] [24.21 effective]	19.150	19.096	352.30	404.27	396.45	403.11	493.20	547.66	538.63	546.91
As-received +30 hrs [37.83 hrs total]	19.269	19.230	332.60	400.64	390.17	396.86	469.30	542.07	531.15	538.02

[34.21 effective]										
As-received +40 hrs [47.83 hrs total] [44.21 effective]	19.360	19.329	318.10	416.87	391.89	401.74	451.50	542.41	531.67	538.11
As-received +60 hrs [67.83 hrs total] [64.21 effective]	19.495	19.474	296.90	397.85	387.34	384.69	425.70	537.20	524.71	522.80
As-received +80 hrs [87.83 hrs total] [84.21 effective]	19.596	19.579	281.50	415.66	382.78	387.99	407.00	526.96	517.75	533.32
As-received +100 hrs [107.83 hrs total] [104.21 effective]	19.675	19.662	269.40	415.66	389.31	388.51	392.20	526.96	535.75	532.58
Min. required [2013As1]:			***345***				***550-690***			

*Effective time, t_{eff}, of exposure to simulated PWHT.

**Calculated tensile properties using the graphical prediction model derived from Hattingh's tests [1987Hat, 2009Met2].

Table A.3: Mechanical tensile properties of shell-to-dome weld of ash lock 210AL-3401 in the as-received condition as well as after simulated PWHT.

Component	**Hp**	**Hp_{eff}**	**Actual YS (ave)** [MPa]**	**Actual UTS (ave)** [MPa]**
As-received [11.93 hrs total] [8.31 hrs effective]	18.821	18.681	609.24	700.56
As-received (+2 hrs) [14.41 hrs total] [10.79 hrs effective]	18.895	18.782	614.49	695.92
As-received (+4 hrs) [16.41 hrs total] [12.79 hrs effective]	18.945	18.848	586.08	674.04
As-received (+6 hrs) [18.41 hrs total] [14.79 hrs effective]	18.990	18.905	592.23	684.01
As-received (+30 hrs) [42.41 hrs total] [38.79 hrs effective]	19.313	19.279	572.69	674.61
As-received (+40 hrs) [52.41 hrs total] [48.79 hrs effective]	19.395	19.368	553.14	665.21
As-received (+60 hrs) [72.41 hrs total] [68.79 hrs effective]	19.521	19.501	521.91	627.02
As-received (+80 hrs) [92.41 hrs total] [88.79 hrs effective]	19.615	19.600	506.67	609.36
Minimum required [2013As1]:			***550-690***	

*Effective time, t_{eff}, of exposure to simulated PWHT.

**Average of tension test results on samples from the external and internal surfaces. Middle values were omitted due to inconsistent test results resulting from the weld root configuration (insufficient weld metal present in the test specimen). External and internal values were comparable and the averages are displayed.

Table A.4: Hardness measurements of shell of ash lock 210AL-3401 in the as-received condition as well as after simulated PWHT.

Component	Hp	Hp_{eff}	Location	Brinell (ave) [HBN]	Vickers (ave) [HV10]	MicroDur Portable Vickers (ave) [HV]
As-received [11.93 hrs total] [8.31 hrs effective*]	18.821	18.681	External	173.2	172.8	176.8
			Middle	164.6	171.1	168.8
			Internal	167.6	166.6	166.0
As-received +2 hrs [14.41 hrs total] [10.79 hrs effective]	18.895	18.782	External	161.3	169.2	167.6
			Middle	170.0	169.9	167.8
			Internal	170.4	167.0	167.6
As-received +4 hrs [16.41 hrs total] [12.79 hrs effective]	18.945	18.848	External	174	171	167
			Middle	169.8	168.7	167.0
			Internal	169.9	169.1	163.4
As-received +6 hrs [18.41 hrs total] [14.79 hrs effective]	18.990	18.905	External	187	167	169
			Middle	169.6	170.2	177.6
			Internal	169.5	168.5	178.4
As-received +8 hrs [20.41 hrs total] [16.79 hrs effective]	19.030	18.954	External	175	165	169
			Middle	166.9	162.1	167.6
			Internal	168.4	162.9	170.0
As-received +10 hrs [22.41 hrs total] [18.79 hrs effective]	19.066	18.998	External	164	169	172
			Middle	164.2	162.5	169.2
			Internal	167.2	164.2	171.0
As-received +12 hrs [24.41 hrs total] [20.79 hrs effective]	19.099	19.037	External	170	167	167
			Middle	166.2	165.3	163.2
			Internal	172.2	166.1	167.2
As-received +14 hrs [26.41 hrs total] [22.79 hrs effective]	19.130	19.072	External	177	170	166
			Middle	168.3	161.3	162.6
			Internal	177.1	173.7	170.8
As-received +16 hrs [28.41 hrs total] [24.79 hrs effective]	19.158	19.105	External	174	166	167
			Middle	169.1	169.3	165.6
			Internal	175.3	169.2	174.0
As-received +18 hrs [30.41 hrs total] [26.79 hrs effective]	19.184	19.135	External	170	162	171
			Middle	169.9	172.4	169.4
			Internal	173.4	171.8	168.0
As-received +20 hrs [32.41 hrs total] [28.79 hrs effective]	19.209	19.163	External	170	167	161
			Middle	169.9	169.3	156.6
			Internal	173.4	167.8	172.2
As-received +30 hrs	19.313	19.279	External	170	163	165

Component	Hp	Hp_{eff}	Location	Brinell (ave) [HBN]	Vickers (ave) [HV10]	MicroDur Portable Vickers (ave) [HV]
[42.41 hrs total] [38.79 hrs effective]			Middle	169.9	159.8	159.8
			Internal	173.4	157.1	154.8
As-received +40 hrs [52.41 hrs total] [48.79 hrs effective]	19.395	19.368	External	170	161	163
			Middle	169.9	156.2	159.7
			Internal	173.4	151.5	156.8
As-received +60 hrs [72.41 hrs total] [68.79 hrs effective]	19.521	19.501	External	170	163	153
			Middle	169.9	158.8	149.4
			Internal	173.4	154.5	149.2
As-received +80 hrs [92.41 hrs total] [88.79 hrs effective]	19.615	19.600	External	170	159	155
			Middle	169.9	156.8	152.3
			Internal	173.4	154.8	149.3
As-received +100 hrs [112.41 hrs total] [108.79 hrs effective]	19.691	19.679	External	170	160	155
			Middle	169.9	158.1	150.6
			Internal	173.4	156.4	150.5

*Effective time, t_{eff}, of exposure to simulated PWHT.

Table A.5: Hardness measurements of dome of ash lock 210AL-3401 in the as-received condition as well as after simulated PWHT.

Component	Hp	Hp_{eff}	Location	Brinell (ave) [HBN]	Vickers (ave) [HV10]	MicroDur Portable Vickers (ave) [HV]
As-received [7.35 hrs total] [3.73 hrs effective*]	18.634	18.371	External	157.0	165.1	168.8
			Middle	154.9	159.5	167.2
			Internal	154.4	164.1	167.8
As-received +2 hrs [9.83 hrs total] [6.21 effective]	18.746	18.568	External	157.0	167.4	166.8
			Middle	154.9	165.4	166.0
			Internal	154.4	170.5	167.8
As-received +4 hrs [11.83 hrs total] [8.21 effective]	18.818	18.677	External	167.8	173	174
			Middle	164.9	172.0	165.7
			Internal	155.6	171.4	171.8
As-received +8 hrs [15.83 hrs total] [12.21 effective]	18.931	18.830	External	149.1	168	169
			Middle	150.4	166.0	164.8
			Internal	150.4	164.0	171.3
As-received +30 hrs [37.83 hrs total] [34.21 effective]	19.269	19.230	External	149.1	164	170
			Middle	150.4	160.6	171.0
			Internal	150.4	160.6	171.3
As-received +40 hrs [47.83 hrs total] [44.21 effective]	19.360	19.329	External	149.1	167	162
			Middle	150.4	155.7	166.2
			Internal	150.4	163.5	170.0
As-received +60 hrs [67.83 hrs total] [64.21 effective]	19.495	19.474	External	149.1	158	158
			Middle	150.4	150.8	151.0
			Internal	150.4	154.4	152.8
As-received +80 hrs [87.83 hrs total] [84.21 effective]	19.596	19.579	External	149.1	151.1	159.6
			Middle	150.4	151.3	152.4
			Internal	150.4	150.2	156.8
As-received +100 hrs [107.83 hrs total] [104.21 effective]	19.675	19.662	External	149.1	144.2	147.2
			Middle	150.4	151.8	152.8
			Internal	150.4	146.1	151.8

*Effective time, t_{eff}, of exposure to simulated PWHT.

Table A.6: Hardness measurements of shell-to-dome weld of ash lock 210AL-3401 in the as-received condition as well as after simulated PWHT.

Component	Hp	Hp_{eff}	Location	Shell parent metal	Shell HAZ	Weld metal
				MicroDur Portable Vickers [HV]	MicroDur Portable Vickers [HV]	MicroDur Portable Vickers [HV]
As-received [11.93 hrs total] [8.31 hrs effective*]	18.821	18.681	External	173.0	205.3	226.0
			Middle	187.0	208.3	215.7
			Internal	160.5	214.0	222.7
As-received +2 hrs [14.41 hrs total] [10.79 hrs effective]	18.895	18.782	External	173.0	205.3	226.0
			Middle	187.0	208.3	215.7
			Internal	160.5	214.0	222.7
As-received +4 hrs [16.41 hrs total] [12.79 hrs effective]	18.945	18.848	External	164	204	232
			Middle	163.6	201.7	220.3
			Internal	164.6	215.0	228.8
As-received +6 hrs [18.41 hrs total] [14.79 hrs effective]	18.990	18.905	External	171	218	236
			Middle	171.8	216.7	220.5
			Internal	168.8	210.8	237.8
As-received +30 hrs [42.41 hrs total] [38.79 hrs effective]	19.313	19.279	External	164	208	233
			Middle	-	-	-
			Internal	152.8	200.3	216.8
As-received +40 hrs [52.41 hrs total] [48.79 hrs effective]	19.395	19.368	External	157	212	233
			Middle	-	-	-
			Internal	158.8	205.6	223.4
As-received +60 hrs [72.41 hrs total] [68.79 hrs effective]	19.521	19.501	External	154	208	232
			Middle	-	-	-
			Internal	158.6	211.0	220.8
As-received +80 hrs [92.41 hrs total] [88.79 hrs effective]	19.615	19.600	External	152	191	233
			Middle	-	-	-
			Internal	150.2	183.4	212.6

*Effective time, t_{eff}, of exposure to simulated PWHT.

Table A.7: Charpy impact toughness of shell samples in an as-received condition and after additional simulated PWHT (tested at 0°C). The highlighted areas are where the values were below minimum requirements [2003Sas].

Condition	Hp_{eff}	Impact toughness External [J]	Average External [J]	Impact toughness Middle [J]	Average Middle [J]	Impact toughness Internal [J]	Average Internal [J]
As-received [8.31 hrs effective*]	18.681	108	104	97	100	107	97
		117		109		80	
		88		95		103	
As-received +2 hrs [10.79 hrs effective]	18.782	189	190	174	174	124	115
		189		170		105	
		191		175		116	
As-received +6 hrs [14.79 hrs effective]	18.905	97	93	115	103	85	80
		102		100		79	
		81		95		77	
As-received +10 hrs [18.79 hrs effective]	18.998	129	139	142	166	147	182
		132		209		121	
		155		147		276	
As-received +14 hrs [22.79 hrs effective]	19.072	93	84	90	80	100	93
		66		82		75	
		92		68		103	
As-received +18 hrs [26.79 hrs effective]	19.135	72	78	95	86	64	100
		80		73		71	
		81		89		164	
As-received +30 hrs [38.79 hrs effective]	19.279	34	39	-	-	44	49
		42		-		50	
		39		-		51	
As-received +60 hrs [68.79 hrs effective]	19.501	78	80	61	72	82	77
		74		79		107	
		86		76		39	
As-received +100 hrs [108.79 hrs effective]	19.679	14	16	15	17	18	18
		16		16		18	
		18		19		16	
Minimum required [2003Sas]:		**35J ave / 24J min**					

*Effective time, t_{eff}, of exposure to simulated PWHT.

Table A.8: Charpy impact toughness of dome samples in an as-received condition and after additional simulated PWHT (tested at 0°C). The highlighted areas are where the values were below minimum requirements [2003Sas].

Condition	Hp_{eff}	Impact toughness External [J]	Average External [J]	Impact toughness Middle [J]	Average Middle [J]	Impact toughness Internal [J]	Average Internal [J]
As-received [3.73 hrs effective*]	18.371	152	132	126	127	122	104
		119		113		111	
		126		143		79	
As-received +2 hrs [6.21 hrs effective]	18.568	150	129	157	165	129	148
		101		174		136	
		135		165		179	
As-received +4 hrs [8.21 hrs effective]	18.677	228	173	247	251	194	158
		161		265		83	
		129		242		198	
As-received +8 hrs [12.21 hrs effective]	18.830	159	155	176	156	168	204
		163		140		243	
		143		151		202	
As-received +60 hrs [64.21 hrs effective]	19.474	53	58	58	54	66	67
		54		52		66	
		66		52		67	
As-received +100 hrs [104.21 hrs effective]	19.662	23	30	21	26	19	26
		23		37		24	
		42		19		33	
Minimum required [2003Sas]:		**35J ave / 24J min**					

*Effective time, t_{eff}, of exposure to simulated PWHT.

Table A.9: Charpy impact toughness of weld samples in an as-received condition and after additional simulated PWHT (tested at 0°C).

Condition	Hp_{eff}	Impact toughness External [J]	Average External [J]	Impact toughness Middle [J]	Average Middle [J]	Impact toughness Internal [J]	Average Internal [J]
As-received +2 hrs [10.79 hrs effective*]	18.782	197	185	-	-	158	152
		182		-		160	
		174		-		137	
As-received +4 hrs [12.79 hrs effective]	18.848	181	187	-	-	189	198
		194		-		187	
		186		-		217	
As-received +6 hrs [14.79 hrs effective]	18.905	152	148	-	-	146	154
		143		-		161	
		-		-		-	
As-received +30 hrs [38.79 hrs effective]	19.279	180	177	-	-	177	179
		180		-		179	
		170		-		181	
As-received +40 hrs [48.79 hrs effective]	19.368	202	185	-	-	195	201
		166		-		227	
		187		-		180	
As-received +60 hrs [68.79 hrs effective]	19.501	183	187	-	-	179	180
		194		-		174	
		181		-		185	
As-received +80 hrs [88.79 hrs effective]	19.600	201	203	-	-	211	213
		192		-		248	
		213		-		180	
Minimum required [2003Sas]:		**35J ave / 24J min**					

*Effective time, t_{eff}, of exposure to simulated PWHT.

APPENDIX B

Table B.1: List of originally installed ash locks, their initial heat treatment condition, tensile properties and chemical composition.

Equipment no.	Component	Initial heat treatment condition (N/T* temperature [°C] time [min])	Tensile Strength (lowest measured values)		Chemical composition % (product analysis)								
			0.2% Y.S [MPa]	T.S [MPa]	C x100	Si x100	Mn x100	P x100	S x100	Mo x100/ Cu x100	Nb x100/ Ni x100	B x1000/ Cr x100	Al x1000/ V x1000
010AL-06	Shell	N 910 × 60 min T 630 × 30 min.	416	579	22	28	144	11	3	49	11	0	0
	Top dome	N 910 × 30 min T 650 × 30 min.	507	651	21	24	146	14	4	50 -	1 -	- 0	19 2
	Bottom cone	N 910 × 30 min T 650 × 30 min.	435	614	20	22	138	16	5	55 -	1 -	- 0	22 3
010AL-07	Shell	N 910 × 60 min T 610 × 30 min.	385	557	20	27	142	8	4	49	11	0	0
	Top dome	N 910 × 30 min T 650 × 30 min.	469	632	22	25	149	14	4	50 -	1 -	- 0	21 8
	Bottom cone	N 910 × 30 min T 650 × 30 min.	533	674	20	25	148	20	4	50 -	1 -	- 0	21 -
010AL-08	Shell	N 910 × 60 min T 640 × 30 min.	395	557	21	27	142	8	4	49	11	0	0
	Top dome	N 910 × 30 min T 650 × 30 min.	507	651	21	24	146	14	4	50 -	1 -	- 0	19 2
	Bottom cone	N 910 × 30 min T 650 × 30 min.	533	674	20	25	148	20	4	50 -	1 -	- 0	21 3
010AL-09	Shell	N 910 × 60 min T 640 × 30 min.	413	587	20	28	138	11	3	51	20	0	0
	Top dome	N 910 × 30 min T 650 × 30 min.	437	637	20	27	153	20	6	48 -	1 -	- 0	7 9
	Bottom cone	N 910 × 30 min T 650 × 30 min.	496	639	19	28	140	16	4	47 -	4 -	- 0	24 3
010AL-10	Shell	N 910 × 60 min T 630 × 30 min.	394	573	19	27	140	10	4	54 -	1 -	- 2	18 1
	Top dome	N 910 × 60 min T 630 × 30 min.	422	586	19	23	144	13	3	54 -	1 -	- 2	16 3
	Bottom cone	N 910 × 60 min T 630 × 30 min.	381	573	18	25	139	14	4	55 -	1 -	- 3	18 2
010AL-13	Shell	N 910 × 60 min T 640 × 30 min.	421	597	21	28	135	11	3	50	20	0	0
	Top dome	N 910 × 30 min T 650 × 30 min.	437	628	20	27	153	20	6	48 -	1 -	- 0	7 9
	Bottom cone	N 910 × 30 min T 650 × 30 min.	463	596	19	27	139	13	4	44 -	1 -	- 0	33 4
010AL-14	Shell	N 910 × 60 min T 640 × 30 min.	413	587	20	28	138	11	3	51	20	0	0
	Top dome	N 910 × 30 min T 650 × 30 min.	516	667	21	25	149	16	4	51 -	1 -	- 0	20 2
	Bottom cone	N 910 × 30 min T 650 × 30 min.	496	639	19	27	140	16	4	47 -	4 -	- 0	34 4
010AL-15	Shell	N 910 × 60 min T 640 × 30 min.	419	584	20	27	139	13	4	50	20	0	0
	Top dome	N 910 × 30 min T 650 × 30 min.	516	667	21	25	149	16	4	51 -	1 -	- 0	20 2
	Bottom cone	N 910 × 30 min T 650 × 30 min.	463	596	19	27	139	13	4	44	1 -	- 0	33 4
010AL-16	Shell	N 910 × 60 min T 640 × 30 min.	419	586	20	27	139	13	4	50	20	0	0
	Top dome	N 910 × 30 min T 650 × 30 min.	451	639	20	25	149	17	7	46 -	1 -	- 0	4 6
	Bottom cone	N 910 × 30 min T 650 × 30 min.	482	636	18	25	146	16	5	45 -	1 -	- 0	26 7
010AL-17	Shell	N 910 × 60 min T 640 × 30 min.	419	586	20	27	139	13	4	50	20	0	0
	Top dome	N 910 × 30 min T 650 × 30 min.	451	639	20	25	149	17	7	46 -	1 -	- 0	4 6
	Bottom cone	N 910 × 30 min T 650 × 30 min.	482	639	18	25	146	16	5	45 -	1 -	- 0	26 7

Equipment no.	Component	Initial heat treatment condition (N/T* temperature [°C] time [min])	Tensile Strength (lowest measured values)		Chemical composition % (product analysis)								
			0.2% Y.S [MPa]	T.S [MPa]	C x100	Si x100	Mn x100	P x100	S x100	Mo x100/ Cu x100	Nb x100/ Ni x100	B x1000/ Cr x100	Al x1000/ V x1000
010AL-18	Shell	N 910 × 60 min T 630 × 30 min.	428	603	21	28	136	11	3	51	20	0	0
	Top dome	N 910 × 30 min T 650 × 30 min.	431	591	21	26	151	14	7	47 -	5 -	- 0	6 6
	Bottom cone	N 910 × 30 min T 650 × 30 min.	571	661	20	26	149	22	4	47 -	1 -	- 0	19 9
010AL-19	Shell	N 910 × 60 min T 640 × 30 min.	428	603	21	28	136	11	3	51	20	0	0
	Top dome	N 910 × 30 min T 650 × 30 min.	431	611	21	26	151	17	14	47 -	2 -	- 0	6 6
	Bottom cone	N 910 × 30 min T 650 × 30 min.	517	661	20	26	149	22	4	47 -	1 -	- 0	19 9
010AL-20	Shell	N 910 × 60 min T 640 × 30 min.	419	584	20	27	139	13	4	51	20	0	0
	Top dome	N 910 × 30 min T 650 × 30 min.	462	424	20	25	148	16	5	47 -	1 -	- 0	8 6
	Bottom cone	N 910 × 30 min T 650 × 30 min.	492	644	18	25	147	16	3	46 -	1 -	- 0	26 7
010AL-21	Shell	N 910 × 60 min T 640 × 30 min.	403	568	20	28	139	11	3	52	20	0	0
	Top dome	N 910 × 30 min T 640 × 30 min.	462	624	20	25	148	16	5	47 -	1 -	- 0	8 6
	Bottom cone	N 910 × 30 min T 650 × 30 min.	492	644	18	25	147	16	3	46 -	1 -	- 0	26 7
010AL-22	Shell	N 910 × 60 min T 630 × 30 min.	378	560	18	25	138	13	4	55 -	1 -	- 3	18 2
	Top dome	N 910 × 60 min T 630 × 30 min.	398	578	19	2	144	13	3	54 -	1 -	- 2	16 4
	Bottom cone	N 910 × 60 min T 630 × 30 min.	397	565	20	25	141	17	4	57 -	2 -	- 3	18 2
010AL-25	Shell	N 910 × 60 min T 640 × 30 min.	436	610	22	26	141	8	3	50	20	0	0
	Top dome	N 910 × 30 min T 650 × 30 min.	446	670	20	25	150	17	6	47 -	1 -	- 0	27 7
	Bottom cone	N 910 × 30 min T 650 × 30 min.	516	653	18	27	145	15	4	45 -	1 -	- 0	- 6
010AL-26	Shell	N 910 × 60 min T 640 × 30 min.	436	610	22	26	141	8	3	50	20	0	0
	Top dome	N 910 × 30 min T 650 × 30 min.	446	670	20	25	150	17	6	47 -	1 -	- 0	27 7
	Bottom cone	N 910 × 30 min T 650 × 30 min.	510	658	19	26	156	19	7	48 -	1 -	- 0	- 5
010AL-27	Shell	N 910 × 60 min T 640 × 30 min.	473	629	22	28	142	9	3	46	20	0	0
	Top dome	N 910 × 30 min T 650 × 30 min.	463	651	19	25	150	17	4	45 -	2 -	- 0	24 7
	Bottom cone	N 910 × 30 min T 650 × 30 min.	510	658	19	26	156	19	7	48 -	1 -	- 0	- 5
010AL-28	Shell	N 910 × 60 min T 640 × 30 min.	473	629	22	28	142	9	3	46	20	0	0
	Top dome	N 910 × 30 min T 650 × 30 min.	463	651	19	25	150	17	4	45 -	2 -	- 0	24 7
	Bottom cone	N 910 × 30 min T 650 × 30 min.	516	653	18	27	145	15	4	45 -	1 -	- 0	- 6
010AL-29	Shell	N 910 × 60 min T 640 × 30 min.	448	602	22	28	141	10	3	48	20	0	0
	Top dome	N 910 × 30 min T 650 × 30 min.	426	659	20	28	149	16	4	45 -	1 -	- 0	24 8
	Bottom cone	N 910 × 30 min T 650 × 30 min.	512	664	19	26	147	20	7	48 -	2 -	- 0	- 6
010AL-30	Shell	N 910 × 60 min T 640 × 30 min.	449	603	22	28	141	19	3	48	20	0	0
	Top dome	N 910 × 30 min T 650 × 30 min.	426	659	20	28	149	16	4	45 -	1 -	- 0	24 8
	Bottom cone	N 910 × 30 min T 650 × 30 min.	512	664	19	26	147	20	7	48 -	2 -	- 0	- 6
010AL-31	Shell	N 910 × 60 min T 640 × 30 min.	448	603	21	28	143	11	4	45	19	0	0
	Top dome	N 910 × 30 min T 650 × 30 min.	488	641	19	26	150	26	4	47 -	1 -	- 0	- 8

Equipment no.	Component	Initial heat treatment condition (N/T* temperature [°C] time [min])	Tensile Strength (lowest measured values)		Chemical composition % (product analysis)								
			0.2% Y.S [MPa]	T.S [MPa]	C x100	Si x100	Mn x100	P x100	S x100	Mo x100/ Cu x100	Nb x100/ Ni x100	B x1000/ Cr x100	Al x1000/ V x1000
	Bottom cone	N 910 × 30 min T 650 × 30 min.	512	648	19	27	148	16	4	45 -	1 -	- 0	- 7
010AL-32	Shell	N 910 × 60 min T 640 × 30 min.	447	603	21	28	143	11	4	45	19	0	0
	Top dome	N 910 × 30 min T 640 × 30 min.	488	641	19	26	150	26	4	47 -	1 -	- 0	- 8
	Bottom cone	N 910 × 30 min T 650 × 30 min.	512	648	19	27	148	16	4	45 -	1 -	- 0	- 7
010AL-33	Shell	N 910 × 60 min T 640 × 30 min.	461	610	22	28	142	11	3	47	20	0	0
	Top dome	N 910 × 30 min T 650 × 30 min.	482	633	18	25	149	26	4	47 -	1 -	- 0	24 8
	Bottom cone	N 910 × 30 min T 650 × 30 min.	439	665	18	25	147	20	4	48 -	1 -	- 0	- 7
010AL-34	Shell	N 910 × 60 min T 630 × 30 min.	379	573	219	27	141	11	4	54 -	1 -	- 2	15 -
	Top dome	N 910 × 60 min T 630 × 30 min.	435	603	20	26	141	17	3	56 -	4 -	- 4	19 2
	Bottom cone	N 910 × 60 min T 630 × 30 min.	413	614	20	25	142	18	4	57 -	1 -	- 3	19 2
010AL-37	Shell	N 910 × 60 min T 640 × 30 min.	461	610	22	28	142	11	3	47	20 -	- 11	- 0
	Top dome	N 910 × 30 min T 650 × 30 min.	482	633	18	25	149	26	4	47 -	1 -	- 0	24 8
	Bottom cone	N 910 × 30 min T 650 × 30 min.	439	605	18	25	147	20	4	48 -	1 -	- 0	- 7
010AL-38	Shell	N 910 × 60 min T 640 × 30 min.	455	608	20	29	144	11	4	46	1 18	- 10	- 1
	Top dome	N 910 × 30 min T 650 × 30 min.	465	625	20	26	151	16	5	45 -	1 -	- 0	7 9
	Bottom cone	N 910 × 30 min T 650 × 30 min.	436	609	18	25	146	20	4	48 -	1 -	- 0	- 7
010AL-39	Shell	N 910 × 60 min T 640 × 30 min.	455	608	20	29	144	11	4	46	1 18	- 10	- 1
	Top dome	N 910 × 30 min T 650 × 30 min.	465	625	20	26	151	16	5	45 -	1 -	- 0	7 9
	Bottom cone	N 910 × 30 min T 650 × 30 min.	436	609	18	25	146	20	4	48 -	1 -	- 0	- 7
010AL-40	Shell	N 900 × 94 min T 650 × 142 min.	400	565	19	22	146	22	5	48 -	1 -	- 0	- 1
	Top dome	N 910 × 30 min T 650 × 30 min.	485	636	19	25	149	24	4	46 -	1 -	- 0	23 8
	Bottom cone	N 910 × 30 min T 650 × 30 min.	502	645	19	26	146	17	4	49 -	1 -	- 0	- 5
010AL-41	Shell	N 900 × 94 min T 650 × 142 min.	400	565	19	22	146	22	5	48 -	1 -	- 0	- 1
	Top dome	N 910 × 30 min T 650 × 30 min.	485	636	19	25	149	24	4	46 -	1 -	- 0	23 8
	Bottom cone	N 910 × 30 min T 650 × 30 min.	502	645	19	26	146	17	4	49 -	1 -	- 0	- 5
010AL-42	Shell	N 900 × 94 min T 650 × 142 min.	434	590	19	23	149	23	6	49 -	1 -	- 0	- 2
	Top dome	N 910 × 30 min T 650 × 30 min.	513	657	21	23	154	23	3	46 -	1 -	- 0	- 3
	Bottom cone	N 910 × 30 min T 650 × 30 min.	464	619	18	27	150	21	4	48 -	3 -	- 0	- 8
010AL-43	Shell	N 900 × 94 min T 650 × 142 min.	400	565	19	22	146	22	5	48 -	1 -	- 0	- 1
	Top dome	N 910 × 30 min T 650 × 30 min.	513	657	21	23	154	23	3	46 -	1 -	- 0	- 3
	Bottom cone	N 910 × 30 min T 650 × 30 min.	464	619	18	27	150	21	4	48 -	3 -	- 0	- 8
010AL-44	Shell	N 910 × 60 min T 650 × 30 min.	452	608	21	27	142	8	3	50	22	11	0
	Top dome	N 910 × 30 min T 650 × 30 min.	517	662	20	23	152	22	3	45 -	1 -	- 0	- 3
	Bottom cone	N 910 × 30 min T 650 × 30 min.	483	636	17	26	146	20	4	46 -	1 -	- 0	- 7
010AL-45	Shell	N 910 × 60 min T 640 × 30 min.	452	608	21	27	142	8	3	50	22	11	

Equipment no.	Component	Initial heat treatment condition (N/T* temperature [°C] time [min])	Tensile Strength (lowest measured values)		Chemical composition % (product analysis)								
			0.2% Y.S [MPa]	T.S [MPa]	C x100	Si x100	Mn x100	P x100	S x100	Mo x100/ Cu x100	Nb x100/ Ni x100	B x1000/ Cr x100	Al x1000/ V x1000
	Top dome	N 910 × 30 min T 650 × 30 min.	517	662	20	23	152	22	3	45 -	1 -	- 0	- 3
	Bottom cone	N 910 × 30 min T 650 × 30 min.	483	636	17	26	146	20	4	46 -	1 -	- 0	- 7
010AL-46	Shell	N 910 × 30 min T 650 × 30 min.	452	608	21	27	142	8	3	50	22	11	
	Top dome	N 910 × 30 min T 650 × 30 min.	406	582	19	23	141	12	4	52 -	2 -	- 2	18 4
	Bottom cone	N 910 × 30 min T 650 × 30 min.	420	607	19	27	142	17	3	58 -	3 -	- 3	26 3
010AL-47	Shell	N 910 × 60min T 640 × 30 min.	438	599	21	28	145	11	5	45	1 19	- 10	- 1
	Top dome	N 900 × 175 min T 650 × 152 min.	514	665	21	26	155	18	7	49 -	1 -	- 0	-2
	Bottom cone	N 900 × 108 min T 650 × 161 min.	507	648	19	26	151	16	4	50 -	1 -		- 2
010AL-48	Shell	N 910 × 60 min T 640 × 30 min.	480	433	22	27	142	11	3	48	20	- 11	
	Top dome	N 900 × 175 min T 650 × 162 min.	496	641	18	27	149	19	5	47 -	1 -		- 2
	Bottom cone	N 900 × 108 min T 650 × 162 min.	410	573	16	23	144	14	6	50 -	1 -		- 2
010AL-49	Shell	N 910 × 60 min T 640 × 30 min.	480	433	22	27	142	1	3	48	20	- 11	
	Top dome	N 900 × 175 min T 650 × 162 min.	496	641	18	27	149	19	5	47 -	1 -		- 2
	Bottom cone	N 900 × 108 min T 650 × 162 min.	410	573	16	23	144	14	6	50 -	1 -		- 2
010AL-50	Shell	N 900 × 94 min T 650 × 142 min.	469	612	18	27	148	18	5	48 -	1 -		- 2
	Top dome	N 900 × 175 min T 650 × 162 min.	445	611	19	27	150	18	8	46 -	1 -		- 1
	Bottom cone	N 900 × 108 min T 650 × 162 min.	408	566	16	23	149	16	6	49 -	1 -		- 1
010AL-51	Shell	N 900 × 94 min T 630 × 142 min.	387	552	18	20	154	13	3	46 -	1 -		- 2
	Top dome	N 900 × 124 min T 650 × 162 min.	499	637	18	26	147	17	5	47 -	1 -		- 1
	Bottom cone	N 890 × 108 min T 650 × 162 min.	398	575	19	20	145	21	4	47 -	1 -		- 1
010AL-52	Shell	N 900 × 94 min T 630 × 142 min.	387	552	18	20	154	13	3	46 -	1 -		- 2
	Top dome	N 900 × 124 min T 650 × 162 min.	499	637	18	26	147	17	5	47 -	1 -		- 1
	Bottom cone	N 900 × 108 min T 650 × 162 min.	395	567	16	23	149	15	5	50 -	1 -		- 1
010AL-53	Shell	N 900 × 94 min T 630 × 142 min.	465	607	19	20	147	21	4	48 -	1 -		- 1
	Top dome	N 900 × 124 min T 650 × 161 min.	409	586	18	19	141	15	5	47 -	1 -		- 1
	Bottom cone	N 900 × 108 min T 650 × 162 min.	430	590	18	19	151	12	3	45 -	1 -		- 1
010AL-54	Shell	N 900 × 94 min T 630 × 142 min.	456	607	19	20	147	21	4	48 -		- 1	
	Top dome	N 900 × 124 min T 650 × 162 min.	486	641	18	27	148	16	5	48 -	1 -		- 1
	Bottom cone	N 900 × 108 min T 650 × 162 min.	430	590	18	19	151	12	3	45 -	1 -		- 1
010AL-55	Shell	N 900 × 94 min T 650 × 142 min.	391	555	19	20	144	19	4	49 -	1 -		- 1
	Top dome	N 900 × 124 min T 650 × 162 min.	486	641	18	27	148	16	5	48 -	1 -		- 1
	Bottom cone	N 890 × 108 min T 650 × 162 min.	398	575	19	20	145	21	4	47 -	1 -		- 1
010AL-56	Shell	N 910 × 60 min T 630 × 30 min.	378	651	17	25	139	14	4	54 -	1 -	- 3	18 2
	Top dome	N 910 × 90 min T 630 × 30 min.	406	582	19	23	141	12	4	52 -	1 -	- 2	18 4
	Bottom cone	N 910 × 60 min T 630 × 30 min.	420	607	19	27	142	17	3	58 -	3 -	- 3	26 3

Equipment no.	Component	Initial heat treatment condition (N/T* temperature [°C] time [min])	Tensile Strength (lowest measured values)		Chemical composition % (product analysis)								
			0.2% Y.S [MPa]	T.S [MPa]	C x100	Si x100	Mn x100	P x100	S x100	Mo x100/ Cu x100	Nb x100/ Ni x100	B x1000/ Cr x100	Al x1000/ V x1000
010AL-57**	Shell												
	Top dome												
	Bottom cone												
010AL-58**	Shell												
	Top dome												
	Bottom cone												
010AL-59**	Shell												
	Top dome												
	Bottom cone												
010AL-60**	Shell												
	Top dome												
	Bottom cone												
010AL-61**	Shell												
	Top dome												
	Bottom cone												
210AL-0101	Shell	N 930 x 145 min T 650 × 155 min.	382	559	17	23	136	13	4	55 -	2 -	- 3	19 1
	Top dome	N 910 × 175 min T 650 × 161min.	506	651	17	26	142	14	4	56 -	1 -	- 2	36 1
	Bottom cone	N 910 × 154 min T 650 × 155 min.	380	579	19	25	142	17	4	58 -	2 -	- 3	20 1
210AL-0201	Shell	N 910 × 145 min T 650 × 155 min.	379	560	18	25	143	12	4	50 -	2 -	- 3	17 1
	Top dome	N 910 × 175 min T 650 × 161min.	420	596	18	23	143	17	4	57 -	2 -	- 3	29 1
	Bottom cone	N 930 × 154 min T 650 × 155 min.	367	554	17	24	144	16	3	55 -	2 -	- 3	19 1
210AL-0301	Shell	N 910 × 45 min T 650 × 155 min.	368	571	18	25	142	13	4	51 -	1 -	- 3	17 1
	Top dome	N 910 × 175 min T 650 × 161min.	405	583	17	22	139	16	4	54 -	1 -	- 3	29 1
	Bottom cone	N 930 × 154 min T 650 × 155 min.	386	571	17	24	145	16	4	56 -	1 -	- 3	19 1
210AL-0401	Shell	N 910 × 145 min T 650 × 155 min.	373	557	18	25	144	13	5	50 -	1 -	- 3	17 4
	Top dome	N 910 × 175 min T 650 × 161min.	405	583	17	22	139	16	4	54 -	1 -	- 3	29 1
	Bottom cone	N 930 × 154 min T 650 × 155 min.	386	571	17	24	145	16	4	56 -	1 -	- 3	19 1
210AL-0501	Shell	N 910 × 145 min T 650 × 155 min.	378	557	18	25	144	13	5	50 -	1 -	- 3	17 1
	Top dome	N 930 × 175 min T 650 × 161 min.	394	584	18	24	139	21	3	56 -	1 -	- 4	22 1
	Bottom cone	N 930 × 154 min T 650 × 155 min.	359	564	17	25	147	16	4	57 -	2 -	- 3	19 1
210AL-0601	Shell	N 910 × 45 min T 650 × 155 min.	365	571	16	25	142	13	4	51 -	1 -	- 3	17 1
	Top dome	N 930 × 175 min T 650 × 161 min.	394	584	18	24	139	21	3	58 -	1 -	- 4	22 1
	Bottom cone	N 930 × 154 min T 650 × 155 min.	381	564	17	25	147	18	4	57 -	2 -	- 3	19 3
210AL-0701	Shell	N 910 × 145 min T 650 × 155 min.	413	610	17	23	138	13	5	51 -	1 -	- 2	13 1
	Top dome	N 930 × 175 min T 650 × 161 min.	394	583	19	24	140	2	4	56 -	5 -	- 4	22 2
	Bottom cone	N 930 × 154 min T 650 × 155 min.	450	634	20	25	144	16	4	60 -	2 -	- 3	19 1

Equipment no.	Component	Initial heat treatment condition (N/T* temperature [°C] time [min])	Tensile Strength (lowest measured values)		Chemical composition % (product analysis)								
			0.2% Y.S [MPa]	T.S [MPa]	C x100	Si x100	Mn x100	P x100	S x100	Mo x100/ Cu x100	Nb x100/ Ni x100	B x1000/ Cr x100	Al x1000/ V x1000
210AL-0801	Shell	N 910 × 145 min T 650 × 155 min.	413	610	17	23	138	13	5	51 -	1 -	- 2	13 1
	Top dome	N 930 × 175 min T 650 × 161 min.	394	583	19	24	140	2	4	56 -	5 -	- 4	22 2
	Bottom cone	N 930 × 154 min T 650 × 155 min.	430	634	20	23	144	16	4	60 -	2 -	- 3	19 2
210AL-0901	Shell	N 910 × 145 min T 650 × 155 min.	399	583	17	24	141	14	4	54 -	3 -	- 4	31 1
	Top dome	N 910 × 175 min T 650 × 161min.	455	624	19	24	148	21	5	59 -	1 -	- 3	29 4
	Bottom cone	N 930 × 154 min T 650 × 155 min.	434	614	20	25	140	14	4	58 -	1 -	- 3	19 1
210AL-1001**	Shell												
	Top dome												
	Bottom cone												
210AL-1301	Shell	N 910 × 145 min T 650 × 155 min.	358	556	17	25	144	13	5	51 -	1 -	- 3	47 4
	Top dome	N 910 × 175 min T 650 × 161min.	412	596	19	24	146	2	4	57 -	4 -	- 4	31 1
	Bottom cone	N 910 × 154 min T 650 × 155 min.	371	563	18	25	145	15	4	57 -	3 -	- 3	19 1
210AL-1401	Shell	N 910 × 145 min T 650 × 155 min.	437	606	17	23	141	16	4	52 -	2 -	- 3	13 1
	Top dome	N 910 × 175 min T 650 × 161min.	413	605	19	23	142	17	5	55 -	1 -	- 3	29 4
	Bottom cone	N 930 × 154 min T 650 × 155 min.	371	563	18	25	145	15	4	57 -	3 -	- 3	19 1
210AL-1501	Shell	N 910 × 145 min T 650 × 155 min.	437	606	17	23	141	16	4	52 -	2 -	- 3	13 1
	Top dome	N 910 × 175 min T 650 × 161min.	413	605	19	23	142	17	5	55 -	1 -	- 3	29 4
	Bottom cone	N 930 × 154 min T 650 × 155 min.	434	614	20	25	140	14	4	58 -	1 -	- 3	19 1
210AL-1601*	Shell												
	Top dome												
	Bottom cone												
210AL-1701	Shell	N 910 × 145 min T 650 × 155 min.	358	556	17	25	144	13	5	51 -	1 -	- 3	17 4
	Top dome	N 910 × 175 min T 650 × 161min.	506	653	18	24	140	17	5	54 -	1 -	- 2	29 4
	Bottom cone	N 910 × 154 min T 650 × 155 min.	469	635	19	25	142	16	5	54 -	1 -	- 2	29 4
210AL-1801	Shell	N 910 × 145 min T 650 × 155 min.	447	609	16	24	140	2	4	51 -	5 -	- 3	13 1
	Top dome	N 910 × 175 min T 650 × 161min.	506	653	18	24	140	17	5	54 -	1 -	- 2	29 4
	Bottom cone	N 930 × 154 min T 650 × 155 min.	422	597	19	25	141	15	4	56 -	2 -	- 3	18 2
210AL-1901	Shell	N 910 × 145 min T 650 × 155 min.	447	609	16	24	140	2	4	51 -	5 -	- 3	13 1
	Top dome	N 910 × 175 min T 650 × 161min.	445	615	18	24	143	15	4	56 -	1 -	- 3	31 3
	Bottom cone	N 910 × 154 min T 650 × 155 min.	397	574	19	28	144	21	5	59 -	1 -	- 4	19 4
210AL-2001	Shell	N 910 × 145 min T 650 × 155 min.	446	603	17	26	141	15	3	52 -	5 -	- 3	22 3
	Top dome	N 910 × 175 min T 650 × 161 min.	445	615	18	24	143	15	4	56 -	1 -	- 3	31 3
	Bottom cone	N 910 × 154 min T 650 × 155 min.	394	574	19	28	144	21	5	59 -	1 -	- 4	19 4
210AL-2101	Shell	N 910 × 145 min T 650 × 155 min.	446	603	17	26	141	15	3	52 -	5 -	- 3	22 3
	Top dome	N 930 × 175 min T 650 × 161 min.	402	594	18	23	139	22	3	54 -	3 -	- 4	22 2

Equipment no.	Component	Initial heat treatment condition (N/T* temperature [°C] time [min])	Tensile Strength (lowest measured values)		Chemical composition % (product analysis)								
			0.2% Y.S [MPa]	T.S [MPa]	C x100	Si x100	Mn x100	P x100	S x100	Mo x100/ Cu x100	Nb x100/ Ni x100	B x1000/ Cr x100	Al x1000/ V x1000
	Bottom cone	N 910 × 154 min T 650 × 155 min.	398	585	19	25	143	17	4	58 -	1 -	- 4	21 3
210AL-2201	Shell	N 910 × 60 min T 630 × 30 min.	378	560	18	25	138	13	4	55 -	1 -	- 3	18 2
	Top dome	N 910 × 60 min T 650 × 155 min.	398	578	19	23	144	13	3	54 -	1 -	- 2	16 4
	Bottom cone	N 910 × 60 min T 630 × 30 min.	397	565	20	25	141	17	4	57 -	2 -	- 3	18 2
210AL-2501	Shell	N 910 × 145 min T 650 × 155 min.	428	587	18	25	141	17	4	53 -	1 -	- 2	29 2
	Top dome	N 910 × 175 min T 650 × 161min.	541	679	18	27	147	15	6	56 -	1 -	- 3	40 1
	Bottom cone	N 910 × 154 min T 650 × 155 min.	385	564	18	24	143	17	4	57 -	1 -	- 4	21 1
210AL-2601	Shell	N 910 × 145 min T 650 × 155 min.	419	583	18	25	145	20	5	56 -	3 -	- 2	29 2
	Top dome	N 910 × 175 min T 650 × 161min.	541	679	18	27	147	15	6	56 -	1 -	- 3	40 1
	Bottom cone	N 910 × 154 min T 650 × 155 min.	385	564	18	24	143	17	4	57 -	1 -	- 4	21 1
210AL-2701	Shell	N 910 × 145 min T 650 × 155 min.	419	583	18	25	145	20	5	56 -	3 -	- 2	29 2
	Top dome	N 910 × 175 min T 650 × 161min.	533	671	18	26	148	16	5	57 -	1 -	- 3	40 1
	Bottom cone	N 910 × 154 min T 650 × 155 min.	402	566	17	24	143	18	4	57 -	1 -	- 4	21 1
210AL-2801	Shell	N 910 × 145 min T 650 × 155 min.	428	587	18	25	141	17	4	53 -	1 -	- 2	29 2
	Top dome	N 910 × 175 min T 650 × 161 min.	533	671	18	26	148	16	5	57 -	1 -	- 3	40 1
	Bottom cone	N 910 × 154 min T 650 × 155 min.	402	566	17	24	143	18	4	57 -	1 -	- 4	21 1
210AL-2901	Shell	N 910 × 145 min T 650 × 155 min.	370	589	18	23	137	15	4	56 -	2 -	- 3	19 1
	Top dome	N 910 × 175 min T 650 × 161min.	505	649	17	24	145	15	3	54 -	1 -	- 2	3601
	Bottom cone	N 930 × 154 min T 650 × 155 min.	410	602	19	25	144	15	4	55 -	2 -	- 4	19 1
210AL-3001	Shell	N 910 x 145 min T 650 × 155 min.	370	589	18	23	137	15	4	56 -	2 -	- 3	19 1
	Top dome	N 910 x 175 min T 650°C x 161 min.	506	649	17	24	145	15	3	54 -	1 -	- 2	36 1
	Bottom cone	N 930 x 154 min T 650°C x 155 min.	410	602	19	25	144	15	4	55 -	2 -	- 4	19 1
210AL-3101	Shell	N 930 × 145 min T 650 × 155 min.	423	575	18	24	144	14	4	52 -	1 -	- 3	- 1
	Top dome	N 910 × 175 min T 650 × 161 min.	389	560	16	23	140	18	5	55 -	1 -	- 3	- 1
	Bottom cone	N 910 × 103 min T 650 × 155 min.	454	605	20	25	141	19	4	57 -	8 -	- 3	- 5
210AL-3201	Shell	N 930 × 145 min T 650 × 155 min.	417	578	19	24	143	13	4	50 -	1 -	- 3	- 1
	Top dome	N 910 × 175 min T 650 × 161 min.	389	560	16	23	140	18	5	55 -	1 -	- 3	- 1
	Bottom cone	N 910 × 103 min T 650 × 155 min.	458	614	19	25	144	18	4	57 -	8 -	- 3	- 6
210AL-3301	Shell	N 930 × 145 min T 650 × 155 min.	423	575	18	24	144	14	4	52 -	1 -	- 3	- 1
	Top dome	N 910 × 175 min T 650 × 161 min.	393	566	17	22	141	18	4	55 -	1 -	- 3	- 1
	Bottom cone	N 910 × 103 min T 650 × 155 min.	454	605	20	25	144	19	4	57 -	8 -	- 3	- 5
210AL-3701	Shell	N 930 × 145 min T 650 × 155 min.	417	578	18	24	143	13	4	50 -	1 -	- 3	- 1
	Top dome	N 910 × 175 min T 650 × 161 min.	393	566	17	22	141	18	4	55 -	1 -	- 3	- 1
	Bottom cone	N 910 × 103 min T 650 × 155 min.	458	614	19	25	144	18	4	57 -	8 -	- 3	- 6
210AL-3801**	Shell												

Equipment no.	Component	Initial heat treatment condition (N/T* temperature [°C] time [min])	Tensile Strength (lowest measured values)		Chemical composition % (product analysis)								
			0.2% Y.S [MPa]	T.S [MPa]	C x100	Si x100	Mn x100	P x100	S x100	Mo x100/ Cu x100	Nb x100/ Ni x100	B x1000/ Cr x100	Al x1000/ V x1000
	Top dome												
	Bottom cone												
210AL-3901**	Shell												
	Top dome												
	Bottom cone												
210AL-4001**	Shell												
	Top dome												
	Bottom cone												
210AL-4101	Shell	N 930 x 145 min T 650 × 155 min.	382	554	17	23	136	13	4	55 -	2 -	- 3	19 1
	Top dome	N 910 × 175 min T 650 × 161min.	506	651	17	26	142	14	4	56 -	1 -	- 2	36 1
	Bottom cone	N 910 × 154 min T 650 × 155 min.	380	579	19	25	142	17	4	58 -	2 -	- 3	20 1
210AL-4201	Shell	N 910 × 145 min T 650 × 155 min.	379	560	18	25	143	12	4	50 -	2 -	- 3	17 1
	Top dome	N 910 × 175 min T 650 × 161min.	446	620	17	24	143	14	4	53 -	1 -	- 2	36 1
	Bottom cone	N 930 × 154 min T 650 × 155 min.	408	607	19	25	145	16	4	55 -	2 -	- 4	19 1
210AL-4301	Shell	N 910 × 145 min T 650 × 155 min.	379	560	18	25	143	12	4	50 -	2 -	- 3	17 1
	Top dome	N 910 × 175 min T 650 × 161min.	420	596	18	23	143	17	4	57 -	2 -	- 3	29 1
	Bottom cone	N 930 × 154 min T 650 × 155 min.	367	554	17	24	144	16	3	55 -	2 -	- 3	19 1
210AL-4401	Shell	N 930 × 145 min T 650 × 155 min.	383	554	17	23	137	15	3	56 -	2 -	- 4	19 1
	Top dome	N 910 × 175 min T 650 × 161min.	506	647	18	23	143	14	4	54 -	1 -	- 2	36 1
	Bottom cone	N 910 × 154 min T 650 × 155 min.	386	602	20	24	139	14	4	57 -	3 -	- 3	20 1
210AL-4501**	Shell												
	Top dome												
	Bottom cone												
210AL-4601	Shell	N 910 × 145 min T 650 × 155 min.	418	583	16	23	140	15	4	54 -	3 -	- 4	31 1
	Top dome	N 930 × 175 min T 650 × 161 min.	402	594	18	23	139	22	3	54 -	3 -	- 4	22 2
	Bottom cone	N 910 × 154 min T 650 × 155 min.	398	585	19	25	143	17	4	58 -	1 -	- 4	21 3
210AL-4701	Shell	N 910 × 145 min T 650 × 155 min.	418	583	16	23	140	15	4	54 -	3 -	- 4	31 1
	Top dome	N 930 × 175 min T 650 × 161 min.	408	590	19	23	137	20	4	53 -	4 -	- 4	22 3
	Bottom cone	N 910 × 154 min T 650 × 155 min.	390	578	19	24	142	16	4	56 -	1 -	- 3	21 3
210AL-4801**	Shell												
	Top dome												
	Bottom cone												
210AL-5601**	Shell												
	Top dome												
	Bottom cone												
210AL-5701**	Shell												

Equipment no.	Component	Initial heat treatment condition (N/T* temperature [°C] time [min])	Tensile Strength (lowest measured values)		Chemical composition % (product analysis)								
			0.2% Y.S [MPa]	T.S [MPa]	C x100	Si x100	Mn x100	P x100	S x100	Mo x100/ Cu x100	Nb x100/ Ni x100	B x1000/ Cr x100	Al x1000/ V x1000
	Top dome												
	Bottom cone												
210AL-5801**	Shell												
	Top dome												
	Bottom cone												
210AL-5901**	Shell												
	Top dome												
	Bottom cone												
210GG-5000-AL**	Shell												
	Top dome												
	Bottom cone												

*N: Normalised; T: Tempered

**Code data book was not available